



National Library
of Canada

Bibliothèque nationale
du Canada

Canadian Theses Service

Services des thèses canadiennes

Ottawa, Canada
K1A 0N4

CANADIAN THESES

THÈSES CANADIENNES

NOTICE

The quality of this microfiche is heavily dependent upon the quality of the original thesis submitted for microfilming. Every effort has been made to ensure the highest quality of reproduction possible.

If pages are missing, contact the university which granted the degree.

Some pages may have indistinct print especially if the original pages were typed with a poor typewriter ribbon or if the university sent us an inferior photocopy.

Previously copyrighted materials (journal articles, published tests, etc.) are not filmed.

Reproduction in full or in part of this film is governed by the Canadian Copyright Act, R.S.C. 1970, c. C-30.

**THIS DISSERTATION
HAS BEEN MICROFILMED
EXACTLY AS RECEIVED**

AVIS

La qualité de cette microfiche dépend grandement de la qualité de la thèse soumise au microfilmage. Nous avons tout fait pour assurer une qualité supérieure de reproduction.

S'il manque des pages, veuillez communiquer avec l'université qui a conféré le grade.

La qualité d'impression de certaines pages peut laisser à désirer, surtout si les pages originales ont été dactylographiées à l'aide d'un ruban usé ou si l'université nous a fait parvenir une photocopie de qualité inférieure.

Les documents qui font déjà l'objet d'un droit d'auteur (articles de revue, examens publiés, etc.) ne sont pas microfilmés.

La reproduction, même partielle, de ce microfilm est soumise à la Loi canadienne sur le droit d'auteur, SRC 1970, c. C-30.

**LA THÈSE A ÉTÉ
MICROFILMÉE TELLE QUE
NOUS L'AVONS REÇUE**

THE UNIVERSITY OF ALBERTA

The Effect of Exfiltration Rate on the ~~Transient~~
Moisture Accumulation in Porous Insulation

by

Raymond Chiu Hon Yu

A THESIS

SUBMITTED TO THE FACULTY OF GRADUATE STUDIES AND RESEARCH
IN PARTIAL FULFILMENT OF THE REQUIREMENTS FOR THE DEGREE
OF MASTER OF SCIENCE

DEPARTMENT OF MECHANICAL ENGINEERING

EDMONTON, ALBERTA

FALL, 1986

Permission has been granted to the National Library of Canada to microfilm this thesis and to lend or sell copies of the film.

The author (copyright owner) has reserved other publication rights, and neither the thesis nor extensive extracts from it may be printed or otherwise reproduced without his/her written permission.

L'autorisation a été accordée à la Bibliothèque nationale du Canada de microfilmer cette thèse et de prêter ou de vendre des exemplaires du film.

L'auteur (titulaire du droit d'auteur) se réserve les autres droits de publication; ni la thèse ni de longs extraits de celle-ci ne doivent être imprimés ou autrement reproduits sans son autorisation écrite.

ISBN 0-315-32342-6

THE UNIVERSITY OF ALBERTA

RELEASE FORM

NAME OF AUTHOR: Raymond Chiu Hon Yu

TITLE OF THESIS: The Effect of Exfiltration Rate on the
Transient Moisture Accumulation in
Porous Insulation.

DEGREE: Master of Science

YEAR THIS DEGREE GRANTED: Fall, 1986

Permission is hereby granted to THE UNIVERSITY OF
ALBERTA LIBRARY to reproduce single copies of this thesis
and to lend or sell such copies for private, scholarly or
scientific research purposes only.

The author reserves other publication rights, and
neither the thesis nor extensive extracts from it may be
printed or otherwise reproduced without the author's
written permission.

(SIGNED) Raymond C. Yu

PERMANENT ADDRESS:

1738 Rochon Street
St. Laurent, Montreal
Quebec, CANADA H4L 1W8

DATE: Oct. 14, 1986

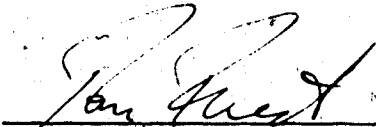
THE UNIVERSITY OF ALBERTA

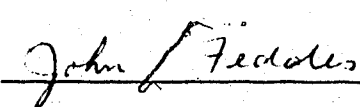
FACULTY OF GRADUATE STUDIES AND RESEARCH

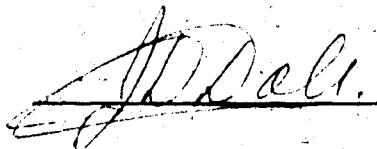
The undersigned certify that they have read, and recommend to the Faculty of Graduate Studies and Research for acceptance, a thesis entitled

The Effect of Exfiltration Rate on the Transient
Moisture Accumulation in Porous Insulation

submitted by Raymond Chiu Hon Yu in partial fulfilment of the requirements for the degree of Master of Science.


(Supervisor)





Date: Aug 11 1986

ABSTRACT

Tests were performed to examine the effects of exfiltration rate on the process of moisture migration and accumulation in a porous media. A 102 mm thick piece of cellulose fibre insulation was tested under an one-dimensional steady-state condition. All tests were conducted under the same temperature and humidity conditions, but the exfiltration rate and the duration of each test were altered. Four tests were carried out with exfiltration rates of 0.4, 0.6, 0.9, and 1.2 air changes per hour (ACH) or 280, 420, 630 and 840 L/hr of air flow, respectively. The length of time for each test was chosen such that the total amount of moist air passing through the cellulose was the same in each test. Eleven calibrated thermal conductivity probes were inserted into various cross sections of the test section to monitor the transient moisture distribution within the cellulose. Seven equally-spaced temperature probes provided the temperature profile across the thickness of the cellulose. Five core samples within the test section were removed at the end of each test. Drying of various cross sections of the core sample provided the final moisture distribution for comparison with the thermal conductivity probe measurements. The overall moisture accumulation within the cellulose for each test was obtained from drying of the

test cellulose in the oven. Both the gravimetric analysis at the end of each test and the probe measurements during the test indicate that significant moisture accumulation only occurs within the cellulose where the temperatures were below freezing. Results in each test show an average of only 20 % moisture by weight (dry basis) in the portion of the cellulose that was above freezing as compared to an average of 150 % moisture in the sub-freezing portion. Measurements of the temperature profiles indicate that higher exfiltration rate raises the internal temperatures within the cellulose. Therefore, the total volume of the cellulose below the freezing temperature decreases as the exfiltration rate increases and results in a decrease in the overall moisture accumulation. Visual inspection, gravimetric analysis and probe measurements all show that the cellulose was divided into a dry and wet portion. Observations made at the end of each test show extensive frost formation within the wet portion of the cellulose. No visible liquid water was found anywhere within the cellulose. Results indicate that sub-freezing temperatures within the cellulose behave as a "sink" for moisture transfer.

ACKNOWLEDGEMENTS

The author wishes to express his sincere appreciation to Dr. T.W. Forest for his encouragement, guidance and invaluable advice in the preparation of this thesis.

Thanks are also extended to the technicians in the Department of Mechanical Engineering for the construction of various experimental apparatus.

Funding for this project was supplied by the Natural Sciences and Engineering Research Council of Canada (NSERC Strategic Grant G1004 and Operating Grant A4201) and R.M. Hardy Engineering Enrichment Fund.

Finally, I would like to thank my family and my wife, Rebecca, for their support and encouragement during my study at the University of Alberta.

TABLE OF CONTENTS

CHAPTER	PAGE
1. INTRODUCTION	1
1.1 Damage to Building Materials Caused by Moisture	2
1.2 The Causes of Moisture Problems	3
1.3 Energy Consideration of Moisture Problems	10
1.4 Methods for Predicting Moisture Accumulation	13
1.5 Present Investigation	17
2. EXPERIMENTAL APPARATUS AND TEST PROCEDURE	19
2.1 Cellulose Insulation	19
2.2 Cold Room	20
2.3 The Box	22
2.4 Tracer Gas Method for Measuring the Exfiltration Rate	27
2.5 Thermal Conductivity Probe	29
2.6 Test Section for the Cellulose Insulation	37
2.7 Data Acquisition System	45
2.8 Test Conditions and Procedure	49
3. DATA REDUCTION	53
3.1 Probe Calibration	53
3.2 Exfiltration Rate and the Temperature Profile	58
3.3 Estimation of Exfiltration Rate from the Total Water Consumption	60
4. RESULTS AND DISCUSSION	62
4.1 Temperature Profiles	62

CHAPTER	PAGE
4.2 Exfiltration Rate	69
4.2.1 MIRAN 1A Gas Analyser	69
4.2.2 Filtration Velocity	71
4.2.3 Overall Water Consumption	71
4.3 Final Moisture Distribution by Gravimetric Analysis	72
4.4 Comparison of Probe Measurements and Gravimetric Analysis	77
4.5 Transient Moisture Profile	82
4.6 The Influence of Exfiltration Rate on the Moisture Distribution and Heat Losses ...	92
4.7 Summary	107
5. CONCLUSIONS AND RECOMMENDATIONS	111
REFERENCES	113
APPENDIX A. MIRAN 1A GAS ANALYSER CALIBRATION PROCEDURE	116
APPENDIX B. SOLUTION OF THE CONTINUITY EQUATION FOR THE TRACER GAS DECAY METHOD	120
APPENDIX C. THEORY OF THE INFINITE LINE HEAT SOURCE .	122
APPENDIX D. SOLUTION FOR THE ENERGY EQUATION	125
APPENDIX E. PSYCHROMETRY OF MOIST AIR	128

LIST OF TABLES

TABLE		PAGE
4.1	Exfiltration rate by three different methods ..	70
4.2	Results of the moisture distribution within the cellulose as obtained from gravimetric analysis (ACH=0.4)	73
4.3	Results of the moisture distribution within the cellulose as obtained from gravimetric analysis (ACH=0.6)	74
4.4	Results of the moisture distribution within the cellulose as obtained from gravimetric analysis (ACH=0.9)	75
4.5	Results of the moisture distribution within the cellulose as obtained from gravimetric analysis (ACH=1.2)	76
4.6	Summary of the overall moisture accumulation and water consumption for each test	100
4.7	Thickness of the frozen portion of the cellulose by locating the 0 °C	100
4.8	Summary of the estimated heat losses due to convection, conduction and latent heat for each test	108

LIST OF FIGURES

FIGURE		PAGE
1.1	The water absorption of various insulation after freeze-thaw exposure following ASTM C666-73 (freeze in air, thaw in water). The Dow Chemical Co., Midland, Mich. 1976	4
1.2	Pressure differences caused by stack effect for a typical structure. Arrows point from higher to lower pressure and indicate direction of air flow	7
2.1	A cross-sectional view of the box	24
2.2	Location of instrumentations and sensors inside the box	26
2.3	Closed-loop schematic flow diagram for the tracer gas decay test method	28
2.4	Typical tracer gas decay test result. The slope of the line represents the exfiltration rate	30
2.5	Details of a typical thermal conductivity probe	33
2.6	Typical temperature rise as measured by a thermal conductivity probe for the dry cellulose insulation	38
2.7	Evaluation of the time correction (tc) for the probe by plotting $dt/d\theta$ versus time	39
2.8	Comparison of thermal conductivity of the cellulose insulation as obtained using the probe and from ASHRAE	40
2.9	Positions of the thermal conductivity probes in the test section	43
2.10	Positions of the temperature probes in the test section	44
2.11	Positions of the sample core holders within the test section	47
2.12	Block diagram of the DASH-8 board	50
2.13	Block diagram of the EXP-16 board	50

FIGURE**PAGE**

3.1	Calibration curves of k_{probe} versus content for a given temperature	56
3.2	Calibration results of k_{probe} versus temperature for a given moisture content	57
4.1	Typical temperature history inside the box and the cold room during a test	63
4.2	Initial and final temperature profiles within the cellulose (ACH=0.4)	64
4.3	Initial and final temperature profiles within the cellulose (ACH=0.6)	65
4.4	Initial and final temperature profiles within the cellulose (ACH=0.9)	66
4.5	Initial and final temperature profiles within the cellulose (ACH=1.2)	67
4.6	Results of the final moisture distribution within the cellulose from gravimetric analysis and probe measurements (ACH=0.4)	78
4.7	Results of the final moisture distribution within the cellulose from gravimetric analysis and probe measurements (ACH=0.6)	79
4.8	Results of the final moisture distribution within the cellulose from gravimetric analysis and probe measurements (ACH=0.9)	80
4.9	Results of the final moisture distribution within the cellulose from gravimetric analysis and probe measurements (ACH=1.2)	81
4.10	The transient moisture profiles as measured by the probes (ACH=0.4)	83
4.11	The transient moisture profiles as measured by the probes (ACH=0.6)	84
4.12	The transient moisture profiles as measured by the probes (ACH=0.9)	85
4.13	The transient moisture profiles as measured by the probes (ACH=1.2)	86
4.14	Results of the overall moisture accumulation by drying and integration of the transient moisture profiles (ACH=0.4)	88

FIGURE

PAGE

4.15 Results of the overall moisture accumulation by drying and integration of the transient moisture profiles (ACH=0.6)	89
4.16 Results of the overall moisture accumulation by drying and integration of the transient moisture profiles (ACH=0.9)	90
4.17 Results of the overall moisture accumulation by drying and integration of the transient moisture profiles (ACH=1.2)	91
4.18 Temperature profiles and the final moisture distribution within the cellulose (ACH=0.4) ...	93
4.19 Temperature profiles and the final moisture distribution within the cellulose (ACH=0.6) ...	94
4.20 Temperature profiles and the final moisture distribution within the cellulose (ACH=0.9) ...	95
4.21 Temperature profiles and the final moisture distribution within the cellulose (ACH=1.2) ...	96
4.22 Overall moisture accumulation versus exfiltration rate for each test	98
4.23 Overall moisture accumulation versus total number of air changes for each test	99
A.1 Closed-loop schematic calibration system for the MIRAN 1A Gas Analyser	117
A.2 Typical calibration curve for the MIRAN 1A Gas Analyser	119

LIST OF PHOTOGRAPHIC PLATES

PLATE	PAGE
2.1 Axial fans inside the cold room	21
2.2 Photo of the inside of the box	23
2.3 Photo of the typical thermal conductivity probes	34
2.4 Photo of the test section	42
2.5 Photo of the thermal conductivity probes in the test section	43
2.6 Photo of the temperature probes in the test section	44
2.7 Photo of a sample core holder	46
2.8 Photo of the sample core holders within the test section	47
2.9 Photo of the completed test section	48
2.10 Photo of the box and the test section	48
4.1 Photo showing the top frozen portion of the cellulose separated easily from the bottom dry portion	104
4.2 Photo of the frost formation within the cellulose under a microscope	105
4.3 Photo of the frost formation within the cellulose under a microscope	105

NOMENCLATURE

Symbol		Units
a	thermal diffusivity.	[m ² /s]
A	cross-sectional area of the test section.	[m ²]
A _{eff}	effective cross-sectional area of the test section.	[m ²]
c	concentration of tracer gas.	[ppm]
C _p	specific heat capacity at constant pressure.	[J/kg·K]
E	exfiltration rate. (Appendix B)	[L/s]
e _s	saturation water vapor pressure.	[Pa]
F	rate of tracer gas injection. (Appendix B)	[L/s]
F	volumetric condensation (or freezing) rate,	[kg/m ³ ·s]
g	gravitational constant (9.8 m ² /s).	[m ² /s]
h	height.	[m]
I	exfiltration rate (ACH).	[hr ⁻¹]
k	thermal conductivity.	[W/m·°C]
k _{probe}	thermal conductivity as measured by the thermal conductivity probe.	[W/m·°C]
ℓ	thickness of the cellulose insulation.	[m]
L	latent heat.	[J/kg]
m	mass.	[kg]
ṁ	mass flow rate.	[kg/s]
P	pressure.	[Pa]
P _{sl}	atmospheric pressure at sea level (101 325 Pa, Appendix E).	[Pa]
q	flow rate of the air.	[m ³ /s]
Q	heat produced per unit length.	[W/m]

Symbol		Units
r	radial distance from the line heat source.	[m]
R _a	gas constant of the air.	[J/kg·K]
RH	relative humidity.	dimensionless fraction
ρ	density.	[kg/m ³]
t	time.	[s]
T	temperature.	[°C or K]
θ	temperature rise.	[°C]
u	filtration velocity.	[m/s]
V	volume.	[m ³]
W	humidity ratio.	dimensionless
x	distance from the warm boundary.	[m]
X, Y, Z	Cartesian coordinates. (Appendix C)	

Subscripts

a	air
b	box
c	conduction
d	dry air
e	exfiltration
i	inside
L	latent heat
m	moisture
o	outside
s	stack
v	water vapour

CHAPTER 1

INTRODUCTION

Living comfort has become an important aspect of life today. When the exterior temperature fluctuates, heat is either supplied or removed from the interior environment to maintain thermal comfort. When the level of humidity changes, moisture is either added to the living space by means of a humidifier or removed by means of a dehumidifier. Many moisture problems in buildings are the direct result of such manipulations of the living environment. Another important aspect of achieving comfortable living space that has implications on the design and thermal performance of the building envelope is ventilation. The supply of fresh air and removal of stale contaminated air is a necessity of any occupied indoor environment. ASHRAE Handbook [1981] recommends a minimum of 2.5 L/s ventilation rate per person in the living space. The constant exchange of inside and outside air can carry a substantial amount of moisture through the building envelope and increase the risk of condensation. The presence of moisture in the living environment is essential to living comfort, but the unwanted condensation and accumulation of moisture in the building envelope can have a detrimental effect on the structure itself. As the ASTM Committee E241, Practices for Increasing Durability

of Building Constructions Against Water-Induced Damages, stated: "Except for structural error, about 90 % of all building construction problems are associated with water in some way.". Therefore, efforts must be made to minimize the damages to building envelope caused by moisture.

1.1 Damage to Building Materials Caused by Moisture

Most building materials except metals and glass have a porous structure that allows moisture to pass through. Moisture can come in contact with building materials in the form of liquid water from condensation, rain penetration or water leakage, or as water vapour in the air, or even as ice and snow in the cold climate areas. The climatic conditions, living habits of the people and construction techniques may vary considerably in different parts of the world, but the physical, thermal and chemical fundamentals of the moisture problems are similar in nature. The presence of moisture in building materials, along with the changes of moisture content and migration of the moisture can have a significant effect on the properties of the materials and their abilities to fulfill their designed functions. In the mildest form, moisture problem appears only as harmless condensation on windows and walls. But in severe cases, moisture can cause structural failure in the building. In between the extremes, excess moisture can result in mold and mildew growth, paint peeling, ceiling stains, etc. ASHRAE

Handbook [1981] points to moisture as the principal or contributing factor in most building material degradation due to physical changes such as spalling of masonry by repeated freeze-thaw cycles, chemical reaction such as rusting of metals, and biological process such as decaying of wood. Dworjadkin and Malinowski [1965] indicated that the volume of light weight concrete swelled and shrank under repeated wetting and drying that resulted in cracking of the concrete. Niskanen [1965] showed that the strength properties of birch plywood decreased as the moisture content in the wood increased. Sneek [1965] gave evidence of typical corrosion failure within the building envelope originating from the presence of moisture on the metal surface. Dechow and Epstein [1978] tested the physical integrity of various insulations under the combination of water absorption and freeze-thaw conditions as outlined in the ASTM Method C666 [1973]. Their results showed the rapid deterioration of some insulation under repeated freeze-thaw cycles (Figure 1.1). The list goes on and on. Clearly, the moisture problems in building materials will take place in many different ways under various environmental conditions, but all result in degradation in performance or complete failure.

1.2 The Causes of Moisture Problems

Moisture problems in buildings are related to the way in which people live, heat, ventilate and insulate

Figure 1.1 has been removed because of the unavailability of copyright permission.

Figure 1.1 The water absorption of various insulation after freeze-thaw exposure following ASTM C666-73 (freeze in air, thaw in water). The Dow Chemical Co., Midland, Mich., 1976.

their buildings. Sources of moisture come from activities such as cooking, bathing, laundering and respiration by the occupants within the living space. ASHRAE Handbook [1981] estimated that a family of four can generate 7 to 12 kg of moisture per day into the living space. Sometimes, additional moisture is purposely added to the living space to improve personal comfort. Nature also adds moisture to the air from rain and snow, or from evaporation of water vapour from the soil.

Moisture-related problems in buildings are most pronounced during the winter months in Canada because of the cold weather. The warm air inside the building during the winter has a much greater water vapour content than the cold air outside. For example, air at 25 °C and 40 % RH contains approximately 0.0078 kg of water per kg of dry air while cold air at -30 °C and 100 % RH contains only 0.0003 kg of water per kg of dry air. Therefore, the vapour pressure inside the building is higher than the outside and this vapour pressure difference causes the water vapour inside the building to move outwards through the building envelope. Most building materials have little resistance to the flow of water vapour, therefore, more resistant material such as a vapour barrier is used to reduce the rate of water vapour movement into the building envelope. However, there are other ways in which moisture can get into the building envelope, namely by infiltration and exfiltration. The term infiltration is used to refer

to air flow from the exterior to the interior; whereas, exfiltration denotes air flow from interior to exterior. Infiltration and exfiltration occur through openings in the building envelope such as cracks and gaps around doors and windows, chimneys, vents, electrical outlets, etc. The cause for infiltration and exfiltration is due to the pressure difference exists across the building envelope. The pressure difference across the building envelope that induces air infiltration and exfiltration can arise naturally by the "stack" effect due to temperature differences and wind action on the building, or artificially by means of mechanical pressurization of the inside of the building. Because warm air is lighter than the cold air, the differences in air density can generate a pressure difference across the building envelope. Figure 1.2 shows the typical pressure distribution over a heated building during the winter under a pure "stack" effect. The level where the interior and exterior pressures are equal is called the Neutral Pressure Level (NPL). The location of the NPL depends on the distribution of openings in the building envelope. If one opening dominates, then the NPL will be near or at the center of the opening. Interior pressure above the NPL is greater than the exterior and the air leaks from inside to outside (exfiltration). Below the NPL, the interior pressure is lower than exterior and the air leaks from outside to inside (infiltration). The "stack" effect pressure at a

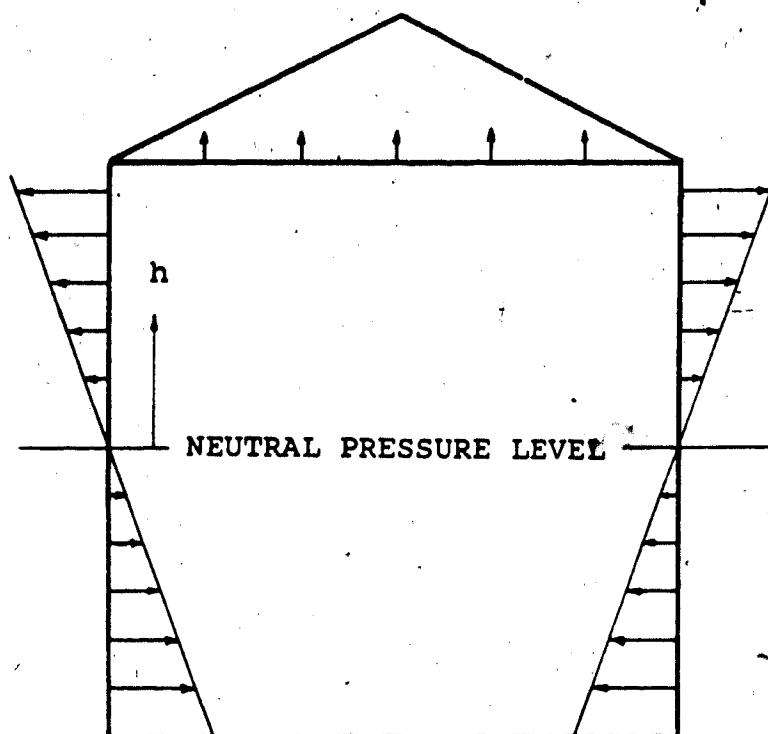


Figure 1.2 Pressure differences caused by stack effect for a typical structure. Arrows point from higher to lower pressure and indicate direction of air flow.

height above (or below) the NPL is given by ASHRAE Handbook [1981] as

$$P_s = (\rho_o - \rho_i) g h - \frac{\rho_i g h (T_i - T_o)}{T_o} \quad (1.1)$$

where P_s is the pressure difference due to the "stack" effect in Pa, ρ_o and ρ_i are the inside and outside air density in kg/m^3 , g is the gravitational constant (9.8 m/s^2), h is the distance to the NPL in m (positive if above the NPL and negative if below), T_i and T_o are the inside and outside temperature in K. Generally speaking, as the height of the building increases, the distance of the NPL to the top of the building also increases and resulting in a larger "stack" effect. Wind around and over a building can create a significant pressure and suction across the building envelope. Positive pressure is generated on the windward side and results in air infiltration; whereas, negative pressure on the leeward side produces air exfiltration. The magnitude of the pressure difference caused by the wind depends entirely on the wind speed and direction. But due to the dynamic nature of the wind and the turbulence caused by the surrounding structures and trees, the effect of wind on infiltration and exfiltration in a building is complex and difficult to account for. Wise [1978] showed that for exposed dwellings, the wind effect dominates the air

leakage; whereas, for sheltered dwellings "stack" effect has a greater influence than the wind. Sometimes a building is pressurized intentionally to minimize air infiltration from the outside by means of a mechanical ventilation system. The purpose is to reduce cold drafts, entrance of noise (traffic, etc) and air pollutants into the living space. Mechanical pressurization of the building provides continuous sustained pressure differences across the building envelope and exfiltration of warm moist air. Under the action of infiltration and exfiltration, a substantial amount of moisture can be carried by the air and passed through the building envelope. During the winter, as the warm moist air exfiltrates through the building envelope, it encounters progressively colder media and moisture in the air will condense onto those surfaces that are below the dew point of the moist air or turn into frost or ice if the surface temperature is below freezing. Therefore, moisture can accumulate within the building envelope and degrade the building materials.

In general, moisture moves from the inside living space through the building envelope to the outside by both diffusion and exfiltration during the winter months. However, the flow of moisture due to exfiltration of warm moist air is found to be more significant than water vapour diffusion. Wilson and Garden [1965] estimated that the amount of moisture accumulated in the masonry due to

exfiltration of warm moist air could be two or more orders of magnitude higher than that due to vapour diffusion. Ford [1982] calculated that for a house with exfiltration rate of 1 air change per hour (ACH) and a volume of 283 m^3 , 130 m^2 wall area, wall permeance of 58 PERM* ($1 \text{ PERM} = 1 \times 10^{-9} \text{ g/s} \cdot \text{m}^2 \cdot \text{Pa}$) and an interior temperature of 20°C , the amount of moisture transfer due to diffusion was about 1 % of that due to exfiltration. Clearly, the process of moisture migration and accumulation in the building envelope is dominated by exfiltration as compared to diffusion.

1.3 Energy Consideration of Moisture Problems

With growing emphasis on energy conservation, the use of thermal insulation in building has increased drastically over the past decade. Both the construction industry and conservationists advocate the use of thicker or higher thermal resistance insulation in the building envelope to reduce heat transmission. However, increased thermal resistance of the building envelope and reduced heat loss will make the outside surface temperature colder, thus raising the temperature difference between the inside and outside surfaces. This increases the potential for condensation to occur within the building

* 1 PERM is defined as $1 \times 10^{-9} \text{ g}$ of moisture absorbed per second per m^2 of the material subjected to 1 Pa vapour pressure difference.

envelope that may not have happened if poorly insulated. Therefore, use of higher thermal resistance or thicker insulation in reducing heat flow also requires action to provide adequate resistance to moisture migration.

The primary function of thermal insulation is to act as a barrier between two environments at different temperatures either to reduce the heat loss from the warmer side towards the cooler side (winter heating), or to reduce the heat entry into the cooler side from the warmer side (summer cooling). Thermal insulation owes much of its insulating value due to the presence of small pockets or pores containing air (or gas) within its structure. These small pores can be formed by fibres, flakes, or by the cells in the material itself. The pores are sufficiently small and provide considerable resistance to the flow of air so that little heat will be transferred by convection from one side of the pores to the others. However, if air leakage is present, sensible heat can be carried by the warm inside air through the insulation and dissipated to the outside. Yarbrough and Toor [1983] showed that the effective thermal resistance of the fibrous insulation decreases as air movement through the insulation increases. When moisture penetrates the insulation, all or part of the air within the pores will be replaced by moisture (vapour, liquid and solid). The thermal conductivity of still air at 25 °C is about 0.025 W/m.°C as compared to 0.6 W/m.°C for water at the

same temperature. For ice, the thermal conductivity at 0°C is approximately $2.2 \text{ W/m}\cdot^{\circ}\text{C}$. Therefore, any presence of moisture within the insulation, liquid or solid form, will increase the conduction of heat. Joy [1957] considered four simple arrangements of moisture within the insulation: series, parallel, bead and foam. In the series arrangement, the moisture is located in layers perpendicular to the direction of the heat flow. In the parallel arrangement, the moisture is assumed to be a series of continuous shafts parallel to the direction of the heat flow. In the bead arrangement, the moisture in a form of small beads is uniformly spaced throughout the insulation. In the foam arrangement, the moisture is assumed to surround the insulation particles or fibres in a form of film joining in a honeycomb or foam structure. With the above simplified models of moisture arrangement, Joy [1957] showed that the effective thermal conductivity of an insulation with 10 % moisture by volume in the parallel arrangement is twice that of the series arrangement with the same amount of moisture. The results indicate that the presence of moisture, as well as the location and arrangement of the moisture within the insulation can increase the effective thermal conductivity of the insulation and the amount of heat transmission. Using heat flow meters, Shuman [1982] has shown that three times as much heat flowed through the roof with wet insulation as compared to the roof with dry insulation.

Beside having a higher conductive value, the movement of the moisture (for vapour and liquid phases) within the insulation also gives rise to an additional convective mode of heat transfer through the insulation. Moisture, whether in vapour or liquid state, carries a substantial amount of energy as latent heat and releases that energy when it condenses or freezes. With the possibility of evaporation, vapour flow and condensation within the pores of the insulation, a large amounts of sensible and latent heat can be transported from the warm side through the insulation to the cold side. Therefore, in addition to the physical degradation to the porous insulation, the presence of moisture can also drastically increase the rate of heat flow.

1.4 Methods for Predicting Moisture Accumulation

Properties of building materials are usually evaluated at their dry states. This information may be useful in comparing different materials, but it does not represent the changes in some properties when moisture is present in the materials. More important, when materials are combined as in the building envelope, one material may fail while others remain intact under the same moisture condition. Such a situation can result in complete failure of the whole building envelope. Lacking data on how moisture affects the properties of building materials always undermines the designers' abilities to provide a

proper design. But evaluation of thermal performance and durability of building materials or combination of materials with the presence of moisture is a very difficult task. In field conditions, factors that can affect the process of moisture migration and accumulation such as temperature, humidity, solar radiation, precipitation, wind speed and direction, etc. are sensitive to the activities inside the building and outside weather. Moisture continuously migrates back and forth within the material according to the changes in the environments. In addition, the amount of moisture accumulation in the building envelope depends on the air leakage rate, humidity ratios of the inside and outside air, temperature gradient and the leakage characteristics of the building.

Moisture migration in a building is a complicated multi-dimensional problem. Accumulation of moisture may be concentrated in the vicinity of the cracks through which air leakage occurs. Distribution of moisture in the building envelope is rarely uniform. Formation of icicles on the walls and around windows in winter are typical examples of the high concentration of moisture in a localized area. Because such multi-dimensional phenomena are extremely difficult to analyse, the process of moisture migration is often simplified to an one-dimensional problem. Because of the complexity of the simultaneous mass and heat transfer associated with

moisture migration and accumulation, only a limited amount of information about the subject has been obtained. Early studies on moisture migration and accumulation in porous materials were concentrated on moisture movement in soil. Gurr et al. [1952] showed that soil column under an imposed temperature gradient causes water vapour to flow from the warm temperature region and condense in the cold temperature region. As the moisture content in the cold region increases, liquid water will flow from the cold region back to the warm region. Klute [1952] used the Darcy's law and continuity equation to derive a numerical method describing the flow of water in unsaturated semi-infinite porous materials. However, the physical dimensions, as well as the boundary conditions experienced by the insulation are different from that of the soil. With the increased use of thermal insulation in building, the subject of moisture migration in porous insulation has received considerable attention over the past years. Various methods have been proposed to predict or estimate the location and/or the amount of moisture accumulation in the building envelope and insulation under a given set of environmental conditions. While some methods are too simplified or inadequate, others are too complicated or need experimental verification. Handegord [1985] used a simplified expression for flow through a sharp-edged orifice to estimate the rate of moisture transfer into the wall due to air leakage. Such an approach may be too

simplified. Tenwolde [1985] proposed a computer model based on a steady-state one-dimensional water vapour movement by diffusion and convection in a multilayered wall to determine the location of condensation and the amount accumulated. The method requires knowing the filtration velocity of the air and predicts that condensation is far more likely to occur on one or more of the interfaces between two different building materials within the multilayered wall. Ogniewicz and Tien [1981] used a set of equations (conservation of energy, mass balance of vapour and liquid) to analyze the problem of condensation in porous insulation under an one-dimensional steady-state heat transfer. The analysis included both the convective and diffusive transport mechanisms, simultaneous heat and mass transfers, material properties and the governing environmental conditions. However, the method is complex and difficult to use. Huang et al. [1979] indicated that the temperature in the porous system plays an important role in mass transfer. The temperature and the concentration gradients are the driving forces for moisture migration and the structure of the porous system in the material dominates the mechanism of moisture movement. Freezing temperatures within the material introduce other considerations such as frost action. Gupta and Churchill [1978] indicated that a sub-freezing temperature within the material can behave as a "sink" for mass transfer that resulted in two distinct wet and dry

zones within the material. The need for a better understanding of the mechanism of moisture migration and accumulation and the interactions with various factors such as temperature and pressure gradients, relative humidities, air leakage, etc. is essential in controlling the moisture problems in building.

1.5 Present Investigation

The tests in the present investigation into moisture migration and accumulation in porous insulation were conducted under an approximated one-dimensional condition. Because exfiltration has been found to be a dominant factor in moisture accumulation within the building envelope, therefore, the exfiltration rate was the only parameter that was varied in each test while other parameters such as temperatures and humidities were held the same. The pressure difference that induces exfiltration was generated by "stack" effect (temperature difference) and mechanical pressurization. The purpose of mechanical pressurization was to simulate the action of wind superimposed on the "stack" effect. Since it is difficult to examine various building materials in this investigation, only cellulose fibre thermal insulation (commonly known as cellulose) was used. The cellulose was tested in a horizontal position similar to the situation in the roof or attic because the imposed pressure difference and effect of gravity were uniform across the

test sample. According to Shuman [1982]: "roof systems, from the exposure-performance standpoint, are the most complex parts of the building system, the effect of moisture on the heat flow through roof system should receive first attention.". By varying the exfiltration rate in each test, the changes in temperature profiles and moisture distributions within the cellulose can be related to the exfiltration rate. Attempts were made to measure the transient moisture profile within the insulation and study the process of moisture build-up within the insulation with respect to time. Very few results on the transient effect of moisture migration and accumulation within porous insulation had been published. Understanding how moisture distributes and accumulates with time within the porous material under the given environmental conditions is important in analysing the process of moisture migration. The aim of the present investigation was to examine the influence of exfiltration rate on the mechanism of moisture migration and accumulation within porous insulation .

CHAPTER 2

EXPERIMENTAL APPARATUS AND TEST PROCEDURE

A slab of 102 mm thick cellulose insulation was tested under similar conditions to those in the attic during the winter months where the insulation is exposed to two different environments. The warm side of the cellulose was exposed to the inside of a box which was maintained at 25 °C and 40 % relative humidity. The cold side was exposed to a temperature of -30 °C inside the cold room. Because the saturated humidity ratio of the air at -30 °C is very small, the relative humidity of the cold air inside the cold room was assumed to be at or near 100 %. The warm and cold environments were held as constant as possible during the test to simulate one-dimensional steady-state heat transfer. The cellulose was under constant imposed pressure difference generated by a "stack" effect and mechanical pressurization. Warm moist air exfiltrated through the cellulose and deposited moisture along its flow path.

2.1 Cellulose Insulation

Cellulose insulation is manufactured from waste newsprint. Special milling equipment is used to process the raw newsprint into a short-fibre cellulosic material and treated with chemicals to control flamability, growth

of fungi, corrosivity, odor emission, etc. The soft, fluffy cellulose contains millions of minute air spaces to resist heat flow. Cellulose is commonly available in two types: loose-fill for blowing and pouring, and spray-on. Loose-fill cellulose passing the Canadian General Standards Board (CGSB) standard 51-GP-60M was used in this study. The thermal conductivity of the cellulose in accordance with ASTM Standard Test Method C-177 [1976] is $0.04 \text{ W/m}\cdot^\circ\text{C}$ at 24°C . Moisture absorption for the cellulose is less than 20 % by weight when subjected to 90 % RH and 50°C until either constant mass is obtained or 168 hours have passed. Taking the density of the newsprint to be approximately 450 kg/m^3 , the porosity of the cellulose insulation at 40 kg/m^3 is about 0.91.

2.2 Cold Room

The cold room is approximately 2.8 by 3.4 m and 2.1 m in height. It is equipped with a two-stage compressor and capable of reaching -50°C inside the room. The air within the room is circulated by four axial fans (Plate 2.1). At a set point temperature of -30°C , the compressor comes on approximately every 10 minutes. The temperature inside the cold room varies slightly (-30 to -28°C) between compressor cycles. A timer activates a defrost cycle every six hours to avoid excess ice build-up in the refrigeration coils. Temperature inside the cold room rises to about -23°C and falls gradually back to



Plate 2.1 Axial fans inside the cold room.

-30 °C during the 15 minutes period of the defrost cycle.

2.3 The Box

The principal component of the apparatus consisted of a plywood box of 762 by 762 mm and 1.5 m in height. The inside of the box was insulated with 25 mm STYROFOAM* S-M insulation boards to reduce heat loss and coated with 6 mil polyethylene vapour barrier to prevent air leakage and diffusion of water vapour through the sides of the box (Plate 2.2). All edges and corners inside and outside of the box were sealed with silicone sealant to ensure air tightness. A cross-sectional view of the box is shown in Figure 2.1.

The inside temperature of the box was set at 25 °C and regulated by a 1500 watt heater-fan unit controlled by a proportional temperature controller. The temperature thermistor-sensing probe for the controller was located at about the mid-height inside the box. A house humidifier was attached to the side of the box with the humidistat set at 40 % RH to provide the desired humidity level for the inside of the box. The humidifier was encased by 76 mm thick STYROFOAM S-M[®] board insulation. A 102 mm diameter fan was installed at the air inlet to the humidifier to circulate the inside air through the humidifier and provide air movement within the box. Calibrated

* Trademark of the Dow Chemical Company.

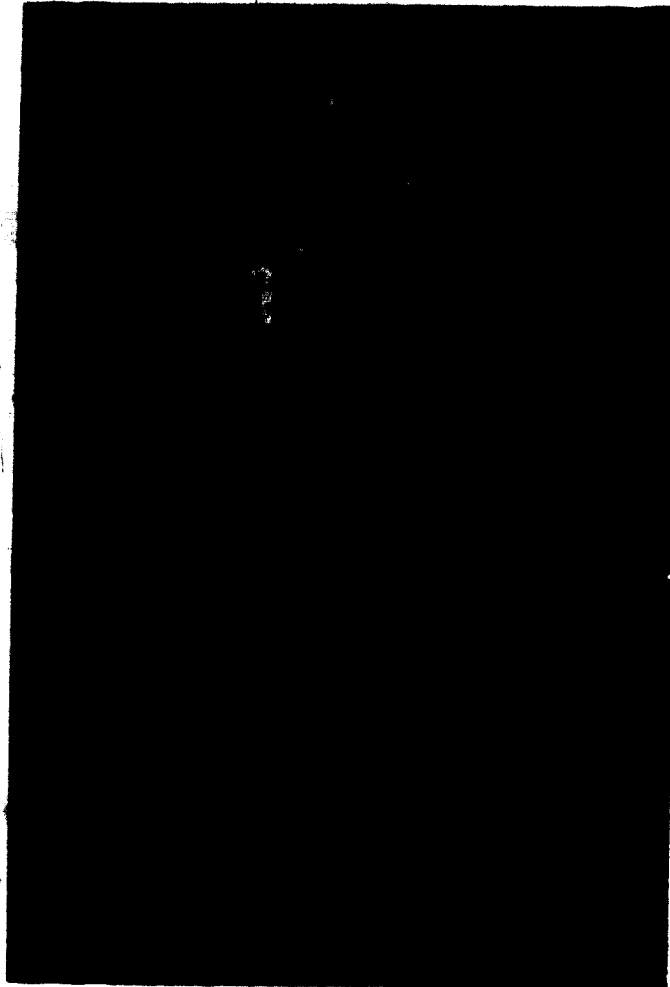


Plate 2.2 Photo of the inside of the box.

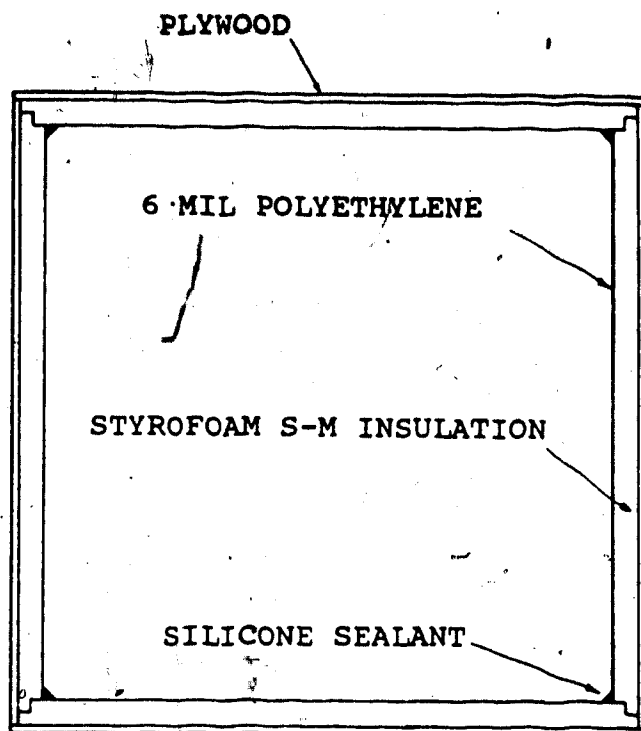


Figure 2.1 A cross-sectional view of the box.

copper-constantan thermocouples were placed at various locations inside the box and the cold room to monitor the temperatures. Wet and dry bulb thermocouples were also installed inside the box to measure the inside relative humidity. A small opening (10 mm in diameter) was made near the bottom of the box for cold air to enter. When the small opening was exposed to the cold room during the test, a pure "stack" effect was generated within the box. By connecting a compressed air source to the small opening, a controlled flow of cold air was forced into the box and an additional pressure difference was induced to simulate the action of wind superimposed onto the "stack" effect. Under the action of the "stack" effect and induced pressure difference, warm moist air flowed through the cellulose insulation at the top of the box and into the cold room. Details are shown in Figure 2.2.

Care was taken to ensure the box was air tight so that cold air only came into the box through the bottom opening and warm moist air left only through the cellulose insulation at the top of the box, rather than through cracks and holes in the sides of the box. In checking for the air tightness, the top of the box was covered with a piece of 13 mm thick plywood and all the edges sealed. The small opening at the bottom was plugged. A small amount of natural gas was injected into the box and positive pressure was applied to the box by means of compressed air. A gas sniffer was used to detect any leaks in the

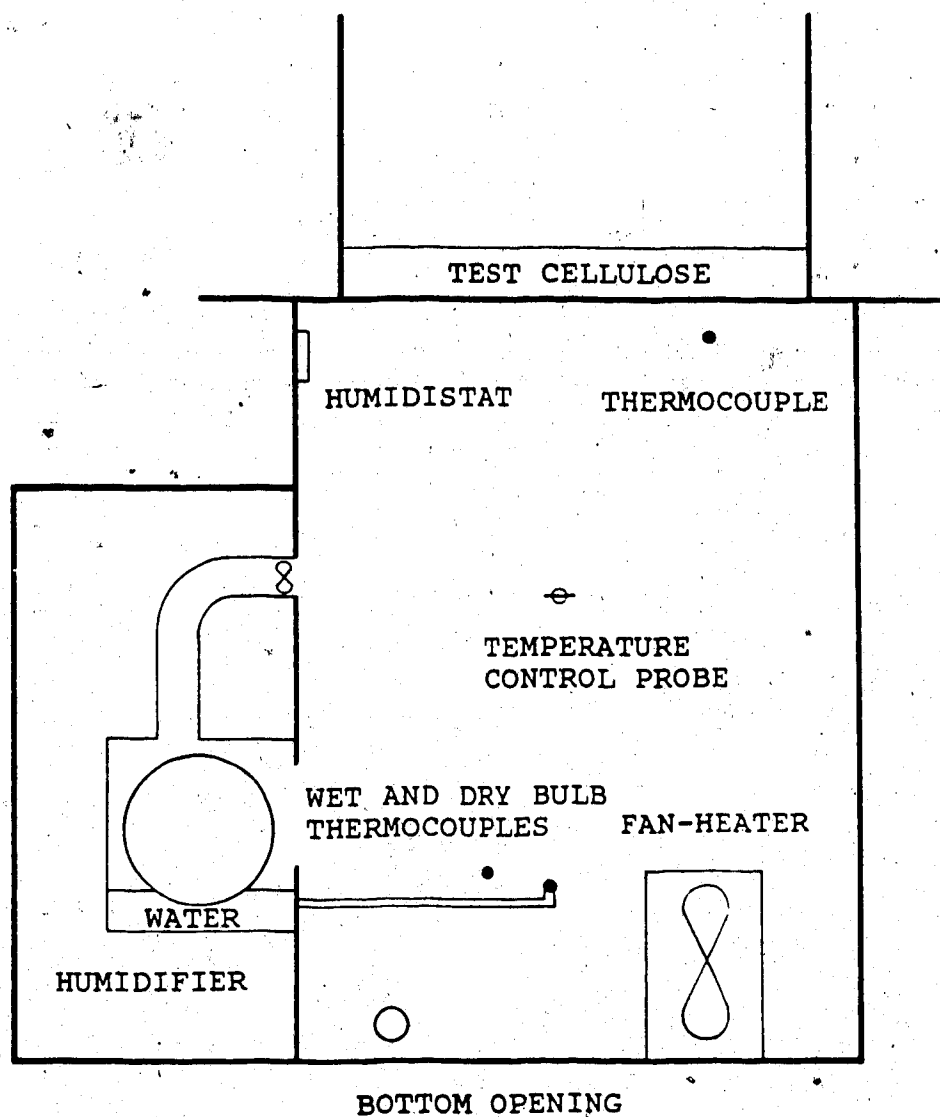


Figure 2.2 Location of instrumentations and sensors inside the box.

set-up. After all the leaks were eliminated, the test section for the cellulose was placed on top of the box. The edges between the test section and the box were also sealed with silicone sealant to avoid air leakage. A baffle was placed in front of the cold room circulation fans to prevent cold air from blowing directly onto the box. Therefore, the air movement inside the cold room had very little effect on the exfiltration rate and moisture migration in the cellulose during the test.

2.4 Tracer Gas Method For Measuring the Exfiltration Rate

The exfiltration rate during each test was measured using the tracer gas decay technique. A schematic of the closed loop flow diagram for the tracer gas method is illustrated in Figure 2.3. A MIRAN 1A Infrared Absorption Gas Analyzer was used along with sulphur hexafluoride (SF_6) as tracer gas for measuring the exfiltration rate of the box. More detailed information regarding the MIRAN Gas Analyzer calibration procedures and calibration curve are included in Appendix A.

To measure the exfiltration rate during the test, a small amount of SF_6 was injected into the box to give a gas concentration of about 5 parts per million (ppm). Both the heater and circulating fans were on during the tracer gas decay test to provide mixing of the air and SF_6 inside the box. Return air circulated through a desiccant flask (for absorbing any moisture in the return air), a filter

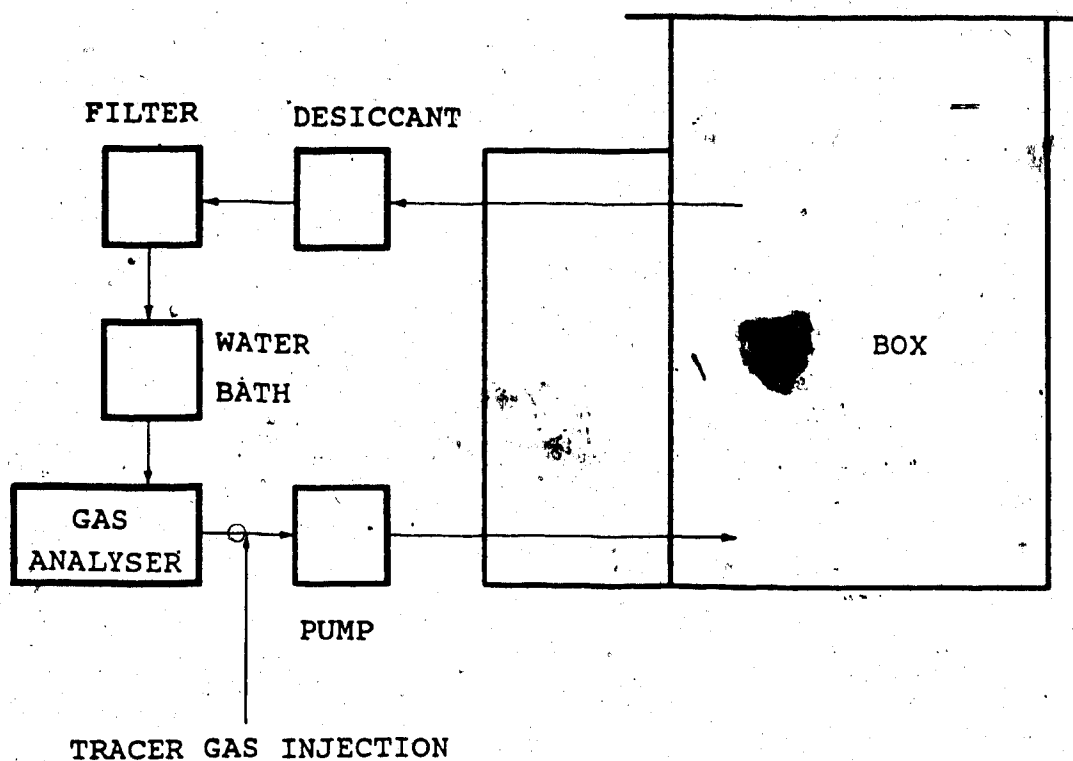


Figure 2.3 Closed-loop schematic flow diagram for the tracer gas decay test method.

(for removing any foreign particles in the return air) and a copper coil water bath (for bringing the return air back to room temperature) before entering the gas analyzer. By connecting the output of the gas analyzer to a strip-chart recorder, the concentration of SF_6 inside the box with respect to time was obtained. From the solution of the continuity equation (Appendix B), the concentration of the tracer gas as a function of time is [ASTM E741, 1983]

$$c(t) = c_0 \exp(-It) \quad (2.1)$$

where $c(t)$ is the concentration of tracer gas at any time, c_0 is the concentration of tracer gas at time = 0, I is the exfiltration (infiltration) rate in air changes per hour (ACH), and t is the time. A plot of natural logarithm of the tracer gas concentration versus time will yield a straight line if the the tracer gas concentration is uniform in the test volume and the exfiltration rate is constant during the test period (Figure 2.4). From the slope of the straight line, the air exfiltration rate for that time interval can be calculated.

2.5 Thermal Conductivity Probe

Moisture migration and accumulation in porous insulation is a continuous process. Since the movement of moisture by diffusion, convection, evaporation and condensation (freezing), etc. inside the porous insulation

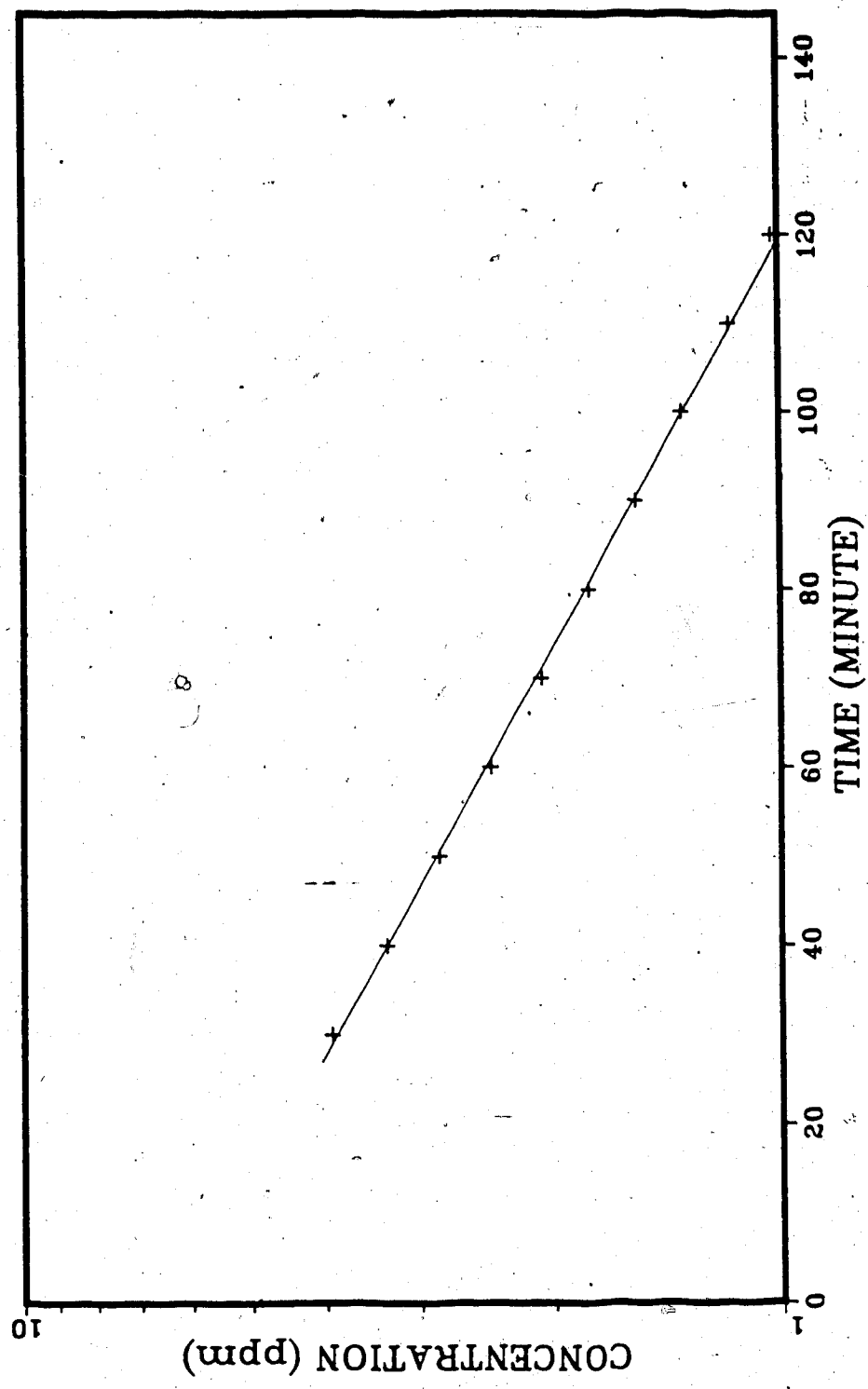


Figure 2.4 Typical tracer gas decay test result. The slope of the line represents the exfiltration rate.

is changing with time, it is more logical and meaningful to determine the moisture content from a transient test method. For steady-state testing of wet material, the moisture will migrate and accumulate under the given environmental conditions. Therefore the final results will not apply to the starting moisture conditions nor the intermediate states during which the moisture redistributes itself. The objective of this experiment requires measurement of moisture content and distribution within the insulation during the course of the experiment. The most accurate and widely used method of determining the moisture content and distribution in materials is by gravimetric analysis; that is, cutting samples at various cross sections and drying the samples in an oven to a constant weight. The change in weight before and after drying represents the moisture content. However, such a method requires cutting up the test insulation frequently and disturbing the test specimen. Thus, the gravimetric analysis is not a practical method for transient, in-situ measurements, but was used to determine the final moisture distribution within the cellulose. Given the objectives and constraints for the experiment, a "thermal conductivity probe" was chosen to measure the moisture content and distribution within the insulation.

For typical building insulation, the thermal conductivity varies from 0.015 to 0.05 W/m·°C at room temperature while water has a thermal conductivity of

about 0.6 W/m·°C. Therefore the higher the amount of moisture within the insulation, the higher the thermal conductivity. The "thermal conductivity probe" consists of a stainless steel tube (2.8 mm O.D. and 2.2 mm I.D.), a line heat source (30 gauge constantan wire) and a thermocouple (30 gauge copper-constantan) as shown in Figure 2.5 and Plate 2.3. The value of the thermal conductivity for a particular material as measured by the probe can be obtained by inserting the probe into the material, connecting the line heat source to a power supply (Hewlett Packard Model 6214A) and measuring the rise in temperature versus time.

The transient line heat source theory on which the probe method is based is given in detail by Carslaw and Jaeger [1959]. The derivations are included in Appendix C. The temperature rise at a point in an "infinite mass of material" heated by a "perfect infinite line heat source" is

$$\theta = \frac{Q}{4 \pi k} \left\{ D - \ln\left(\frac{r^2}{4 a t}\right) + \left(\frac{r^2}{4 a t}\right) - \frac{1}{4} \left(\frac{r^2}{4 a t}\right)^2 + \cdots + O\left(\frac{r^2}{4 a t}\right)^3 \right\} \quad (2.2)$$

where θ is the temperature rise in °C, Q is the amount of heat produced per unit time per unit length in W/m, k is the thermal conductivity of the material in W/m·°C, D is a constant (0.5772), r is the radial distance away from the

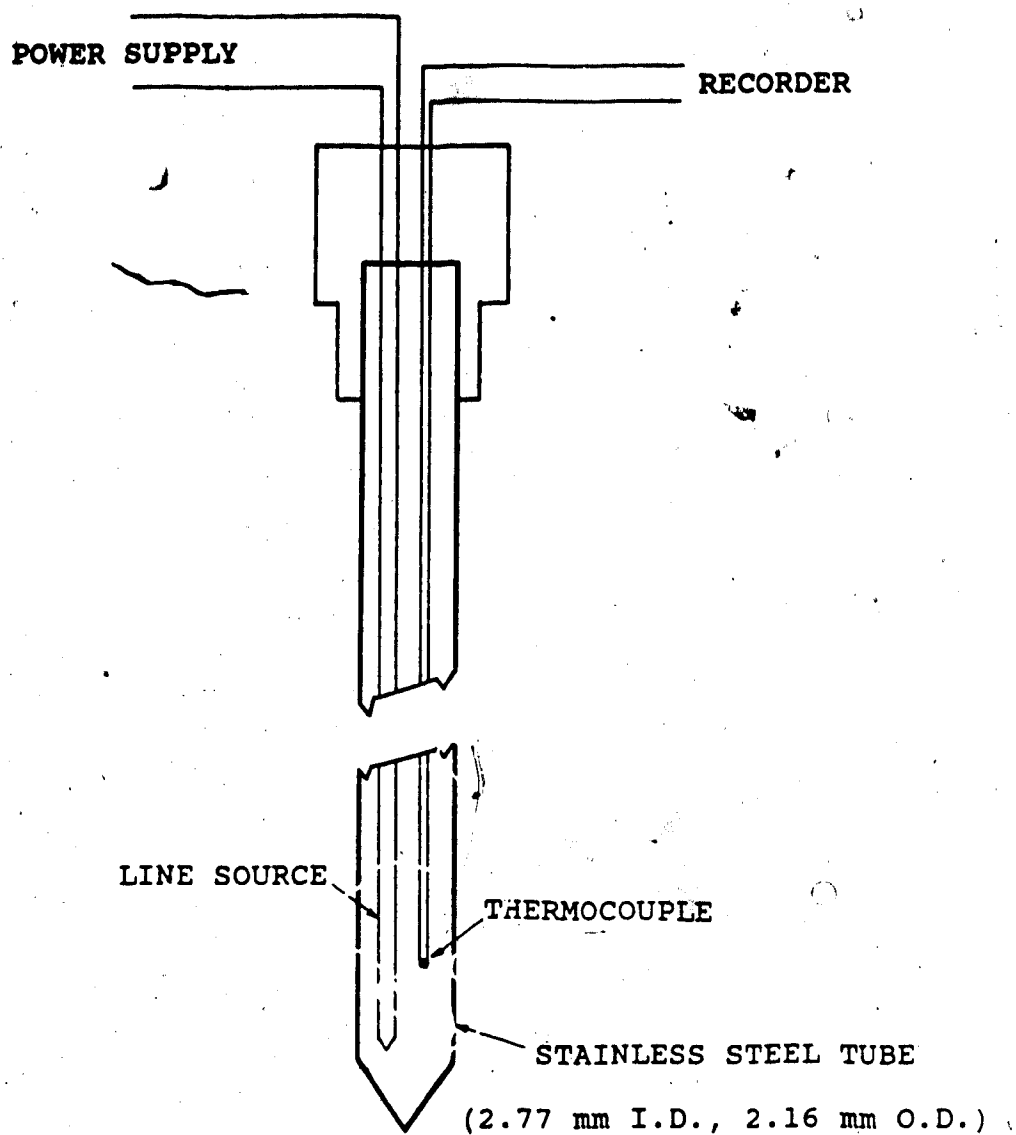


Figure 2.5 Details of a typical thermal conductivity probe.

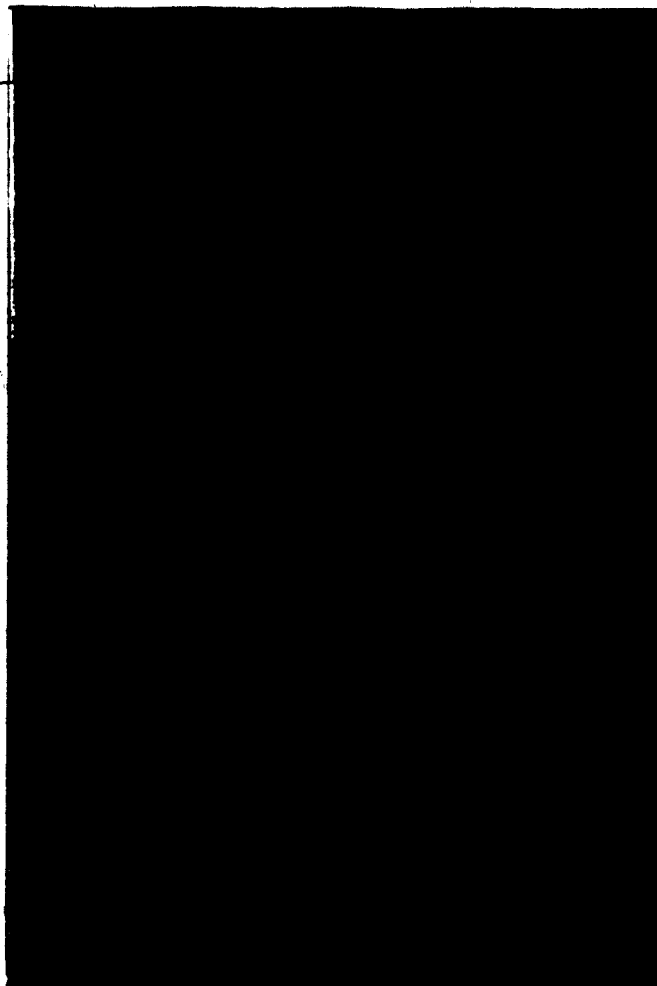


Plate 2.3 Photo of the typical thermal conductivity probes.

line heat source in m, a is the thermal diffusivity of the material in m^2/s , and t is the time in s. Assuming r is equal to 1 mm (reasonable assumption for a 2.2 mm I.D. tube) and taking $7 \times 10^{-7} \text{ m}^2/\text{s}$ as the value of thermal diffusivity for the cellulose, the term $r^2/4at$, corresponding to a given time is

$$t = 60 \text{ s} \quad r^2/4at = 0.006$$

$$t = 120 \text{ s} \quad r^2/4at = 0.003$$

Therefore, as time increases the term $r^2/4at$ decreases. If the temperature rise in the first couple of minutes is ignored, then the term $r^2/4at$ is small and Equation 2.2 can be simplified as follows

$$\theta = \frac{Q}{4 \pi k} \left\{ D - \ln\left(\frac{r^2}{4 a t}\right) \right\} \quad (2.3)$$

Taking the difference in temperature at two different times t_1 and t_2 yields

$$\begin{aligned} \theta_2 - \theta_1 &= \frac{Q}{4 \pi k} \left\{ \left[D - \ln\left(\frac{r^2}{4 a t_2}\right) \right] - \left[D - \ln\left(\frac{r^2}{4 a t_1}\right) \right] \right\} \\ &= \frac{Q}{4 \pi k} \ln\left(\frac{t_2}{t_1}\right) \quad (2.4) \end{aligned}$$

Solving for k yields

$$k = \frac{Q}{4 \pi} \frac{\ln(t_2/t_1)}{\theta_2 - \theta_1} \quad (2.5)$$

Note that for $(r^2/4at) \ll 1$, the thermal conductivity is independent of other thermophysical properties such as thermal diffusivity, α . A plot of temperature rise versus $\ln(\text{time})$ yields a straight line. Knowing the slope of the line and the power input (Q), one can obtain the thermal conductivity of the material.

When the line heat source theory is used in the probe method, the line heat source is neither ideal nor of infinite length and the material is finite in size. In addition, the presence of the metal tube of the probe and the deletion of the higher order terms of $r^2/4at$ will have an effect on the measurement. Van der Held and Van Drunen [1949] have studied the above departures from the ideal conditions in detail and recommended a time correction t_c be added to Equation 2.4 for the probe method to yield accurate results, i.e.

$$\theta_2 - \theta_1 = \frac{Q}{4 \pi k} \ln\left(\frac{t_2 - t_c}{t_1 - t_c}\right) \quad (2.6)$$

$$\text{or } k = \frac{Q}{4 \pi} \left\{ \frac{\ln[(t_2 - t_c)/(t_1 - t_c)]}{\theta_2 - \theta_1} \right\} \quad (2.7)$$

If Equation 2.6 is written in the form of a differential equation, then the value of t_c can be obtained by taking the derivative of time with respect to the temperature

rise ($dt/d\theta$) to yield

$$\frac{dt}{d\theta} = \frac{4 \pi k}{Q} (t - t_c) \quad (2.8)$$

The value of t_c is simply the intercept of the time axis by plotting $dt/d\theta$ versus t . For example, Figure 2.6 shows the temperature rise within the cellulose insulation as measured by the probe. Figure 2.7 illustrates how the time correction (t_c) can be obtained by plotting $dt/d\theta$ versus time. Figure 2.8 shows the results of the thermal conductivity for the dry cellulose using the probe at various temperatures as compared to the values given by ASHRAE Handbook [1981].

The probe was calibrated using samples of cellulose with different uniform moisture contents at several temperature settings. A series of calibration curves for the cellulose involving the measured thermal conductivity, temperature and moisture content were obtained. By measuring the thermal conductivity using the probe and knowing the temperature of the cellulose, the moisture content can be obtained. Details of the probe calibration are presented in Chapter 3.

2.6 Test Section For The Cellulose Insulation

A 610 x 610 mm square hole was cut in the middle of a 13 mm thick plywood plate. Strips of 76 x 102 mm STYROFOAM S-M insulation formed a 610 x 610 mm bracket and

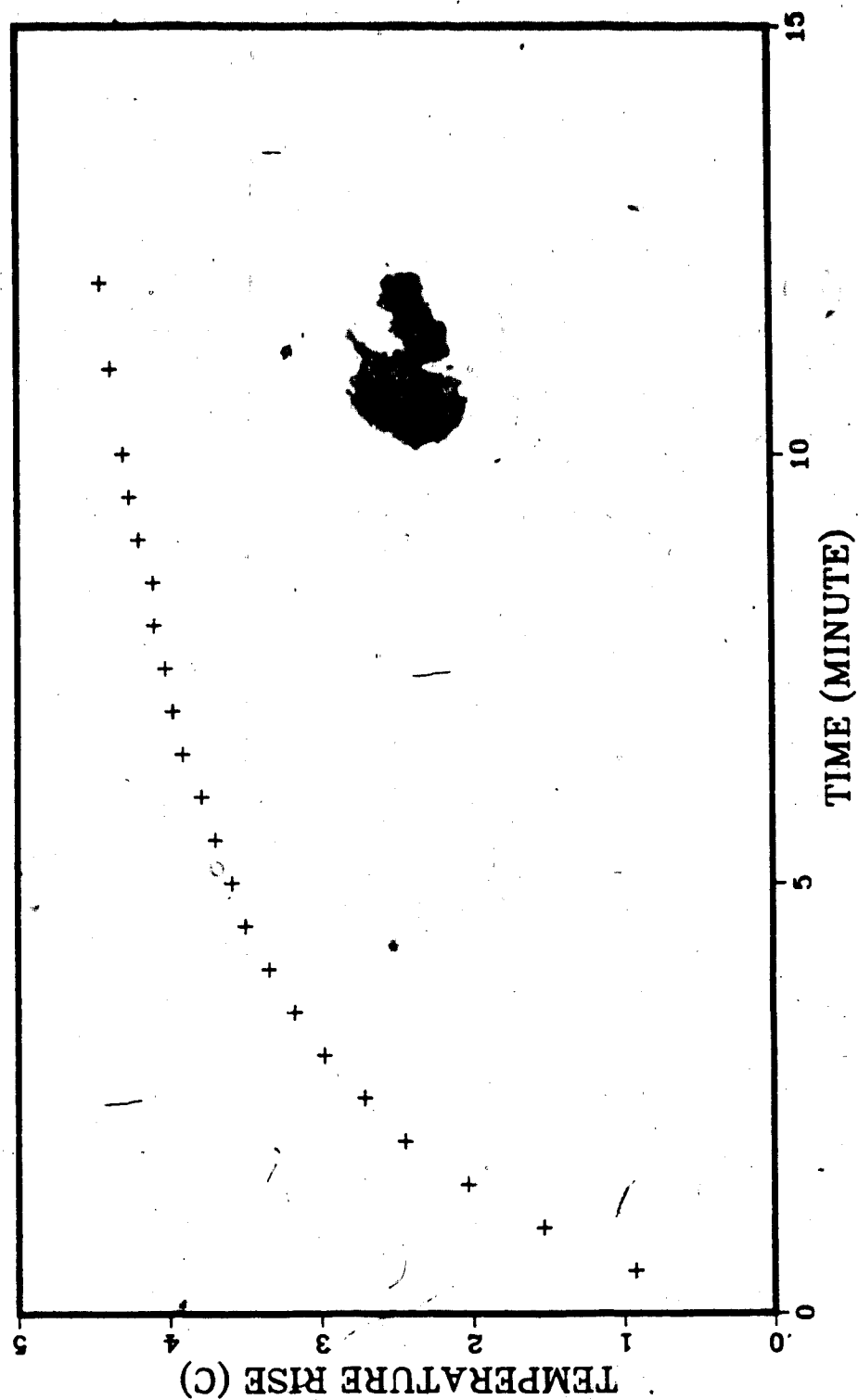


Figure 2.6 Typical temperature rise as measured by a thermal conductivity probe for the dry cellulose insulation.

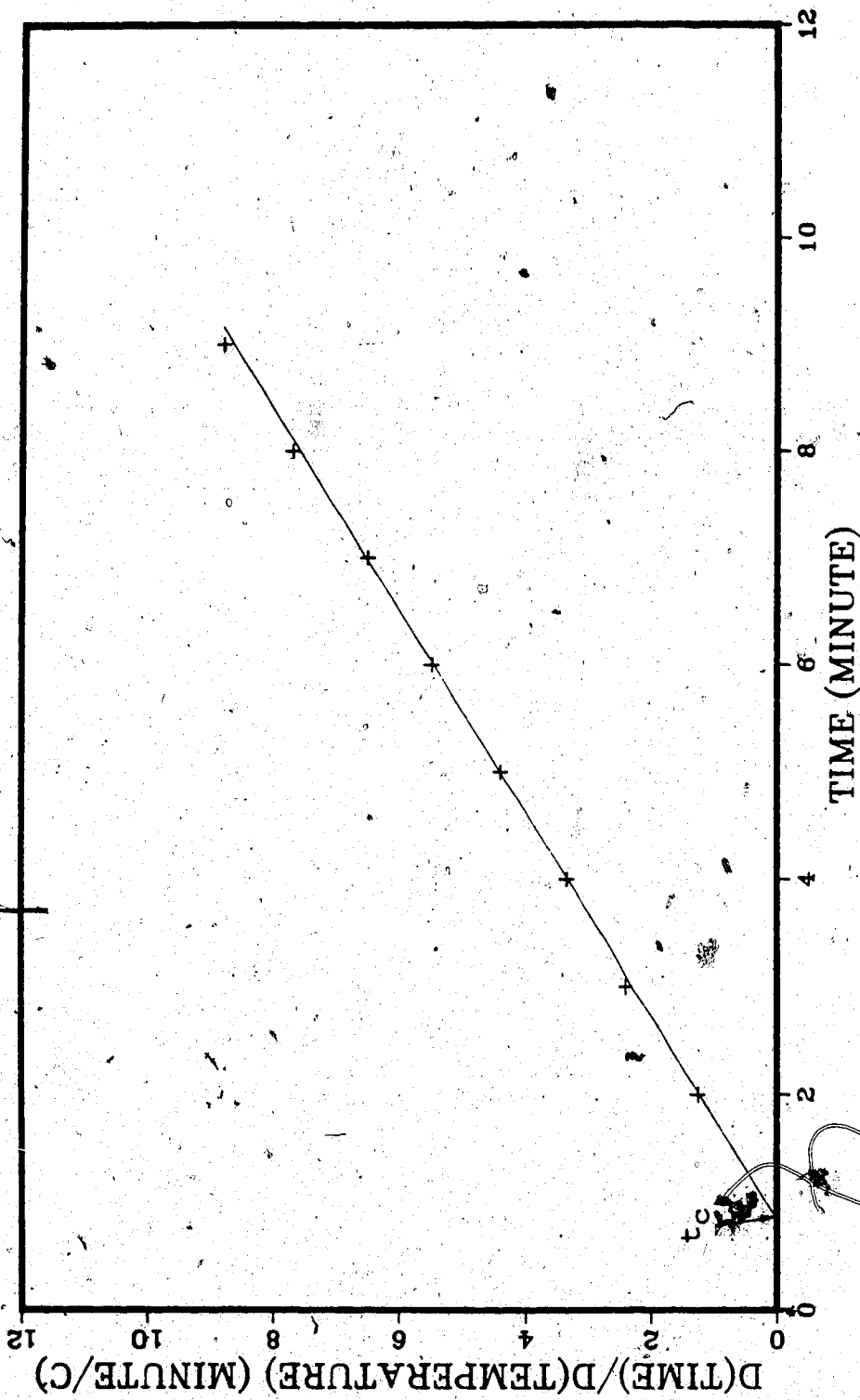


Figure 2.7 Evaluation of the time correction (t_c) for the probe by plotting $d t/d\theta$ versus time.

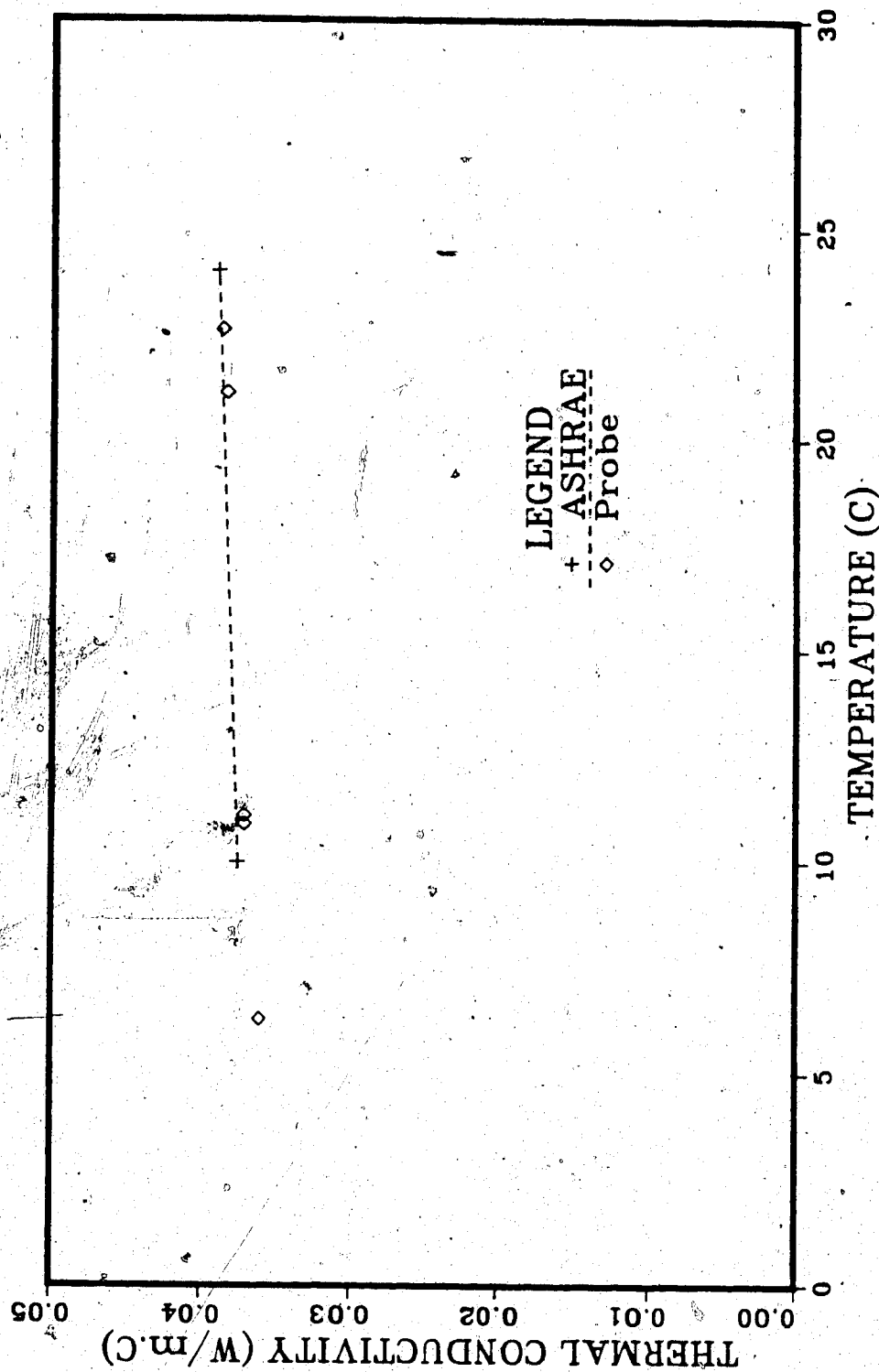


Figure 2.8 Comparison of thermal conductivity of the cellulose insulation as obtained using the probe and from ASHRAE.

coated with epoxy for added water resistance. A fibreglass screen was sandwiched between the bracket and the opening on the plywood plate to form the test section for supporting the loose fill cellulose in place (Plate 2.4). At 40 kg/m^3 test density and 102 mm test thickness, the total weight of the cellulose was calculated to be 1156 g. Eleven identical thermal conductivity probes were inserted into the side of the test section at various levels for measuring the moisture contents and distributions (Figure 2.9 and Plate 2.5). Seven equally spaced thermocouple probes were also inserted into the middle of one side of the test section to measure the temperature profile across the cellulose insulation (Figure 2.10 and Plate 2.6).

Since it would be impossible during the test to remove a sample core of the test insulation for weighing and drying without disturbing the process of moisture movement, attempts were made to at least verify the probe measurements at the end of the test with gravimetric analysis. To do so, five sample core holders were constructed. The donut rings were 63.5 mm in diameter and 3.2 mm thick and made of plexiglas with 3 holes drilled on the ring. A fibreglass screen was attached at the bottom and 12.7 mm long wooden pegs were inserted into the holes on the ring for spacing and support. Total volume for each 12.7 mm cross-section was calculated to be $3.66 \times 10^{-5} \text{ m}^3$. At 40 kg/m^3 test density, the required amount of cellulose

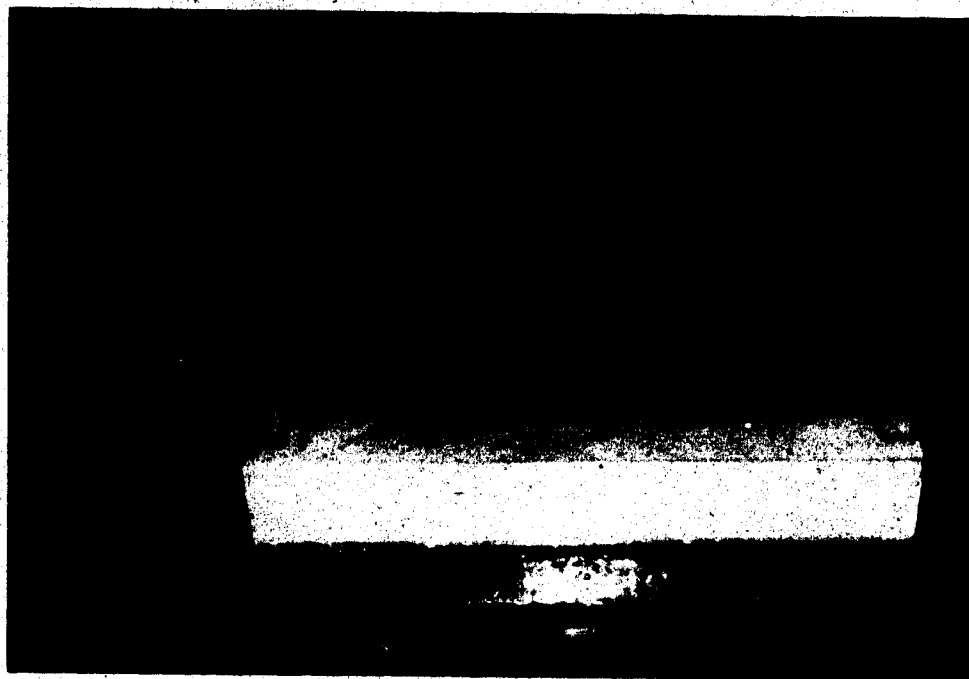


Plate 2.4 Photo of the test section.

COLD BOUNDARY

• (88.9 mm)	• (95.25 mm)	
		• (82.55 mm)
• (69.85 mm)	• (76.2 mm)	
		• (63.5 mm)
• (50.8 mm)	• (57.15 mm)	
		• (38.1 mm)
	• (25.4 mm)	
• (12.7 mm)		

WARM BOUNDARY

number in brackets represents distance from
the warm boundary

Figure 2.9 Positions of the thermal conductivity probes in the test section.

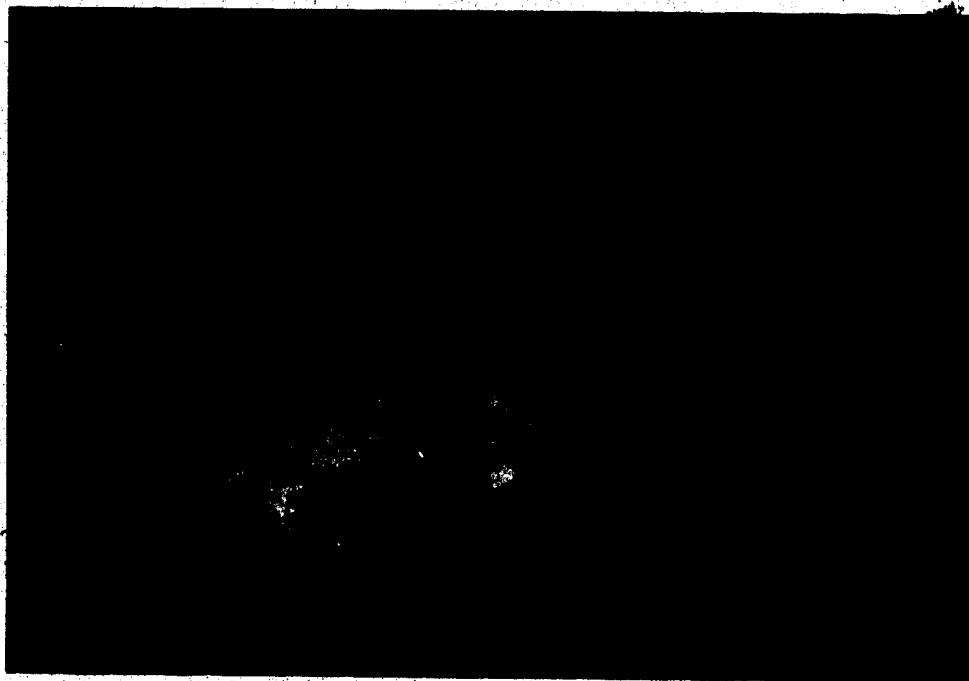


Plate 2.5 Photo of the thermal conductivity probes in the test section.

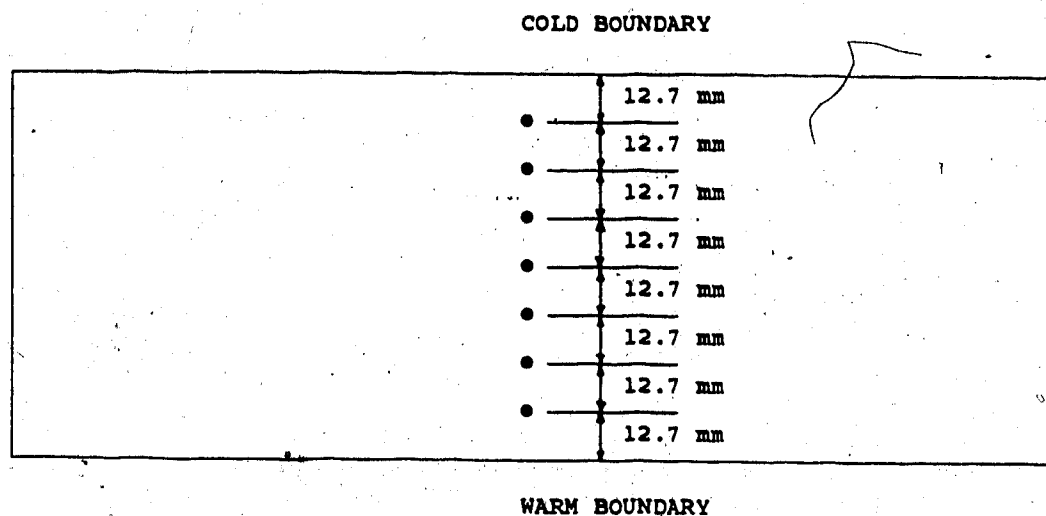


Figure 2.10 Positions of the temperature probes in the test section.

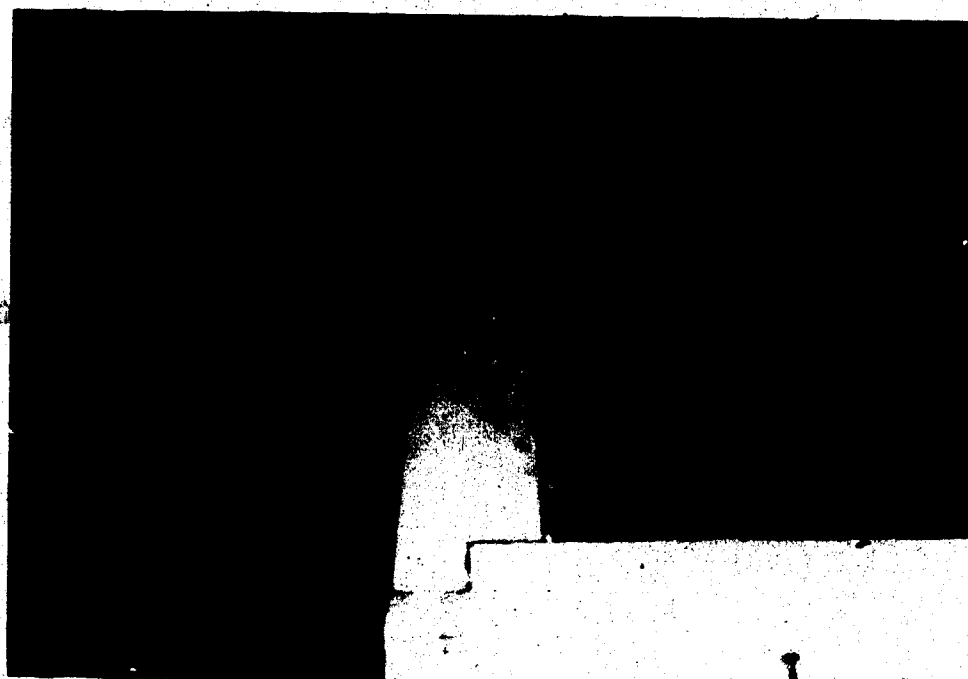


Plate 2.6 Photo of the temperature probes in the test section.

was carefully weighed to 1.46 ± 0.01 g to fill each cross-section. Care was taken to fill each cross-section as uniformly as possible. Then the next cross-section would be placed on top of the previous one and filled with the exact amount of cellulose. The process was repeated until the holder was completed. Each holder was encased with a fibreglass screen tube (Plate 2.7). Five sample core holders were placed at different locations within the test section to observe any multi-dimensional effects during the test (Figure 2.11 and Plate 2.8). The remaining space was then carefully filled with cellulose at 40 kg/m^3 density (Plate 2.9). After the test section was ready, it was placed on top of the test box. An additional 457 mm high bracket was placed on top of the test section to avoid air movement directly above the test cellulose (Plate 2.10). All cellulose was oven dried before each test and this oven-dried state was used as the basis of the dry weight for the insulation.

2.7 Data Acquisition System

The data acquisition system used in this experiment consisted of a MetraByte DASH-8 A-D converter (manufactured by MetraByte Corporation), a MetraByte Universal Expansion Interface (Model No. EXP-16) and an IBM * Personal Computer. The system provides 16

* Trademark of International Business Machines Corporation.

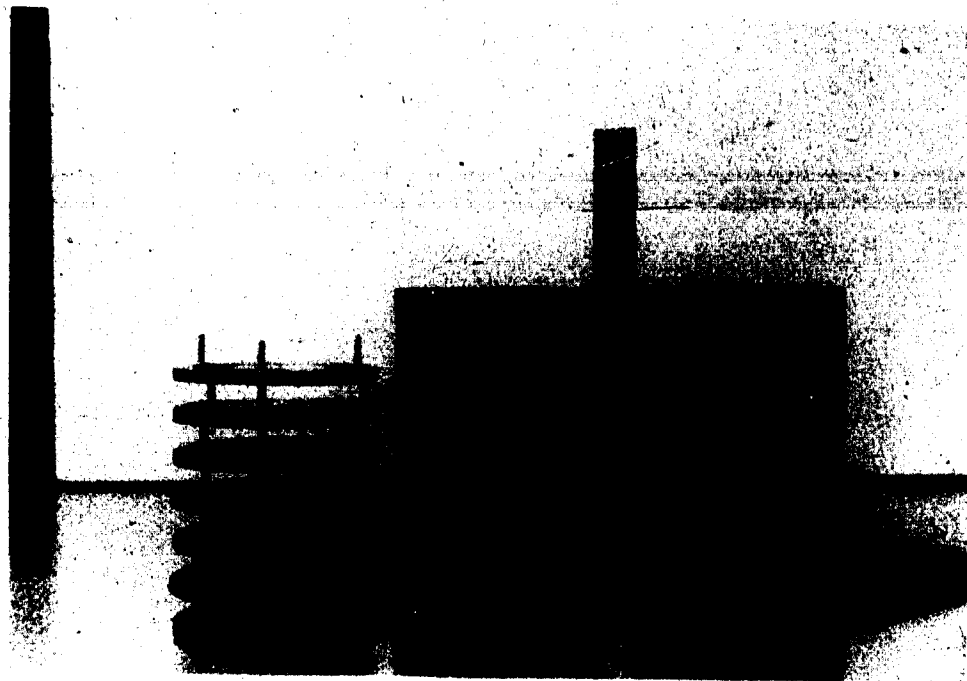


Plate 2.7 Photo of a sample core holder.

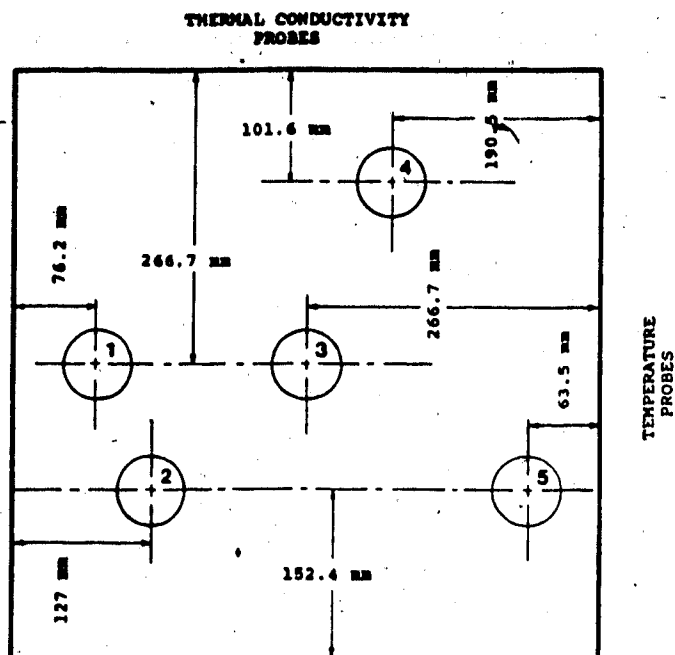


Figure 2.11 Positions of the sample core holders within the test section.



Plate 2.8 Photo of the sample core holders within the test section.

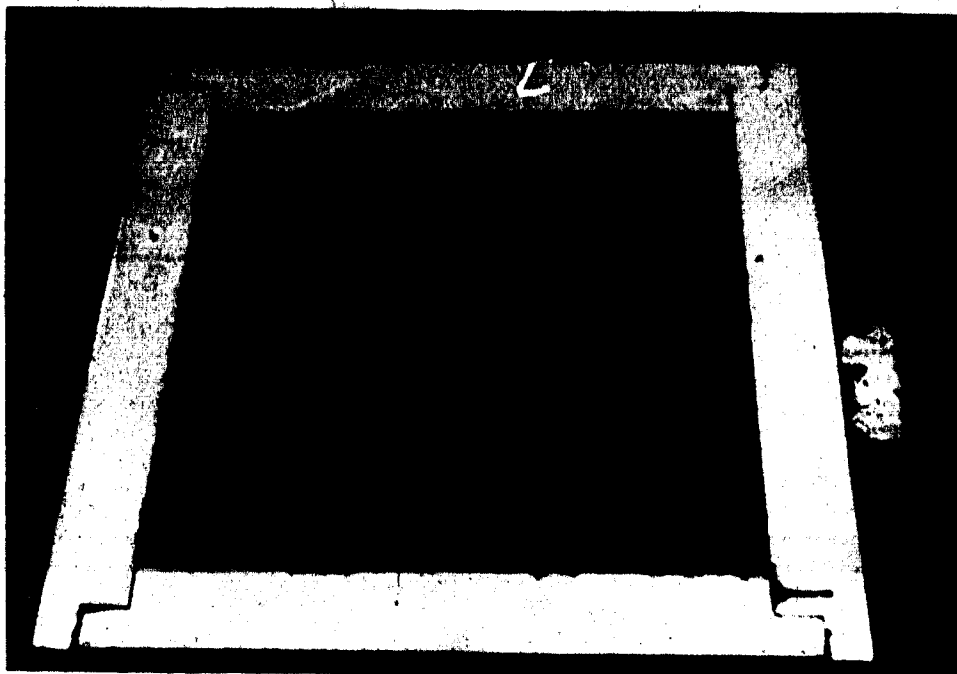


Plate 2.9 Photo of the completed test section.

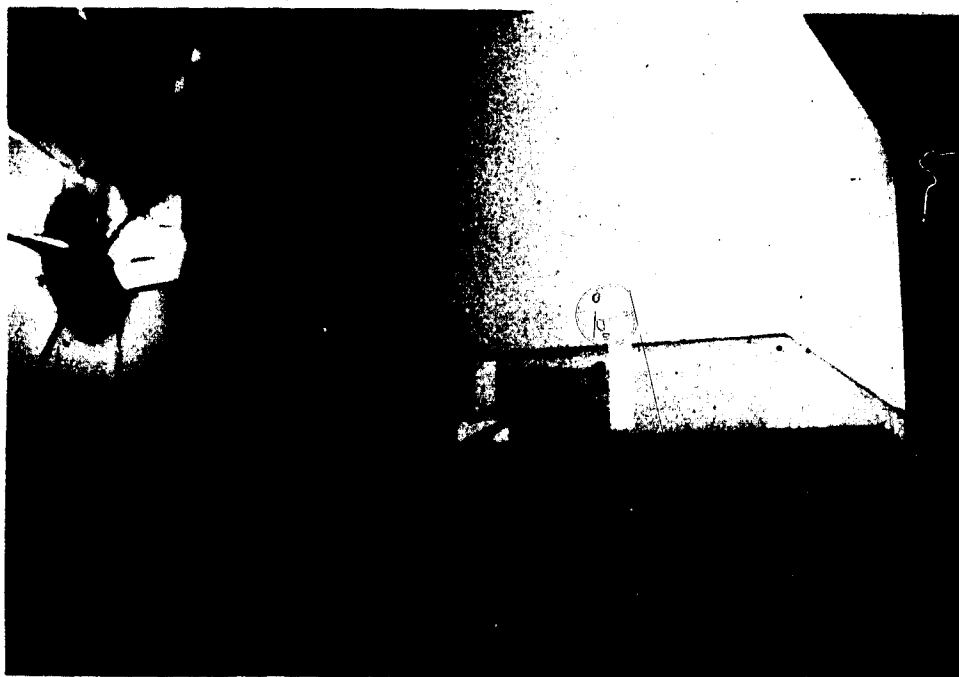


Plate 2.10 Photo of the box and the test section.

differential analog input channels for data collection.

The DASH-8 is an 8-channel 12 bit high speed (up to 4000 samples/second) A/D converter and time/counter board for the IBM PC. All connections are made through a standard connector at the rear of the computer (Figure 2.12).

The EXP-16 is an expansion multiplexer/amplifier system that can be used with any data acquisition system. Each EXP-16 concentrates 16 differential analog input channels into one analog output channel and also provides signal amplification, filtering and conditioning. The board includes cold-junction sensing and compensation circuitry for thermocouples measurements (Figure 2.13).

2.8 Test Conditions And Procedure

Four sets of tests were performed with different conditions. The inside temperature (25 °C) and relative humidity (40 %), cold room temperature (-30 °C), thickness and density of the test cellulose insulation (102 mm and 40 kg/m³) were the same for all tests while the duration of the test and the exfiltration rate were varied in each test. For test #1, the small opening near the bottom of the box was simply exposed to the cold room and the system itself regulated the amount of cold air being drawn into the box through the opening. The exfiltration rate as measured by the gas analyser was 0.4 ACH or 280 L/hr of air flow and the test lasted

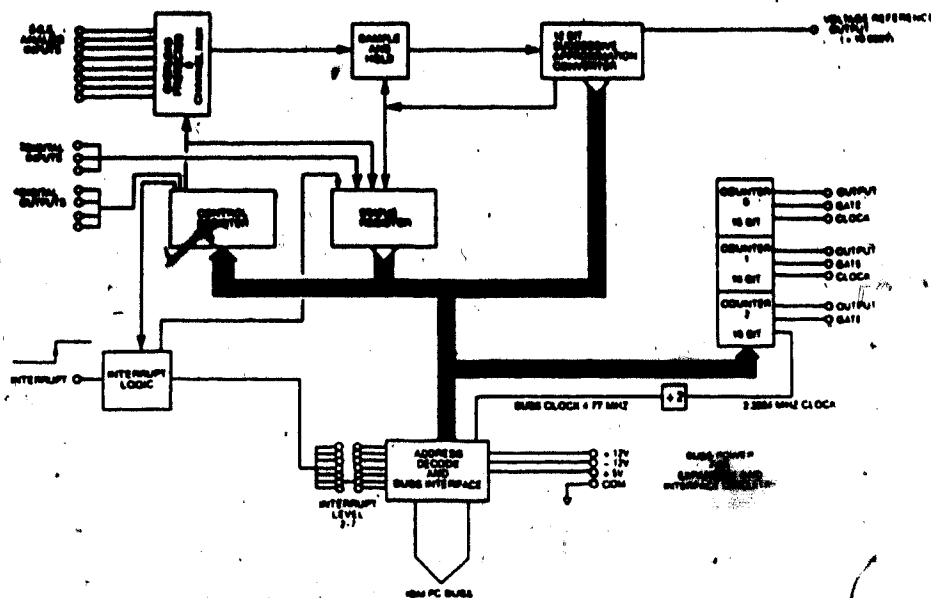


Figure 2.12 Block diagram of the DASH-8 board.

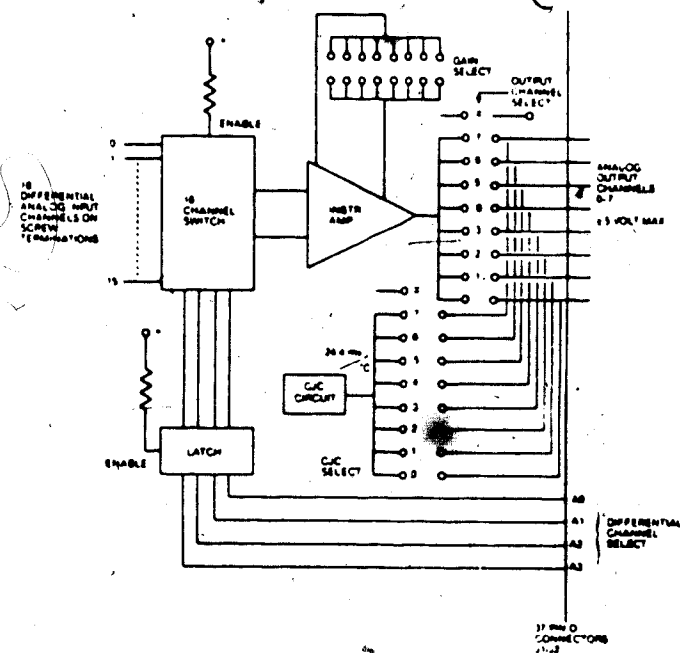


Figure 2.13 Block diagram of the EXP-16 board.

504 hours (21 days). For test #2, a small amount of cold air was forced into the box via the small opening at the bottom of the box to give an exfiltration rate of 0.6 ACH or 420 L/hr of air flow. The test ended after 336 hours (14 days). In test #3, the exfiltration rate was increased to 0.9 ACH or 630 L/hr of air flow and the test completed in 224 hours (9.3 days). In test #4, the exfiltration rate was 1.2 ACH or 840 L/hr of air flow and the test ran for 168 hours (7 days). The situation in Test #1 modelled the moisture migration and accumulation under a pure "stack effect". Tests #2, 3 and 4 simulated situations where a "stack" effect and induced pressure are present. The length of time for each test was chosen such that the total amount of moist air flow through the test insulation was constant for all tests, i.e.

$$\text{ACH} \times (\text{time duration of the test}) = \text{constant}$$

The main item of interest was to determine the effect of exfiltration rate on the moisture distribution and the rate of accumulation within the cellulose.

Testing procedure was identical in every test. Just before the start of each test, probe measurements on the cellulose were taken to ensure uniform packing of the insulation. After the start of the test, the daily moisture content and distribution within the cellulose were obtained by using the probes. Temperature profiles

across the cellulose were recorded daily using the temperature probes. The exfiltration rate was measured by the MIRAN Gas Analyser every day. Also, the inside temperature, inside humidity and cold room temperature were monitored on a daily basis to ensure constant test conditions. The total amount of water consumed by the humidifier to maintain the test condition of 40 % relative humidity was recorded. At the end of each test, the sample core holders were removed and the cellulose in each cross-section was weighed and dried to obtain the final moisture content and distribution. The remaining cellulose was collected and dried to obtain the overall moisture content. Visual inspection was made to check the compaction of the cellulose, traces of liquid water within the cellulose, the extent of frost formation and any sign associated with the process of moisture migration. The cellulose was touched by hand to feel any liquid water or dampness.

CHAPTER 3

DATA REDUCTION

The ability of measuring the transient moisture distribution within the cellulose was crucial in the present investigation. A relation between probe measurement, moisture content and temperature of the cellulose was required in order to convert the probe measurement into corresponding moisture content in the cellulose. A probe calibration was carried out to obtain such a relation. Beside using the tracer gas decay method, other measurements such as the temperature profile within the cellulose and the overall water consumption for the test were also used in estimating the exfiltration rate.

3.1 Probe Calibration

The thermal conductivity of the insulation given by the manufacturer or obtained from standard measurement techniques are usually for dry insulation only. There is currently no acceptable standard test method (steady-state, or transient) for measuring the effective thermal conductivity of wet insulation. Langlais et al. [1983] indicated that the values of thermal conductivity of wet insulation obtained using the probe method represent a quasi-steady state and might be unrealistic. Therefore, in order to avoid confusion, the values

obtained by the probe on the wet cellulose will be referred to as k_{probe} and served only as a measure of the moisture content. The values do not necessarily imply the effective thermal conductivities of the wet cellulose. At a given density, the value of k_{probe} for the insulation is a function of temperature and moisture content of the insulation. Before the probe can be used as a device to measure the moisture content in insulation, it must be calibrated against a range of moisture contents and temperature settings for that particular insulation.

For the calibration process, a 203 mm in diameter and 254 mm in height cylindrical container was used to hold the test sample. At 40 kg/m^3 density, the dry weight (oven dry) was calculated to be 330 g and 5 test samples were carefully weighed and put into different containers. Different amounts of water were sprayed onto each test sample and mixed thoroughly to give an approximately uniform moisture content within each test sample. The samples were covered and placed in a temperature controlled environment for conditioning. After 3 hours the samples were mixed again and after 6 hours of conditioning, the samples were weighed to obtain the moisture contents by weight. Each sample was carefully mixed and packed in the cylindrical container with the probe inserted in the middle. A constant current of 0.2 ampere was supplied to the line heat source and the temperature rises, measured by the thermocouple inside the

probe, were recorded and the value of k_{probe} for that temperature and moisture content was calculated. The process was repeated for various moisture contents (0 to 400 %) and temperature settings (20 to -20 °C). A series of calibration curves of k_{probe} versus moisture content for a temperature setting was obtained (Figure 3.1). A fifth order least square polynomial was used to fit the data in Figure 3.1. Using the results of the fitted values in Figure 3.1 and replotting with temperature as the independent variable for various moisture contents, a series of straight lines with correlation factors (R^2) of 0.995 to 1.0 was obtained (Figure 3.2). From the coefficients of the least square straight lines in Figure 3.2, a single equation representing the k_{probe} value for a given temperature and moisture content in the cellulose was derived using a third order least square polynomial

$$\begin{aligned}
 k_{\text{probe}} = & (3.726E+2 + 5.347E-4 \times MC - 1.394E-6 \times MC^2 \\
 & + 1.992E-9 \times MC^3) + T \times (1.418E-4 + 1.297E-6 \times MC \\
 & - 4.798E-8 \times MC^2 + 7.002E-11 \times MC^3)
 \end{aligned} \tag{3.1}$$

where k_{probe} is the calibration value corresponding to a given moisture content and temperature in $W/m \cdot ^\circ C$, MC is the moisture content by weight (dry basis) in % and T is the temperature in °C. Equation 3.1 was used to calculate the moisture content from the measured k_{probe} value and

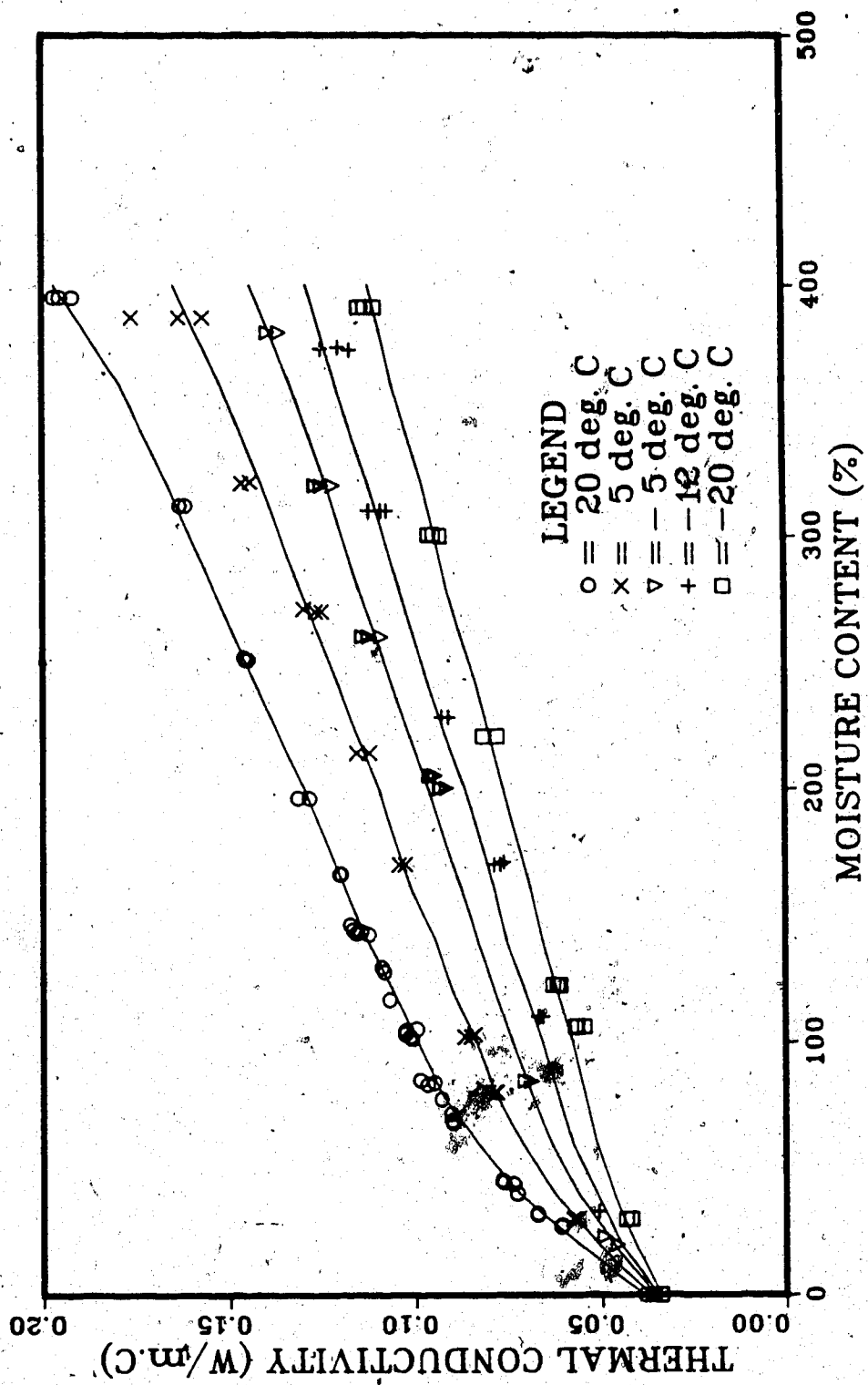


Figure 3.1. Calibration curves of k_{probe} versus moisture content for a given temperature.

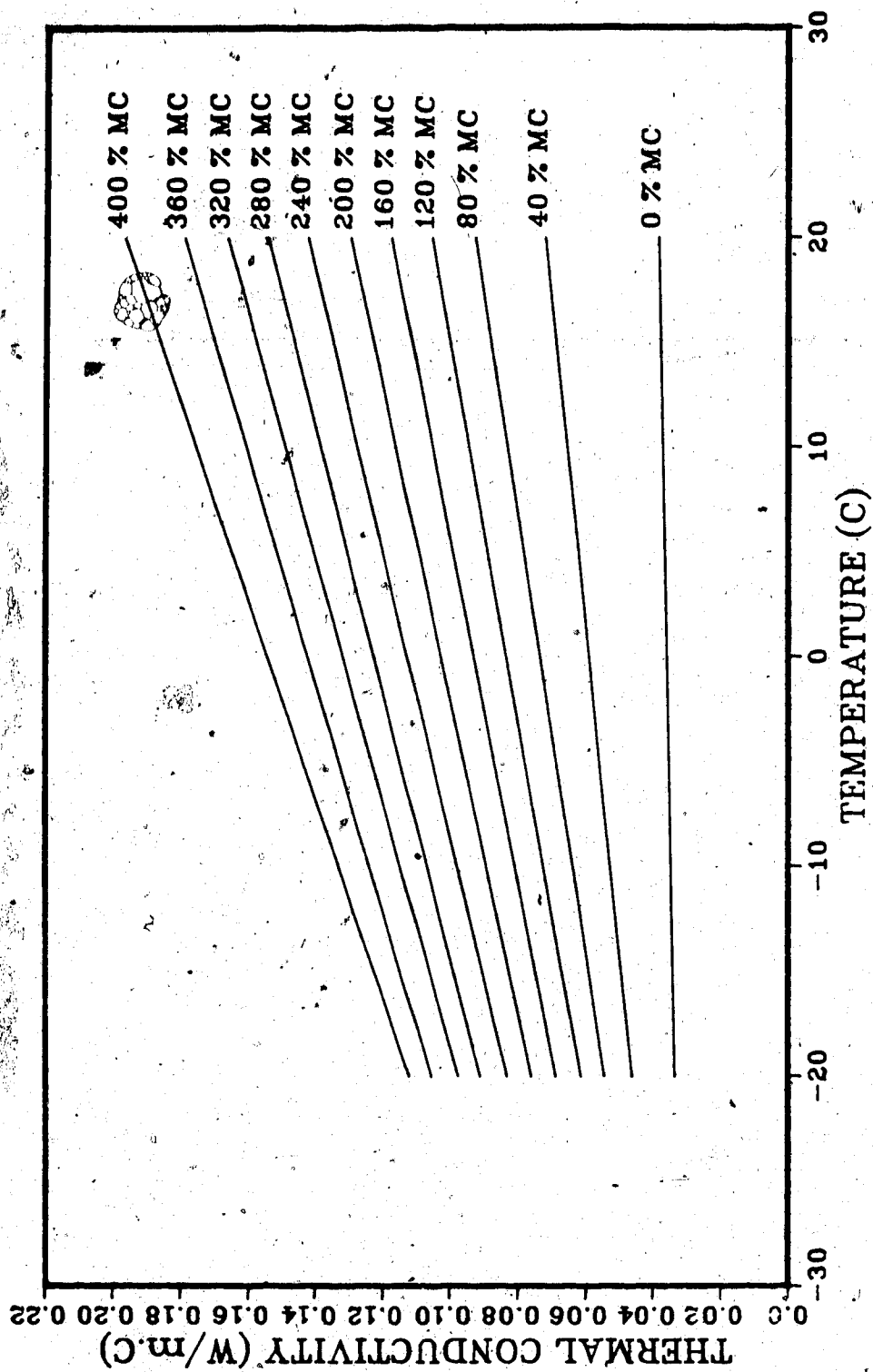


Figure 3.2 Calibration results of k_{probe} versus temperature for a given moisture content.

temperature during the test. The average percent error in k_{probe} between the calibration data and curve fitted results from Equation 3.1 is less than 5 %.

3.2 Exfiltration Rate and the Temperature Profile

Most porous insulation is permeable to air intrusion and the temperature profile within the insulation depends on the given boundary temperatures and the amount of air intrusion (infiltration or exfiltration). Consider the case of permeable insulation subjected to a warm boundary temperature T_i at $x=0$ and a cold boundary temperature T_o at $x=l$, with a steady exfiltrative flow of warm air from warm to cold boundaries due to an imposed pressure difference. Berlad et al. [1980] have shown that the energy equation is

$$\rho u C_p \frac{dT}{dx} = k \frac{d^2T}{dx^2} \quad (3.2)$$

where ρ is the density of the air in kg/m^3 , u is the velocity of the air flow through the insulation (which will be termed "filtration velocity") in m/s , C_p is the specific heat capacity of the air in $\text{J/kg}\cdot\text{K}$, T is the temperature in K , x is the distance from the hot boundary in m , and k is the thermal conductivity of the insulation in $\text{W/m}\cdot\text{°C}$. The solution for Equation 3.2 (Appendix D) is

$$T = T_i - (T_i - T_o) \left[\frac{\exp(\rho u C_p x/k) - 1}{\exp(\rho u C_p l/k) - 1} \right] \quad (3.3)$$

The term $\rho u C_p x/k$ is called the Peclet Number (Pe) and represents the relative magnitude of heat transfer by convection as compared to heat transfer by conduction. Solution to Equation 3.2 in the form of Equation 3.3 is valid only if the properties such as ρ , C_p and k are constant. As moisture accumulates within the cellulose, the effective thermal conductivity of the insulation changes and Equation 3.2 will not be applicable. Deviation from the measured temperature profile described by Equation 3.3 indicates changes in properties due to moisture accumulation. If the average property values for ρ , C_p and k are assumed and the temperature profile is provided, the average filtration velocity can be estimated from Equation 3.3. Knowing the filtration velocity, the exfiltration rate can be approximated as

$$I = \frac{u A_{eff}}{V_b} (3600 \text{ s/hr}) \quad (3.4)$$

where I is the exfiltration rate in ACH, A_{eff} is the effective cross-section area of the test section (cross-section area times the porosity) in m^2 , and V_b is the volume of the box in m^3 . Equation 3.4 is only used as a rough estimate of the exfiltration rate and provides an additional check on the tracer gas decay test result.

3.3 Estimation of Exfiltration Rate from the Total Water Consumption

Water vapour in the air also can be used as a tracer gas. The air temperature and relative humidity inside the box were controlled at 25 °C and 40 % RH. From psychrometry (Appendix E), the humidity ratio of the air was calculated to be 0.0078 kg H₂O/kg dry air. At the outside temperature of -30 °C and assuming 100 % RH, the humidity ratio of the cold air was 0.0003 kg H₂O/kg dry air. Therefore the humidifier supplied approximately 0.0075 kg of water for every kg of cold air entered into the box in order to maintain the desired test conditions. From the total amount of water consumed by the humidifier over the entire test period, the total amount of air which entered into the box was

$$\dot{m}_a = \frac{m_w}{(0.0075 \text{ kg H}_2\text{O/kg air}) \cdot t} \quad (3.5)$$

where \dot{m}_a is the mass flow rate of the air in kg/hr, m_w is the mass of water consumed in the entire test period in kg, and t is the duration of the test in hr. Knowing the density of the air and the volume of the box, the exfiltration rate was estimated to be

$$I = \frac{\dot{m}_a}{\rho V_b} \quad (3.6)$$

Calibration of the probe measurement provides an easy conversion of the measured k_{probe} value and temperature of the cellulose into moisture content. Eleven thermal conductivity probes at various levels of the cellulose provided a moisture profile within the insulation. With a daily moisture profile, the progress of moisture migration and accumulation within the cellulose was studied. The estimations of the exfiltration rate from the temperature profile and overall water consumption provided useful checks on the tracer gas decay test. Because the exfiltration rate was the only variable that was changed from one test to another, therefore, it was important to verify and compare the tracer gas test result with other measurements.

CHAPTER 4

RESULTS AND DISCUSSION

Four sets of tests were performed in this investigation of moisture migration in porous insulation. Test conditions were held constant for all tests with the exception of the exfiltration rate. The length of the test was chosen such that the total amount of moist air passing through the cellulose was the same for each test. Results were correlated with the measured temperature profile within the cellulose and the exfiltration rate during the test. Estimation of the heat losses due to conduction, convection and latent heat are also included for each test.

4.1 Temperature Profiles

As mentioned in Chapter 2, the cold room temperature varied with the compressor cycle and defrost cycle and the temperature inside the box fluctuated slightly as the heater came on and off (Figure 4.1). The fluctuation of the boundary temperatures were small and should not influence the temperature profile within the cellulose. Figures 4.2 to 4.5 show the initial (about 1 day after the start of the test) and final (the last day of the test) temperature profiles for each test. The dew point temperature of the warm moist air and the 0 °C are

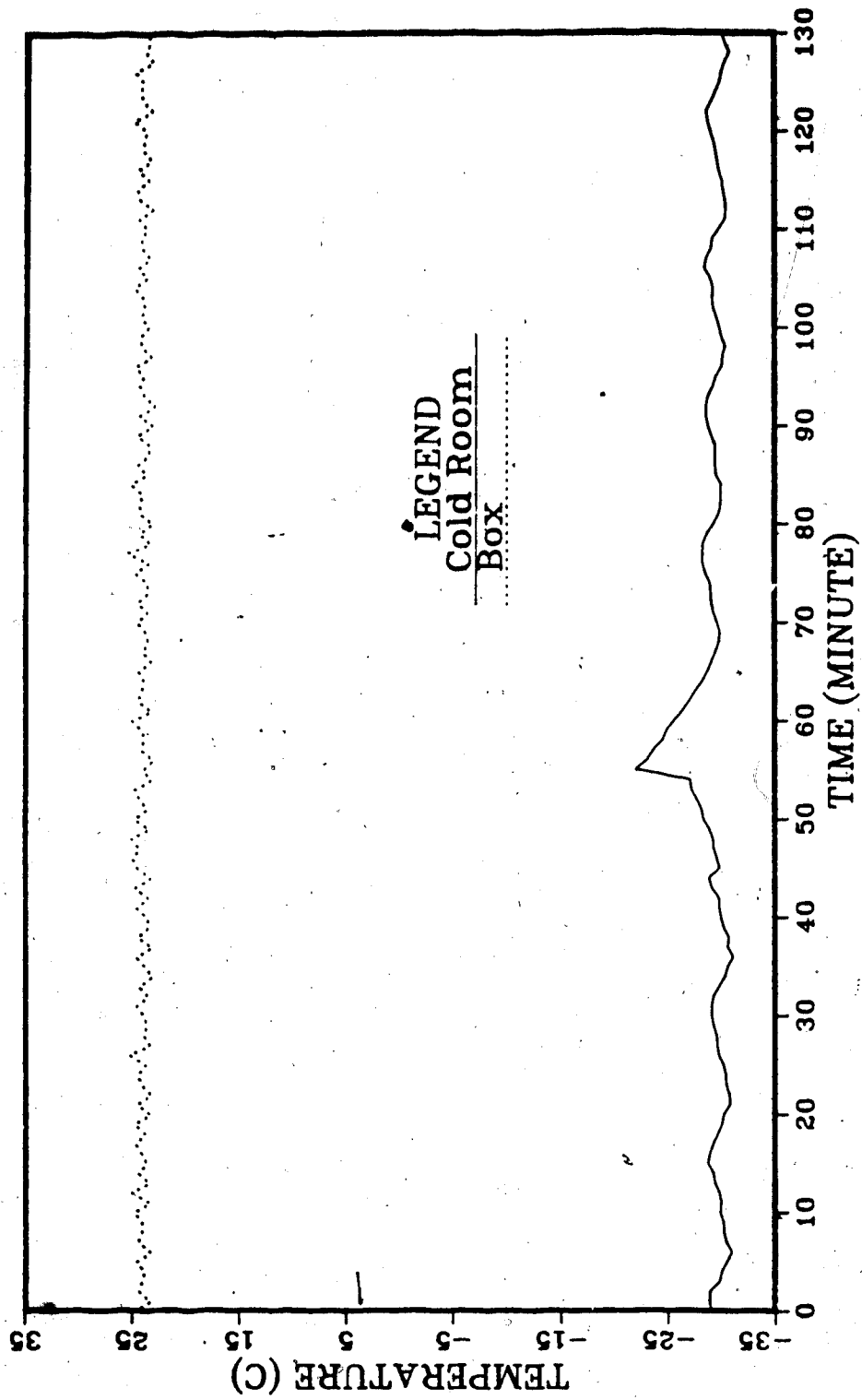


Figure 4.1 Typical temperature history inside the box and the cold room during a test.

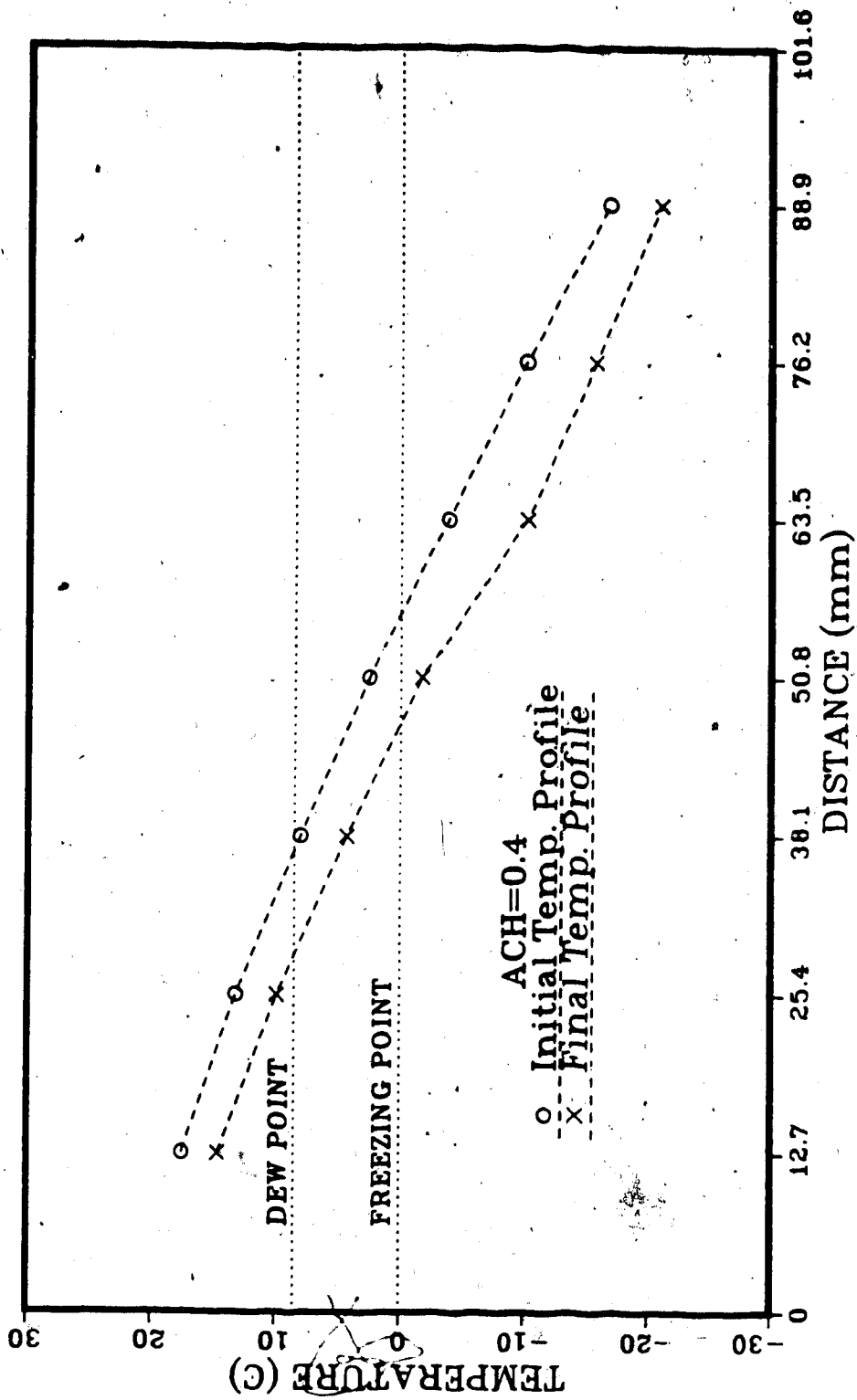


Figure 4.2 Initial and final temperature profiles within the cellulose (ACH=0.4).

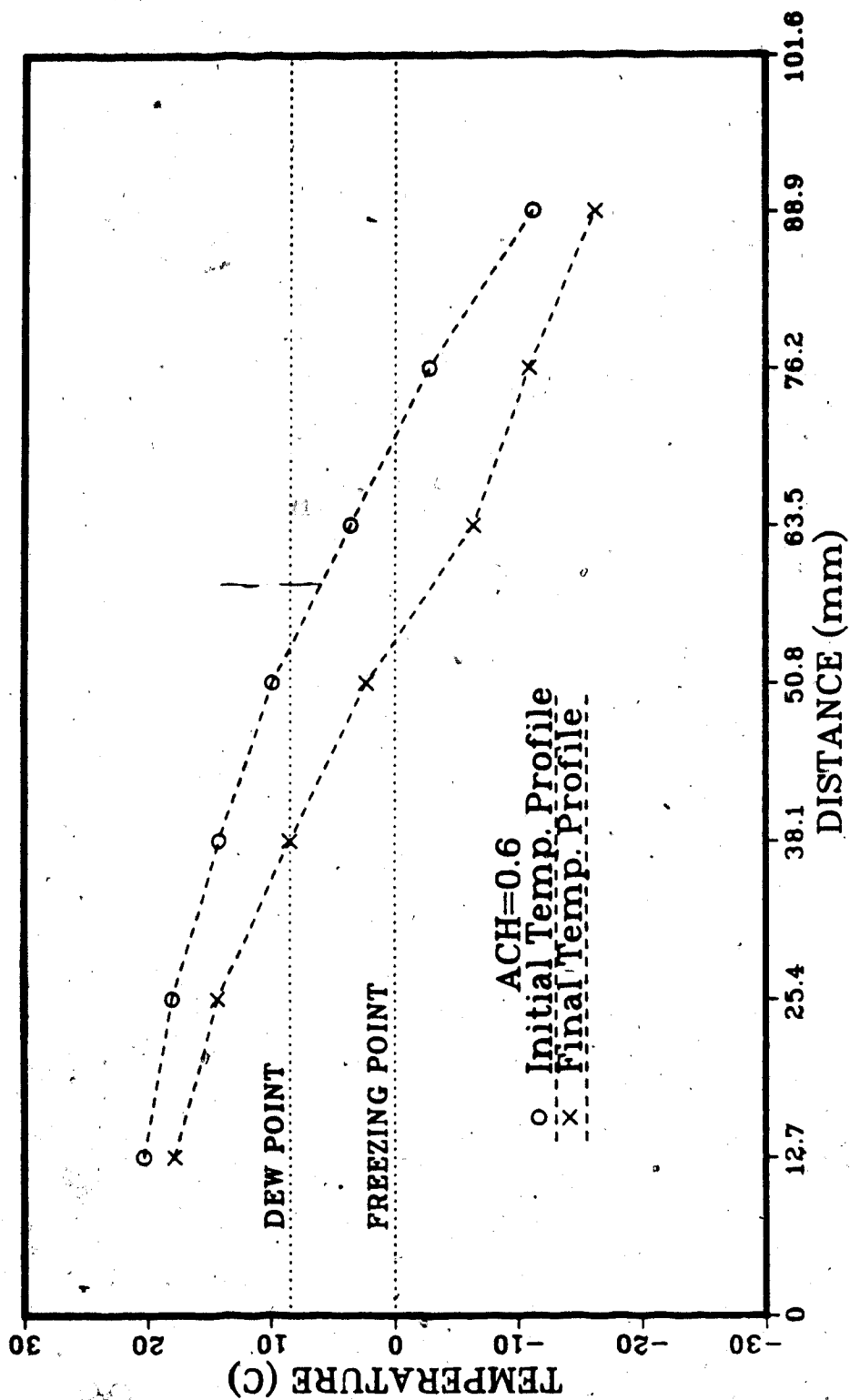


Figure 4.3 Initial and final temperature profiles within the cellulose (ACH=0.6).

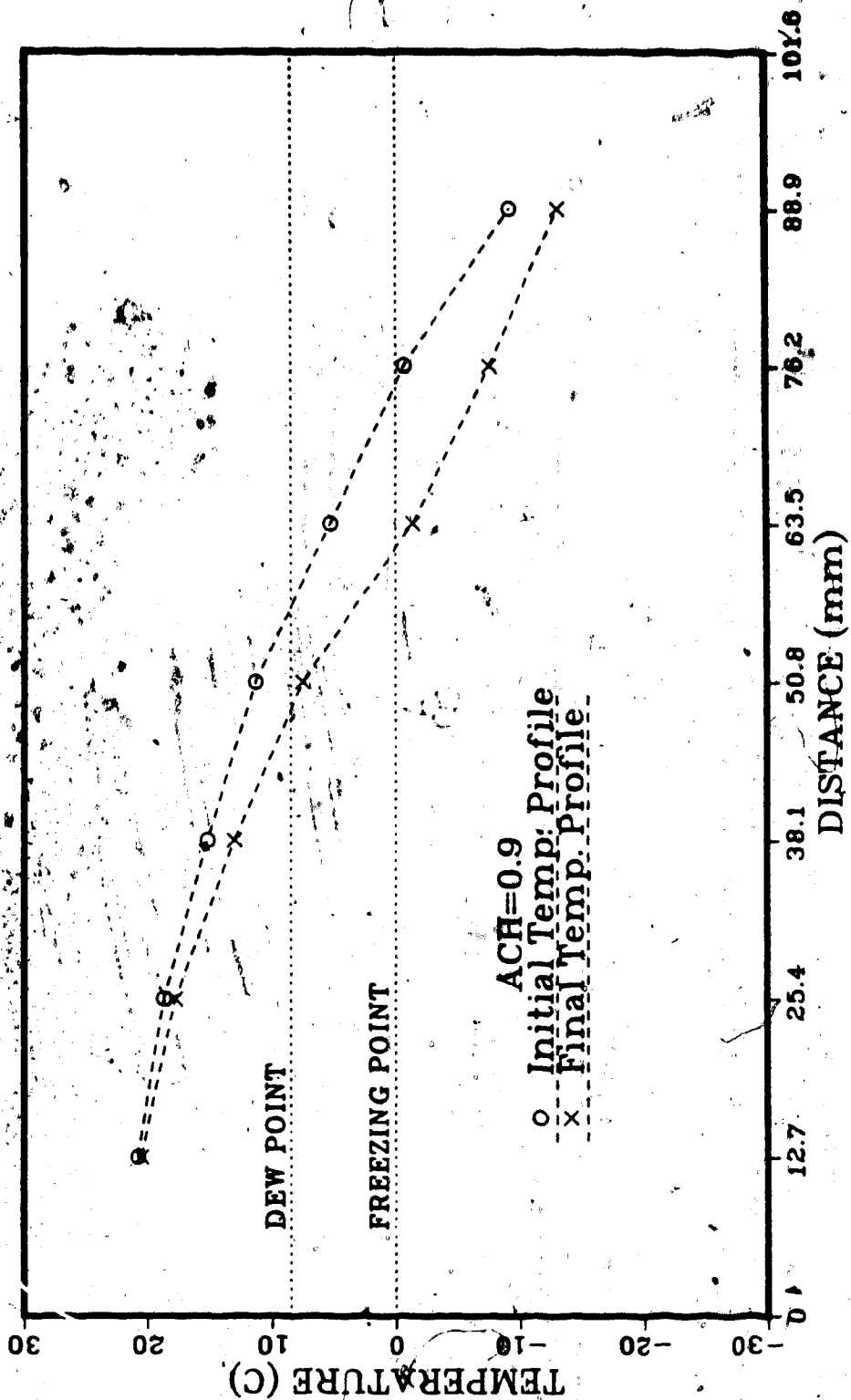


Figure 4.4 Initial and final temperature profiles within the cellulose (ACH=0.9).

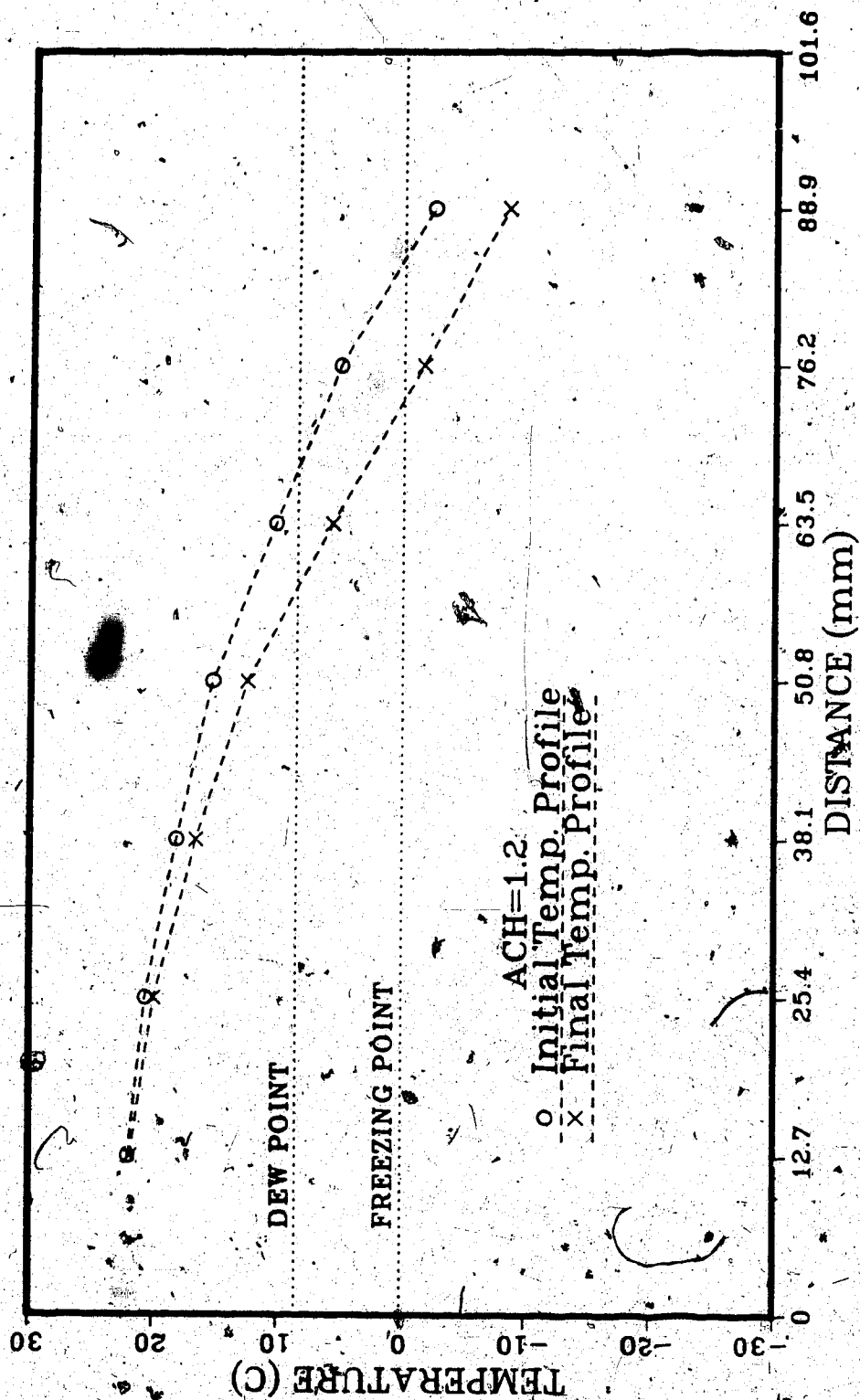


Figure 4.5 Initial and final temperature profiles within the cellulose (ACH=1.2).

included. When there is no moisture accumulation within an insulation, the energy equation is given by Berlad et al. [1980] in the form of Equation 3.2. If ρ , C_p and k were assumed constant, then the temperature within an insulation is given by Equation 3.3

$$T = T_i - (T_i - T_o) \left[\frac{\exp(\rho u C_p x/k) - 1}{\exp(\rho u C_p l/k) - 1} \right] \quad (3.3)$$

When moisture is accumulating within an insulation, Ogniewicz and Tien [1981] proposed that a latent heat term, LF , be added to Equation 3.2

$$\rho u C_p \frac{dT}{dx} + L \Gamma \frac{d^2 T}{dx^2} = 0 \quad (4.1)$$

where L is the latent heat in J/kg and Γ is the volumetric moisture accumulation in $\text{kg/m}^3 \cdot \text{s}$. Again, if ρ , C_p , k and Γ were assumed constant, the temperature within an insulation can be showed (similar to the solution of Equation 3.2 in Appendix D) as

$$T = T_i - \left[(T_i - T_o) + \frac{L \Gamma l}{\rho u C_p} \right] \left[\frac{\exp(\rho u C_p x/k) - 1}{\exp(\rho u C_p l/k) - 1} \right] \quad (4.2)$$

If moisture condenses or freezes within an insulation, the term LF is positive. Comparison of Equations 3.3 and 4.2 shows that the presence of moisture will lower the temperatures within an insulation as compared to no

moisture accumulation. The drops in temperatures within the cellulose as shown in the measured temperature profiles (Figures 4.2 to 4.5) are the indication of moisture accumulation within the cellulose. The inside and outside surface temperatures of the cellulose are obtained by extrapolating the measured temperature profiles. The results clearly show that as exfiltration rate increases, the outside surface temperature of the cellulose also increases.

4.2 Exfiltration Rate

The exfiltration rate for each test was measured by three different methods: a direct measurement using the MIRAN Gas Analyser, estimations from the filtration velocity and from the overall water consumption. The results are listed in Table 4.1. Results obtained by the tracer gas decay test using the MIRAN 1A Gas Analyser are considered to be the best measure of the exfiltration rate. Because of the set-up of the experiment, other information such as filtration velocity and overall water consumption were also used to estimate the exfiltration rate and provided additional checks on the gas analyser's measurements. Results on the exfiltration rate by the three methods are consistent with each other.

4.2.1 MIRAN 1A Gas Analyser

The largest source of error for the tracer gas decay method is the mixing of the tracer gas. But with

Table 4.1 Exfiltration rate by 3 different methods.

Exfiltration Rate (MIRAN 1A Gas Analyser, ACH)	0.40	0.60	0.90	1.20
Average Filtration Velocity ($\times 10^{-4}$ m/s)	3.0	4.3	6.6	8.7
Exfiltration Rate (Equation 3.3, ACH)	0.41	0.58	0.89	1.16
Overall Water Consumption (mL)	1332	1352	1410	1437
Duration of the Test (hours)	504	336	224	168
Exfiltration Rate (Equation 3.6, ACH)	0.46	0.70	1.09	1.48

both the heater fan and circulating fan running at all time, it is believed that the concentration of SF_6 within the box was uniform. The results of the tracer gas decay tests showed very little changes in the exfiltration rate over the entire test period.

4.2.2 Filtration Velocity

The filtration velocity of the air in the solution to Equation 3.2 assumed constant values for ρ , C_p and k . In reality, ρ and C_p for the air depends on the temperature and relative humidity while k for the insulation depends on the temperature and moisture content. Because the amount of moisture accumulation in the above freezing portion of the cellulose was small (about 20 % moisture content by weight), therefore temperature measurements in this portion were used to calculate the filtration velocity. Exfiltration rates obtained from Equation 3.3 represent only an approximation.

4.2.3 Overall Water Consumption

The water level control valve on the humidifier is not designed to regulate the water level precisely, therefore the overall water consumption used to estimate the exfiltration rate is only an estimation. The water consumption rate by the humidifier was not constant. When the humidifier was on, more water was being consumed. But averaging over the entire test period, an average exfiltration rate can be obtained.

4.3 Final Moisture Distribution by Gravimetric Analysis

Moisture distribution from the gravimetric analysis for the 0.4 ACH test was slightly different from the other tests in that the results were obtained by direct coring of the cellulose at the end of the test. The core samples were cut into four 25 mm thick cross sections for weighing and drying. The core sample holders were employed for the 0.6, 0.8, and 1.2 ACH tests because of the difficulties in direct coring of the cellulose. The purpose of placing the core sample holders at various locations within the test section was to determine if there was any significant variation in the moisture content with respect to the location, that is to observe any multi-dimensional effect present within the test section. Tables 4.2 to 4.5 list the results of the gravimetric analysis for each test. The results indicate some spatial variations. Although the test section was insulated with 76 mm thick STYROFOAM S-M insulation, some heat loss through the side of the test section was expected. Because the set-up was not truly an one-dimensional heat transfer, temperatures at the edges and corners of the test section were expected to be lower than the center and therefore some multi-dimensional effects were present. Some local variations of density in the test sample due to packing were also anticipated. The small temperature and density differences will cause some

Table 4.2 Results of the moisture distribution within the cellulose as obtained from gravimetric analysis (ACH=0.4).

COLD BOUNDARY

D

C

B

A

WARM BOUNDARY

Moisture content (% by weight, dry basis)

Sample Core Holder							
Level	1	2	3	4	5	Mean	St.Dev.
A	15	13	17	14	17	15.2	1.8
B	18	38	36	23	15	26.0	10.5
C	156	178	175	158	182	169.8	12.0
D	183	214	191	244	233	213.0	26.2

Table 4.2 Results of the moisture distribution within the cellulose as obtained from gravimetric analysis (ACH=0.6).

COLD BOUNDARY

H

G

F

E

D

C

B

A

WARM BOUNDARY

Moisture content (% by weight, dry basis)

Sample Core Holder							
Level	1	2	3	4	5	Mean	St.Dev.
A	10.7	10.1	9.9	13.8	10.3	11.0	1.6
B	10.9	11.6	11.0	14.7	11.0	11.8	1.6
C	13.0	12.7	12.2	16.2	13.0	13.4	1.6
D	15.0	15.1	14.9	18.3	16.2	15.9	1.4
E	20.8	20.9	19.6	24.8	23.7	22.0	2.2
F	183.8	196.1	182.5	202.9	216.5	196.4	14.1
G	303.8	290.7	288.3	276.0	275.3	286.8	11.8
H	141.1	140.8	132.4	145.1	138.8	138.8	5.2

Table 4.4 Results of the moisture distribution within the cellulose as obtained from gravimetric analysis (ACH=0.9).

COLD BOUNDARY

H

G

F

E

D

C

B

A

WARM BOUNDARY

Moisture content (% by weight, dry basis)

Sample Core Holder							
Level	1	2	3	4	5	Mean	St. Dev.
A	9.5	10.5	8.1	8.0	7.8	8.8	1.2
B	9.8	9.2	8.1	9.2	9.6	9.2	0.7
C	11.4	11.0	9.2	10.2	11.8	10.7	1.0
D	13.6	13.5	11.3	13.4	15.0	13.4	1.3
E	17.9	17.4	13.8	17.9	16.8	16.8	1.7
F	81.4	59.7	64.4	77.7	69.2	70.5	9.0
G	245.3	283.5	255.7	258.0	266.7	261.8	14.3
H	251.2	228.8	231.4	222.2	231.9	233.1	10.8

Table 2.5 Results of the moisture distribution within the cellulose as obtained from gravimetric analysis (ACH=1.2).

COLD BOUNDARY

H

G

F

E

D

C

B

A

WARM BOUNDARY

Moisture content (% by weight, dry basis)

Sample Core Holder							
Level	1	2	3	4	5	Mean	St.Dev.
A	5.8	9.4	5.8	6.6	5.6	6.6	1.6
B	7.3	9.6	5.9	6.9	5.9	7.1	1.5
C	8.7	9.4	7.1	7.1	6.2	7.7	1.3
D	10.9	11.0	7.9	9.4	7.5	9.3	1.6
E	11.9	12.8	9.1	9.9	9.9	10.7	1.6
F	16.5	15.8	10.3	12.8	12.0	13.5	2.6
G	79.6	87.4	83.0	79.2	88.0	83.4	4.2
H	199.9	213.1	180.5	179.8	215.2	197.7	17.1

variation of moisture content in the same plane within the cellulose. The mean value and standard deviation of the gravimetric analysis for different cross-sections show the magnitude of the spatial variations was relatively small. The results of the gravimetric analysis also indicate there is a large sudden increase in the moisture content somewhere within the cellulose for all the tests. For example, at the end of the 0.6 ACH test the moisture content 57 mm from the warm side of the cellulose was 22 % as compared to 196 % at 70 mm, an increase of about 174 %. This sudden increase suggests the existence of an interface within the cellulose where the moisture content changes significantly.

4.4 Comparison of Probe Measurements and Gravimetric Analysis

Figures 4.6 to 4.9 show the results of the final moisture distribution within the cellulose as obtained by average gravimetric analysis and by the probes. The spatial variations mentioned above also affected the probe measurements similar to that of the gravimetric analysis. Because the probe senses a small region surrounding itself, therefore, the measurement may be in error if the probe is inserted in a region with large moisture gradient. For example, if the probe is inserted into a relatively dry region with a high moisture content plane near by, then the probe measurement will indicate a higher moisture content than that of gravimetric analysis because

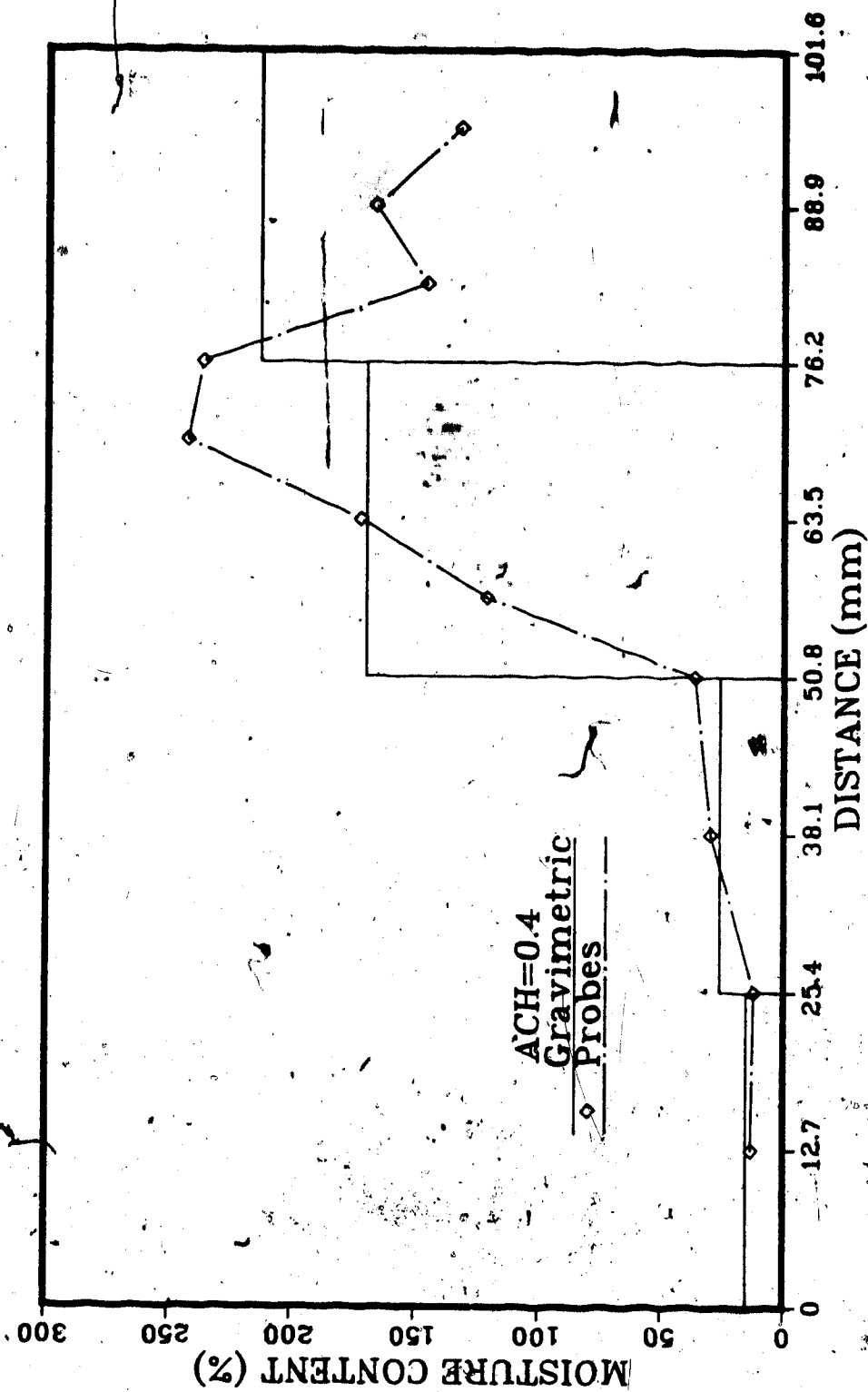


Figure 4.6 Results of the final moisture distribution within the cellulose from gravimetric analysis and probe measurements (ACH=0.4).

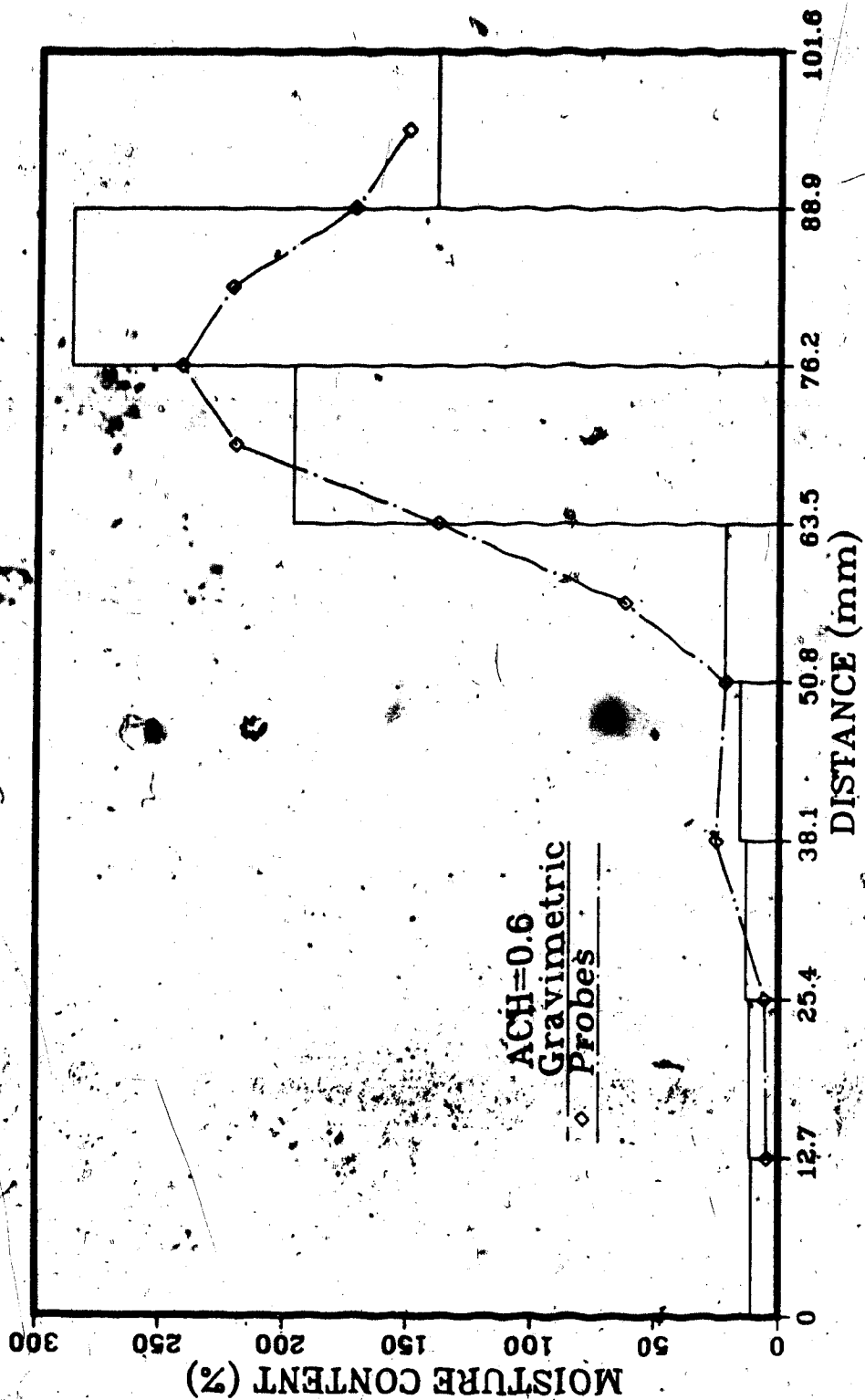


Figure 4.7 Results of the final moisture distribution within the cellulose from gravimetric analysis and probe measurements (ACH=0.6).

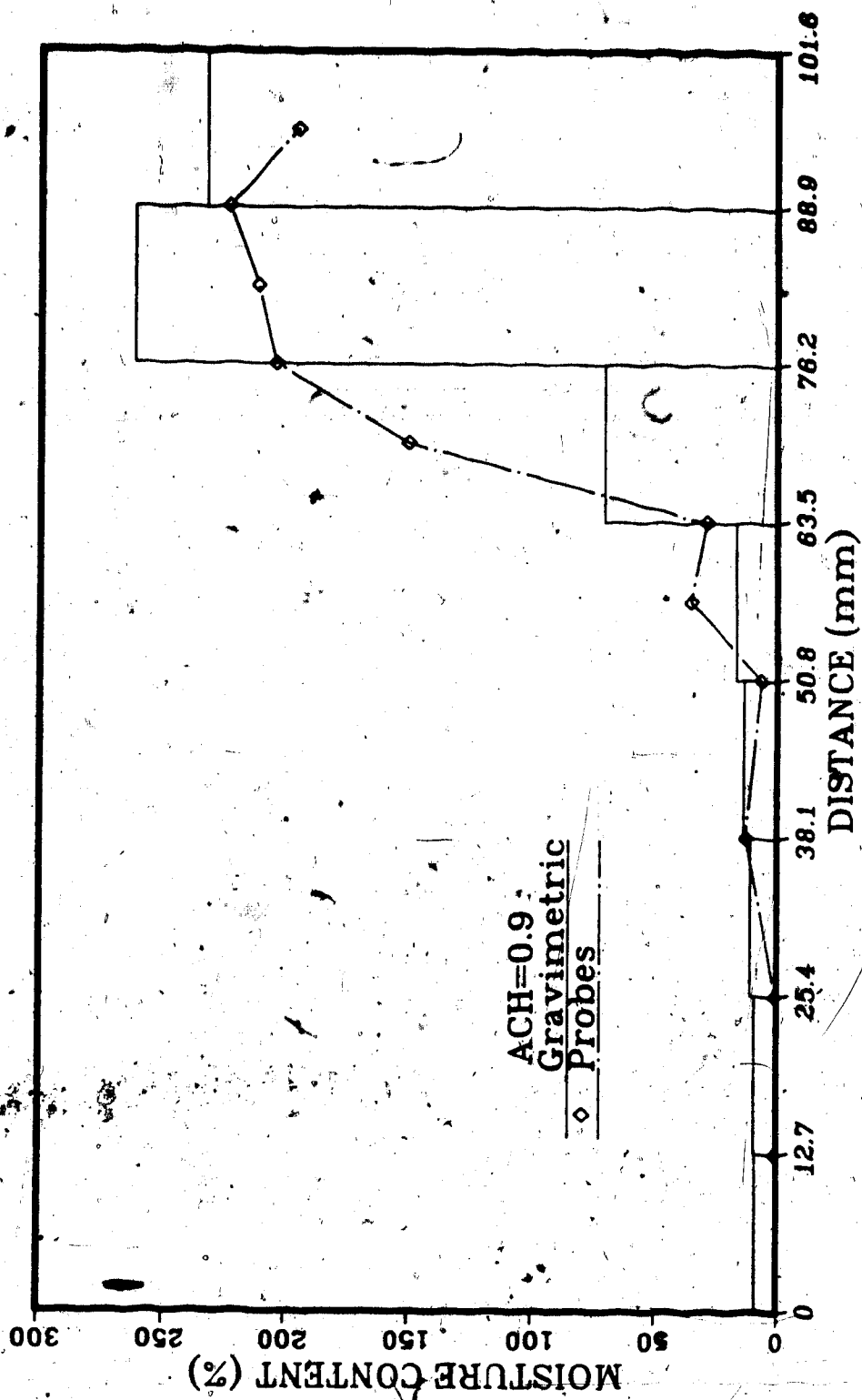


Figure 4.8 Results of the final moisture distribution within the cellulose from gravimetric analysis and probe measurements (ACH=0.9).

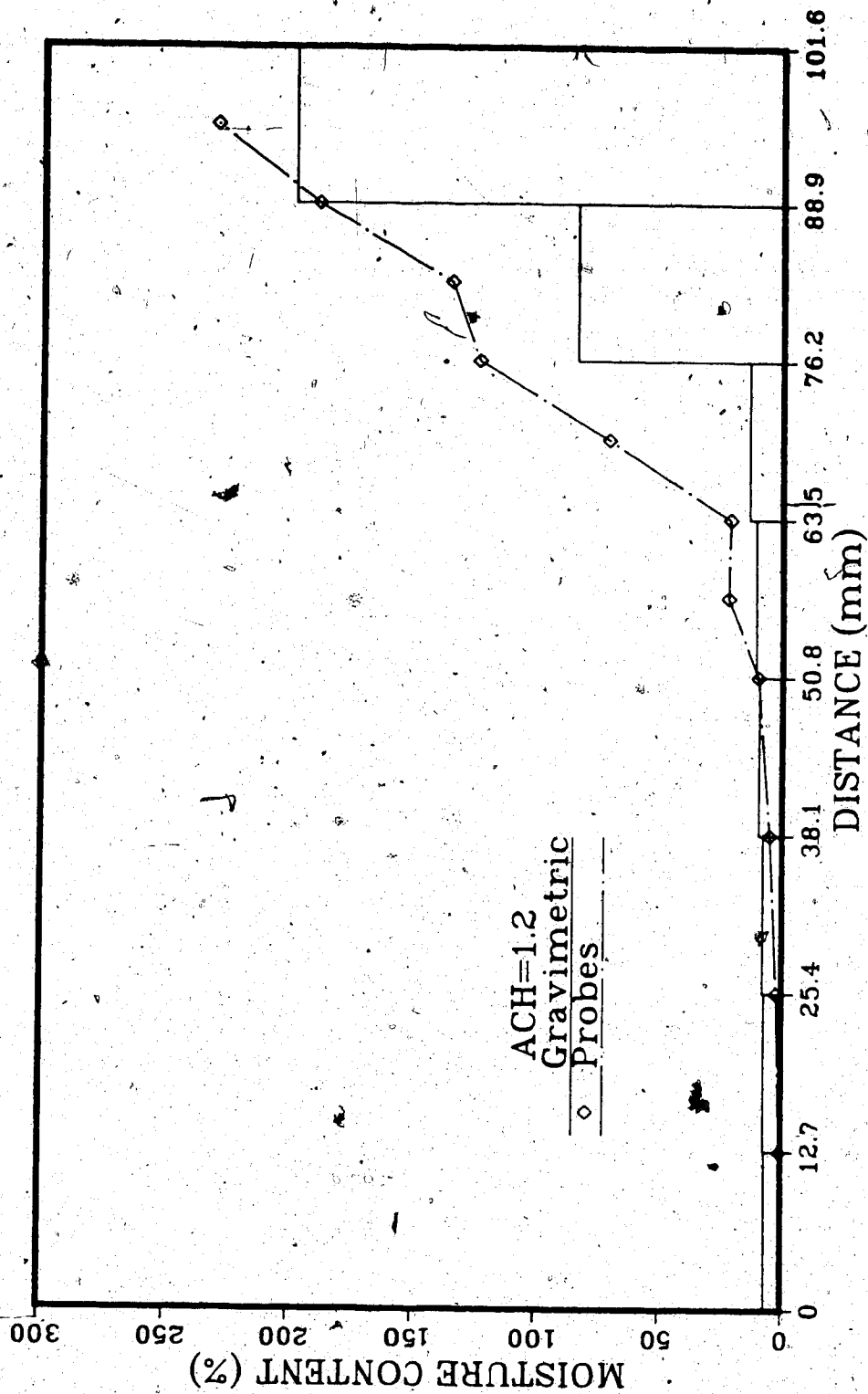


Figure 4.9 Results of the final moisture distribution within the cellulose from gravimetric analysis and probe measurements (ACH=1.2).

of the influence of the high moisture content plane. The probe measurements at or near the interfaces within the cellulose were generally higher than the gravimetric results. Also there are some errors associated with the calibration process and curve fitting of the calibration data. The probe results follow the same trend as the gravimetric analysis. Both results indicate the cellulose was relatively dry starting from the warm boundary but increased suddenly at the interface which corresponds to the 0 °C isotherm within the cellulose as shown later on. The location of the interface was shifted toward the cold boundary as the exfiltration rate increased. The shifting of the interfaces was due to the increase in temperatures within the cellulose because of the higher exfiltration rate. The results of the probe measurement and the gravimetric analysis demonstrated that the probe can be used as a device in measuring the moisture content in porous insulation if properly calibrated.

4.5 Transient Moisture Profile

The transient moisture profiles within the insulation as measured by the probes for each test are illustrated in Figures 4.10 to 4.13. Moisture content near the warm boundary reached the final value very quickly and remained relatively dry; whereas, the moisture content near the cold boundary increased with time. Again the results clearly indicate the existence of an interface

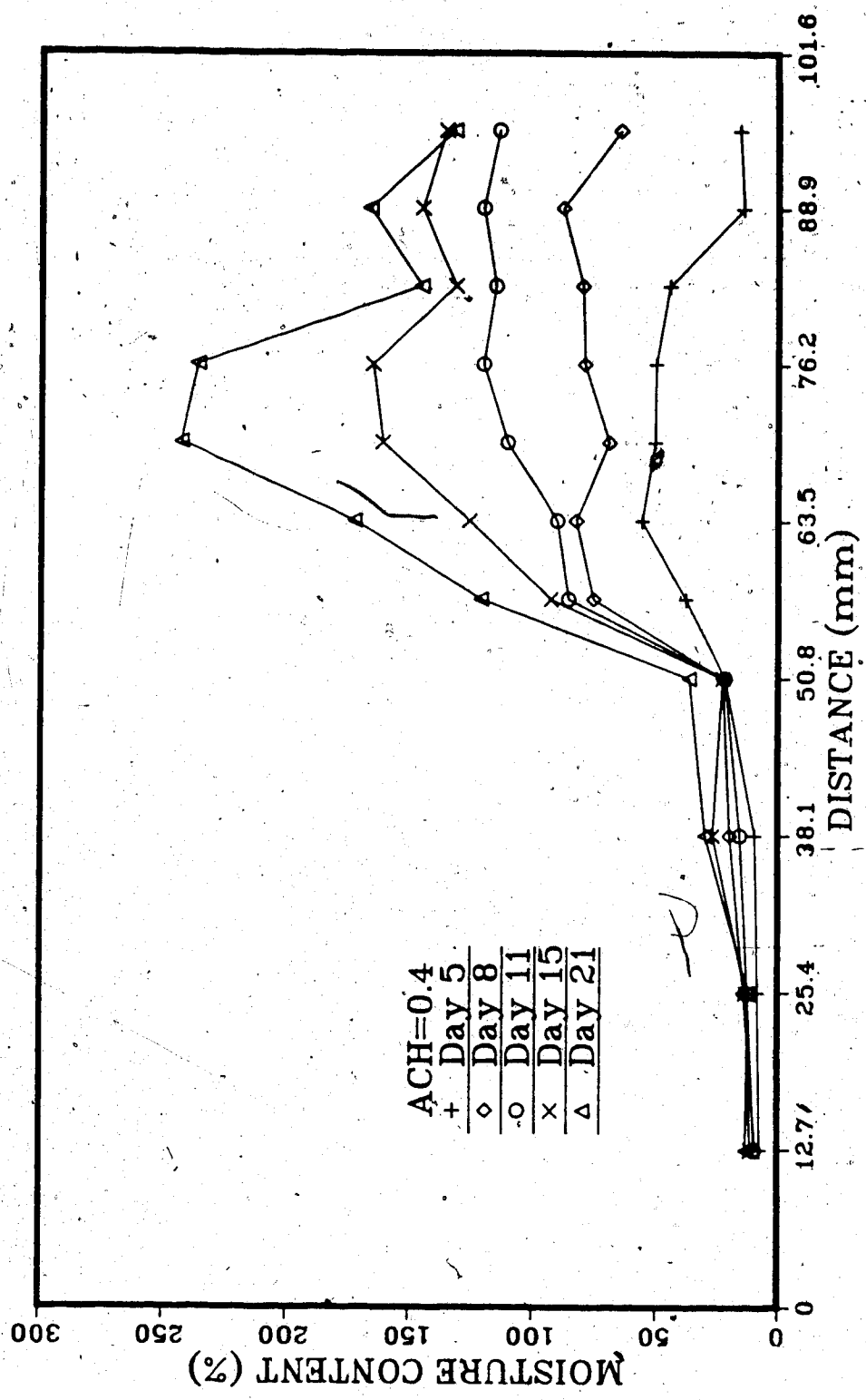


Figure 4.10 The transient moisture profiles as measured by the probes (ACH=0.4).

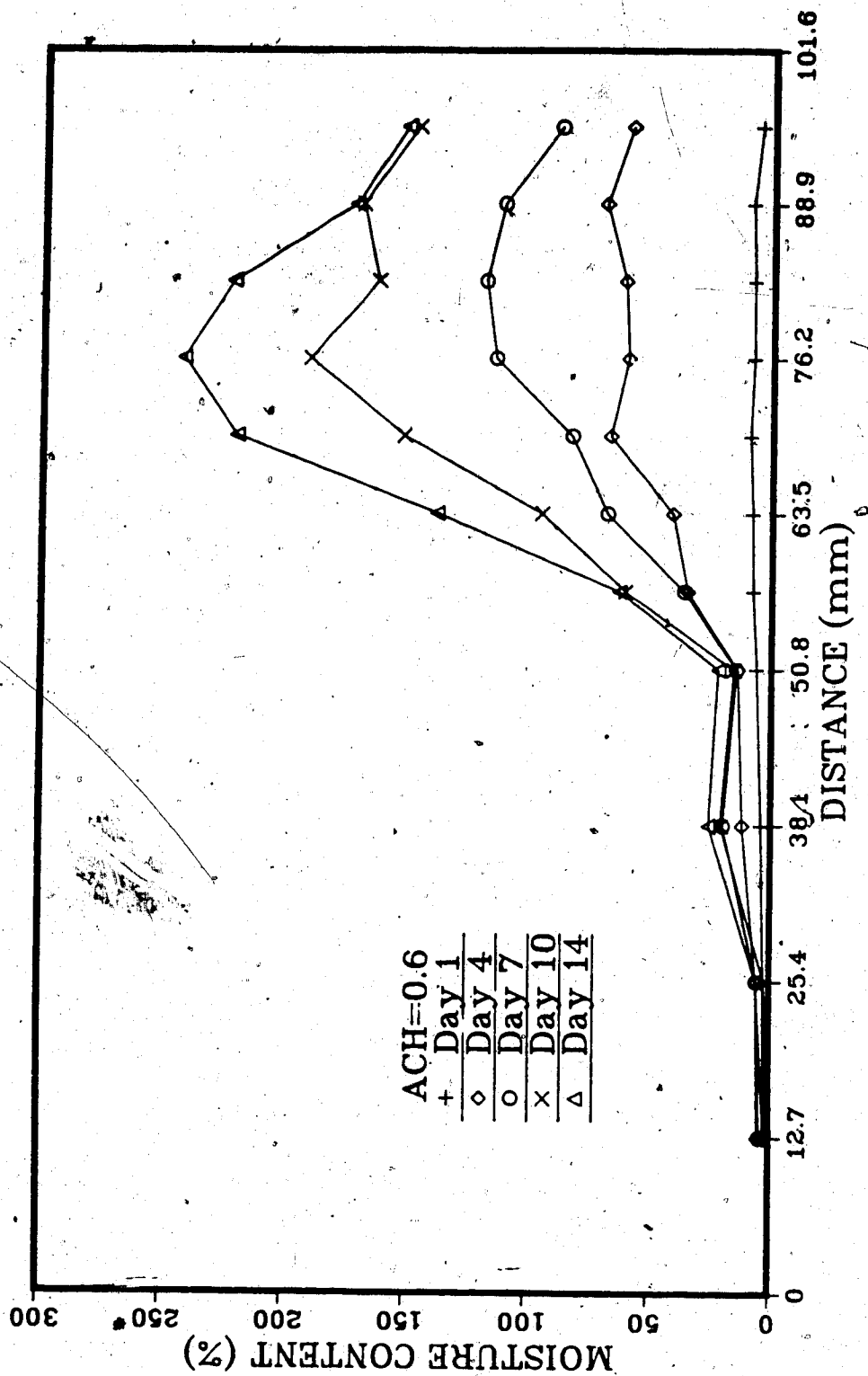


Figure 4.11 The transient moisture profiles as measured by the probes (ACH=0.6).

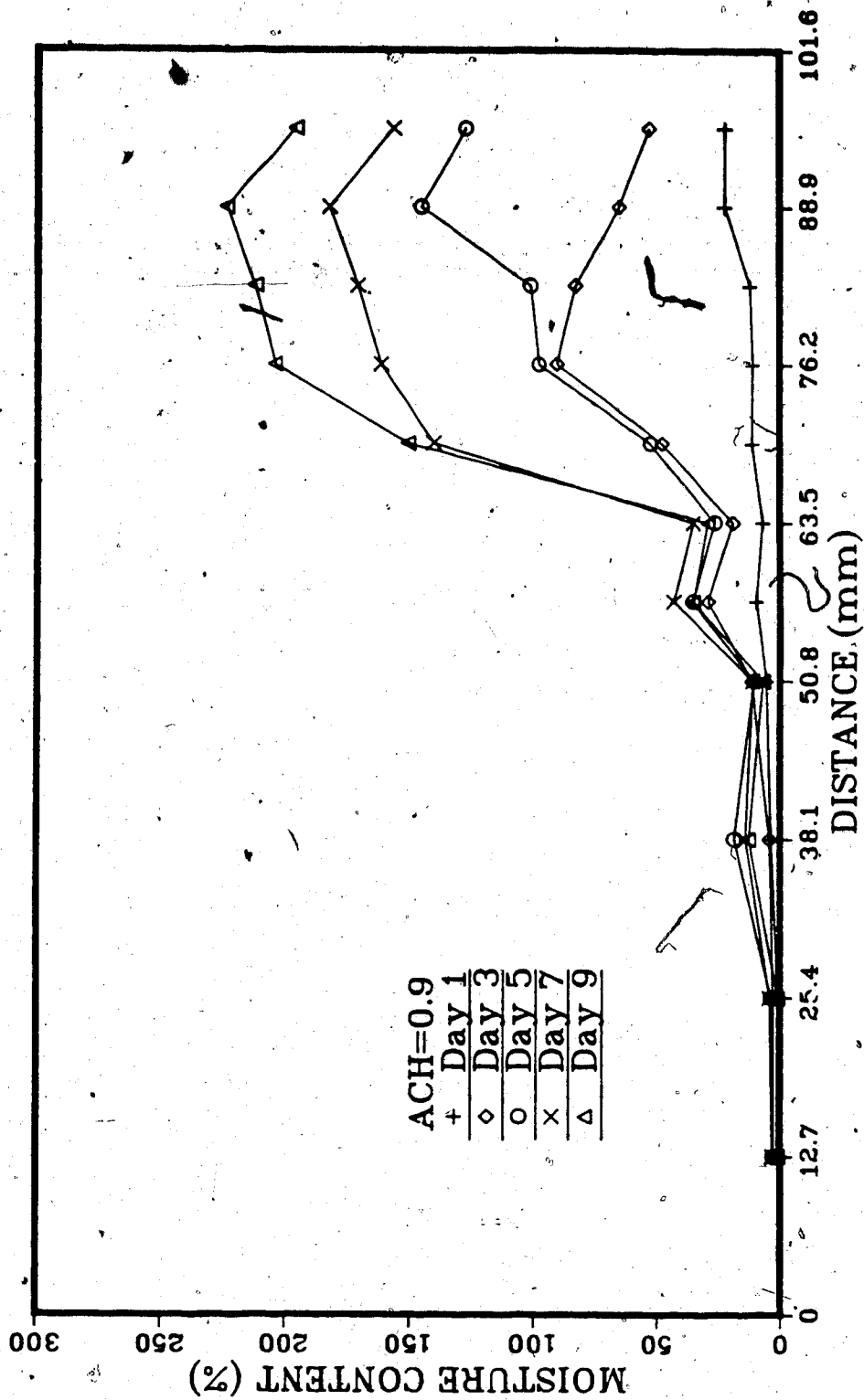


Figure 4.12 The transient moisture profiles as measured by the probes (ACH=0.9).

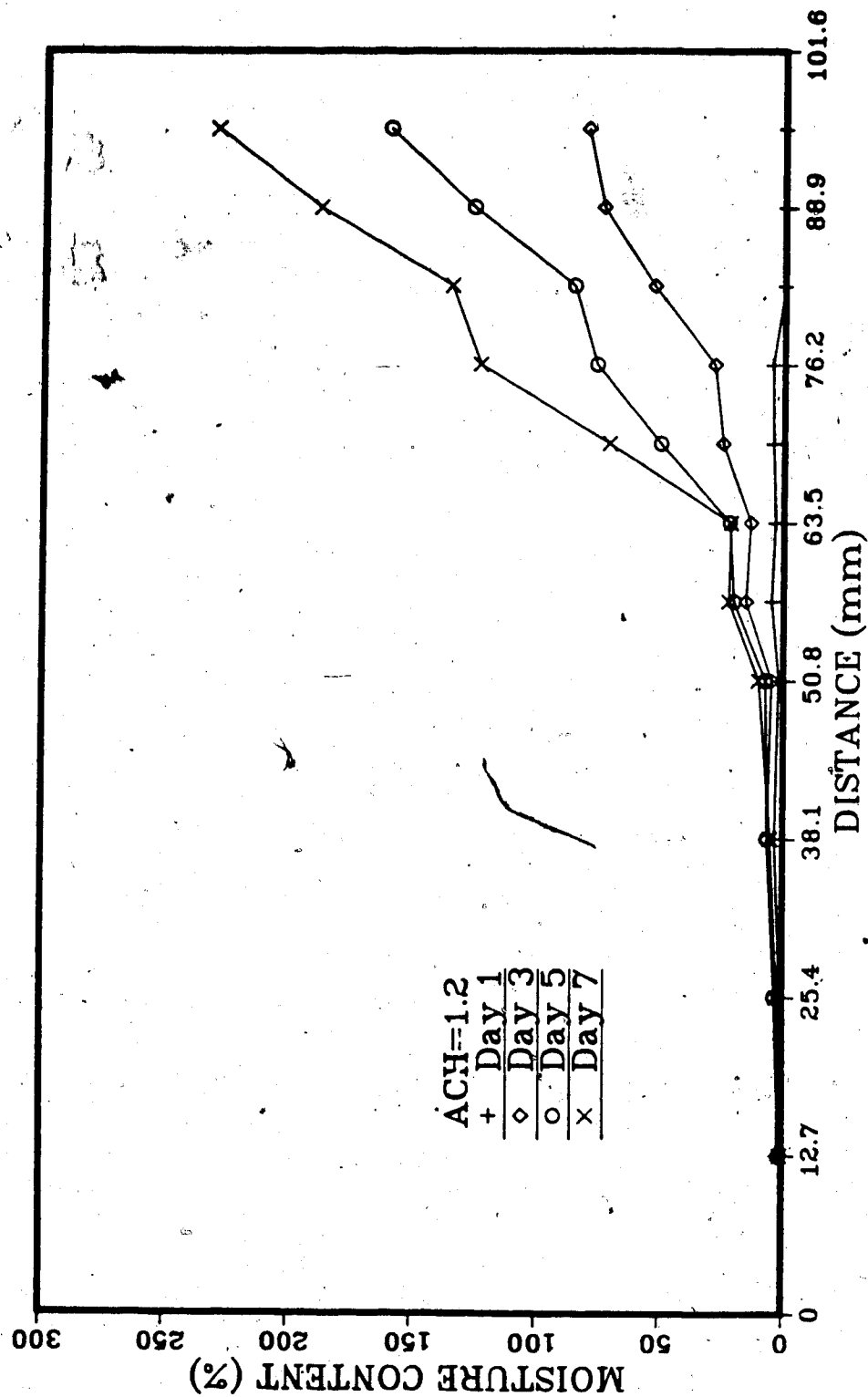


Figure 4.13 The transient moisture profiles as measured by the probes (ACH=1.2).

where the moisture content was low on the warm side of the interface and high, on the cold side. The insulation was divided into a dry and wet portion. This phenomena will be discussed later in this chapter. By integrating the transient moisture profiles as measured by the probes, a moisture accumulation rate was obtained. Figures 4.14 to 4.17 illustrate the moisture accumulation rate for various exfiltration rates. The final results by gravimetric analysis on the overall test sample are also included. Knowing that there was no moisture accumulation at the beginning of each test, a straight line was used to connect the initial moisture accumulation at the start and the final overall moisture accumulation at the end of each test. The results of the daily moisture accumulation obtained by integrating the transient moisture profile appear to follow a straight line, indicating that the moisture accumulation rate within the cellulose was constant during the test period. Undoubtedly, if the moisture accumulation reaches a very large value, the flow resistance of the cellulose will increase because the effective area of the cellulose will decrease. This will result in a reduction of exfiltration rate and a decrease in the moisture accumulation rate. In a recent study by Modi and Benner [1985], moisture gain by spray-applied fiberglass and cellulose exposed to air at relative humidities of 30, 50 and 70 % and temperature differences of 20 and 27 °C, show a constant rate of moisture

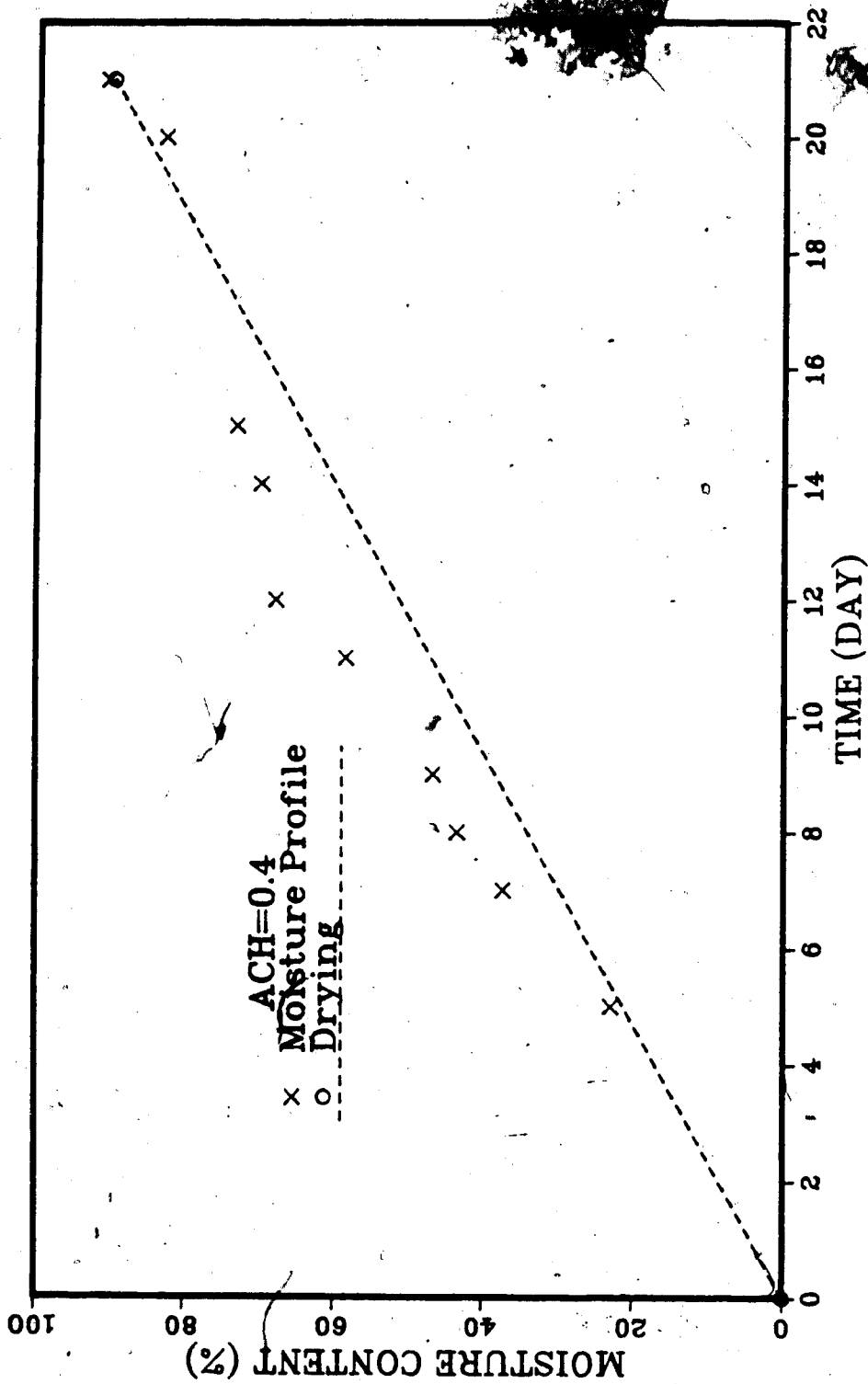


Figure 4.14 Results of the overall moisture accumulation by drying and integration of the transient moisture profiles (ACH=0.4).

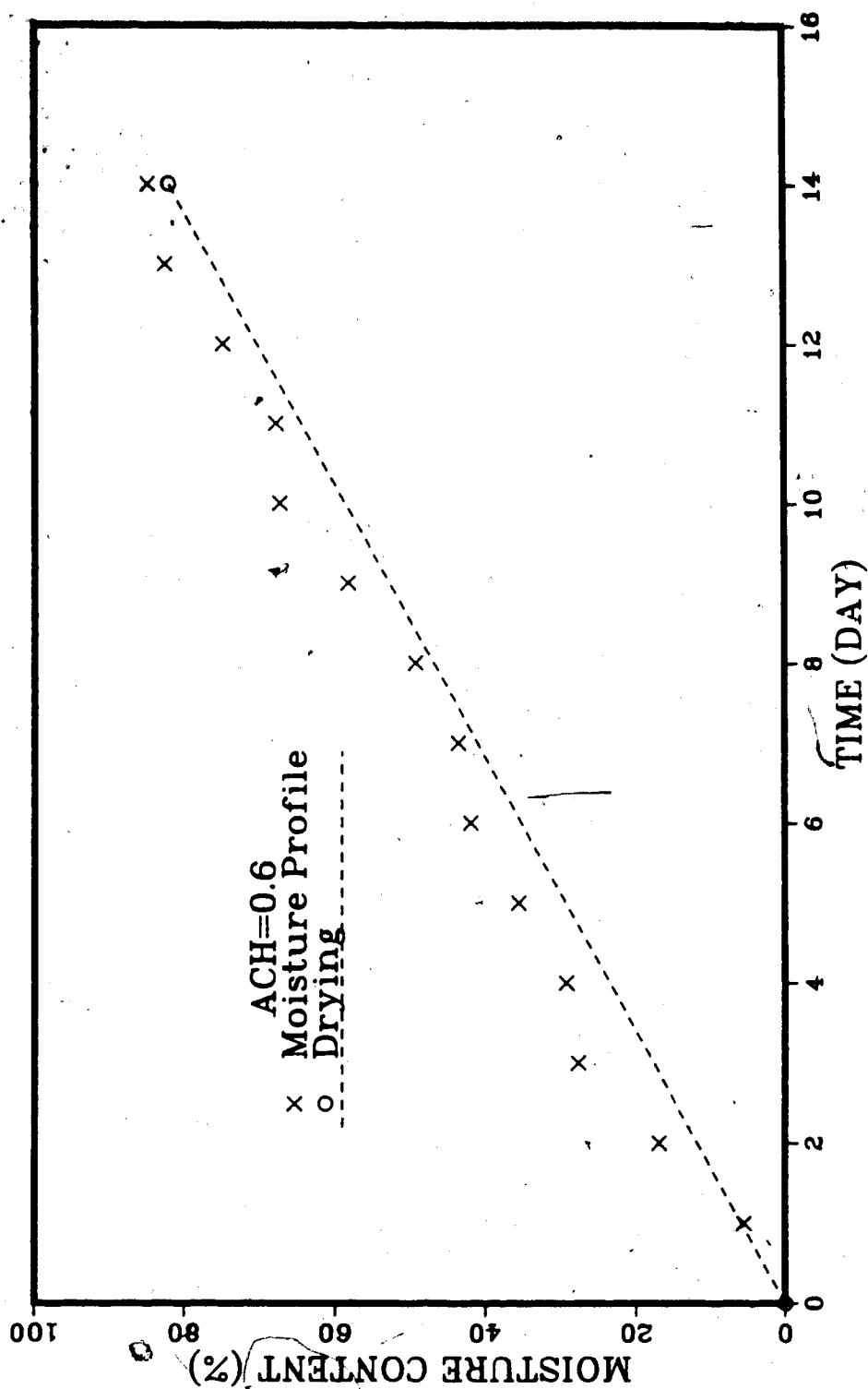


Figure 4.15 Results of the overall moisture accumulation by drying and integration of the transient moisture profiles (ACH=0.6).

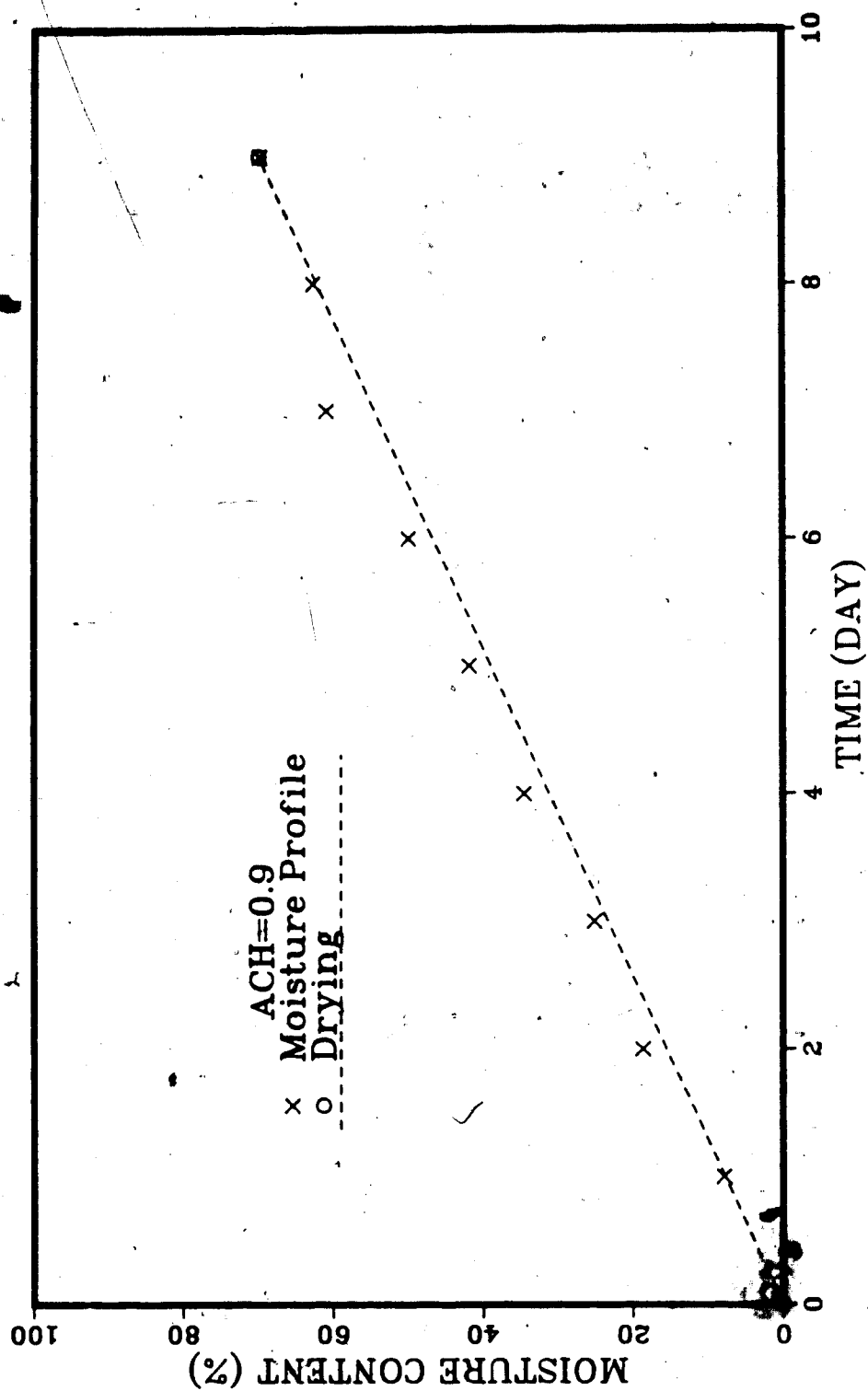


Figure 4.16 Results of the overall moisture accumulation by drying and integration of the transient moisture profiles (ACH=0.9).

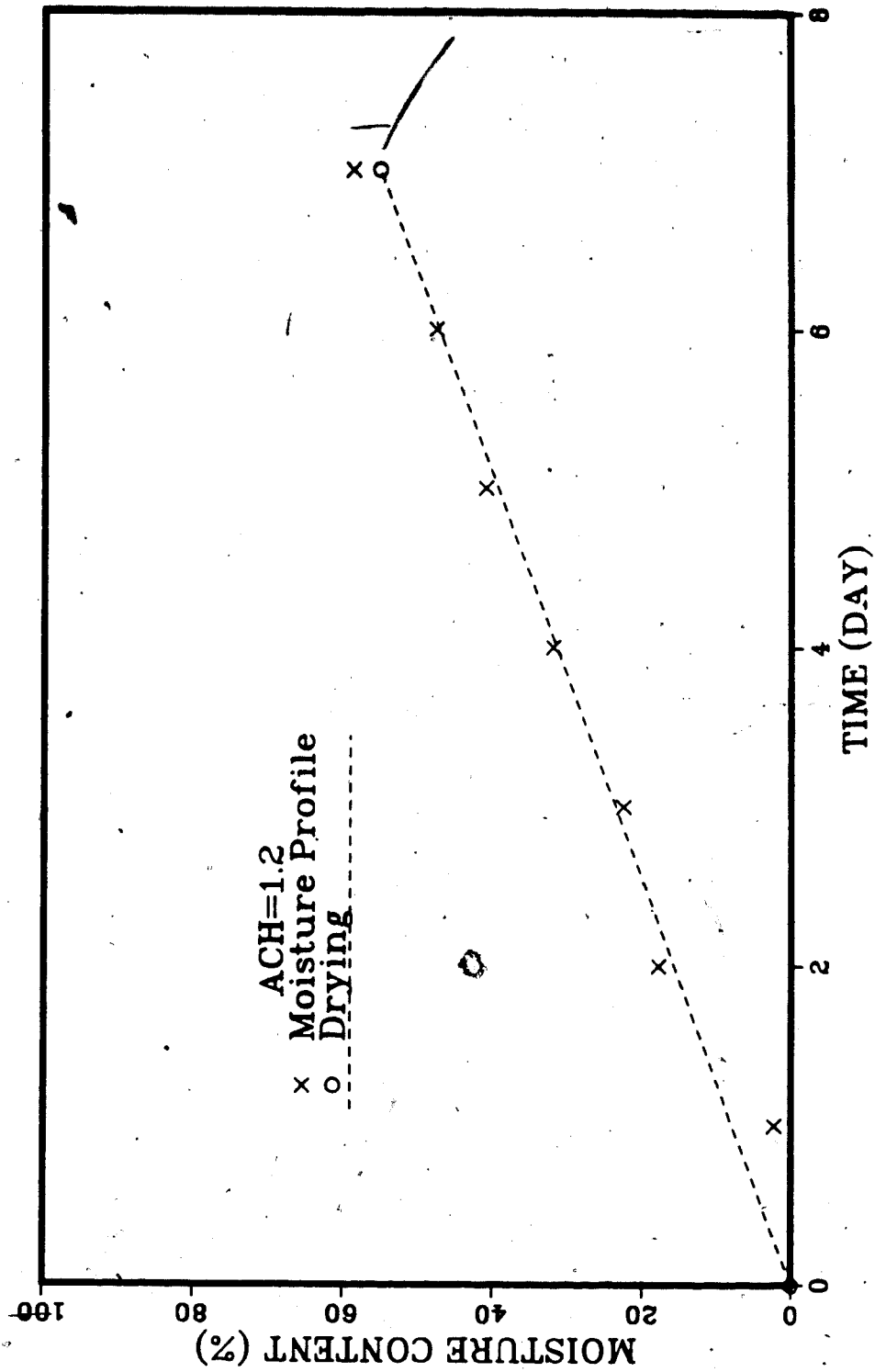


Figure 4.17 Results of the overall moisture accumulation by drying and integration of the transient moisture profiles (ACH=1.2).

accumulation initially but decreased gradually over time. The measured exfiltration rate by the tracer gas decay method was constant during each test. This indicates that very little change occurs in the flow resistance of the cellulose during each test and therefore a constant rate of moisture accumulation is expected. The scatter of the transient moisture accumulation results by integration of the transient moisture profiles in Figures 4.14 to 4.17 is due to spatial variations and gradient effects affecting the probe measurements.

4.6 The Influence of Exfiltration Rate on the Moisture Distribution and Heat Losses

Superposition of the temperature profiles on the final moisture distributions within the insulation shows a definite pattern (Figures 4.18 to 4.21). The results indicate that significant moisture accumulation within the insulation only occurred in the region that was below the freezing point temperature (0°C). The average moisture content within the cellulose above the freezing point temperature remained relatively dry at about 20 % for the duration of each test. Results indicate that little or no condensation occurs between the dew point and 0°C . Also, as the exfiltration rate increased, the internal temperature of the cellulose was raised and the freezing point temperature was pushed further towards the cold boundary. This resulted in a smaller portion of sub-freezing cellulose to allow moisture accumulation.

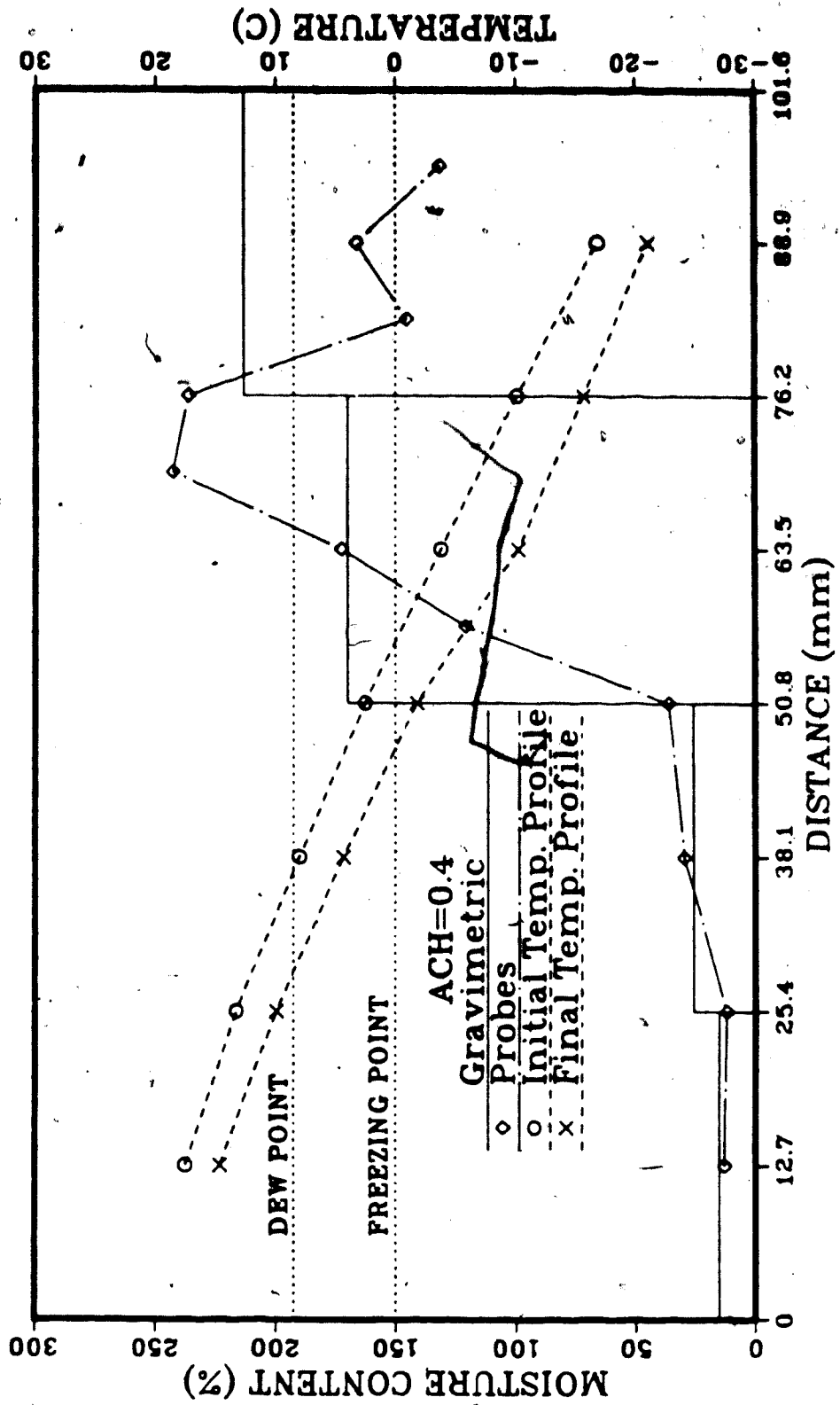


Figure 4.18 Temperature profiles and the final moisture distribution within the cellulose (ACH=0.4).

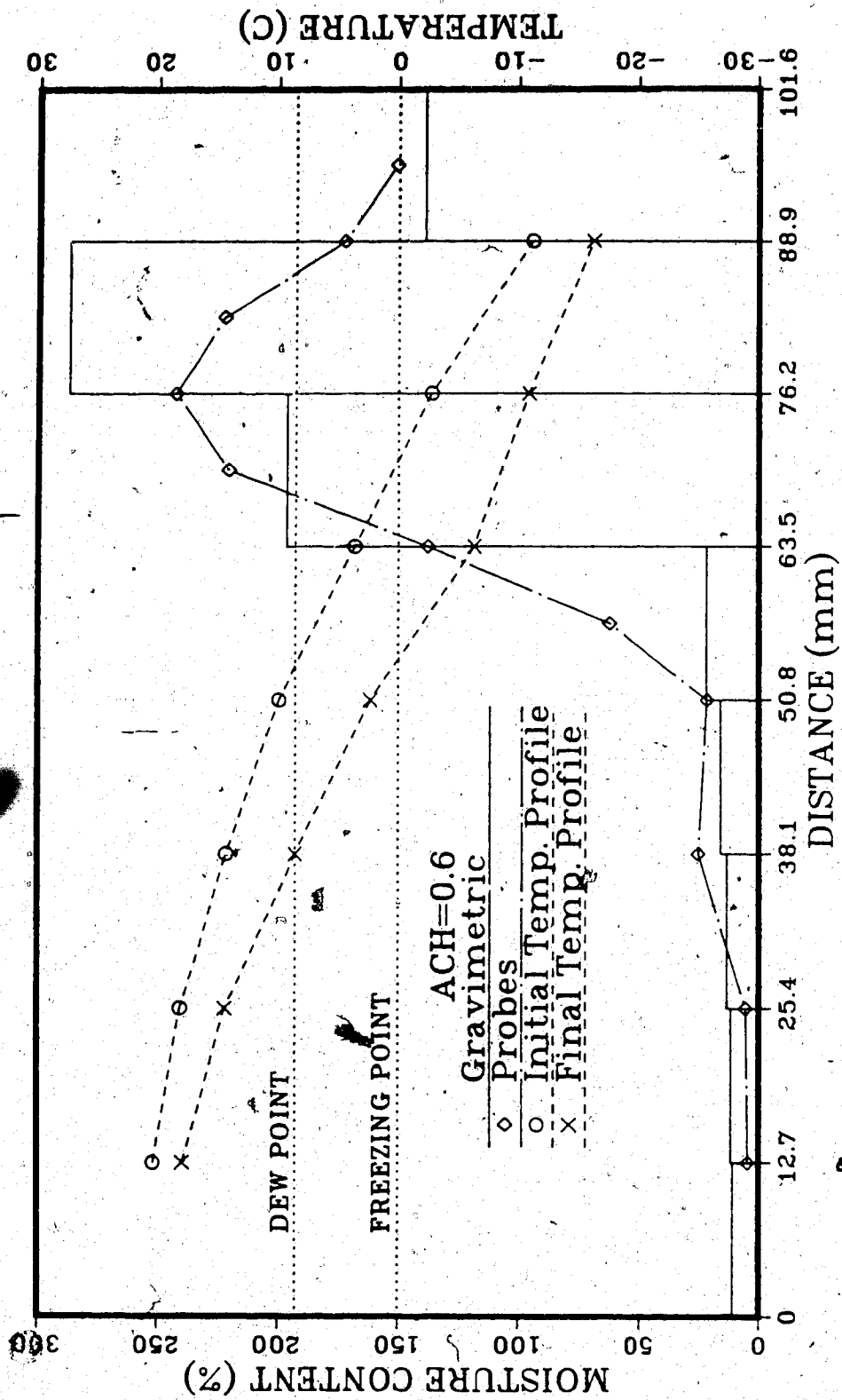


Figure 4.19 Temperature profiles and the final moisture distribution within the cellulose (ACH=0.6).

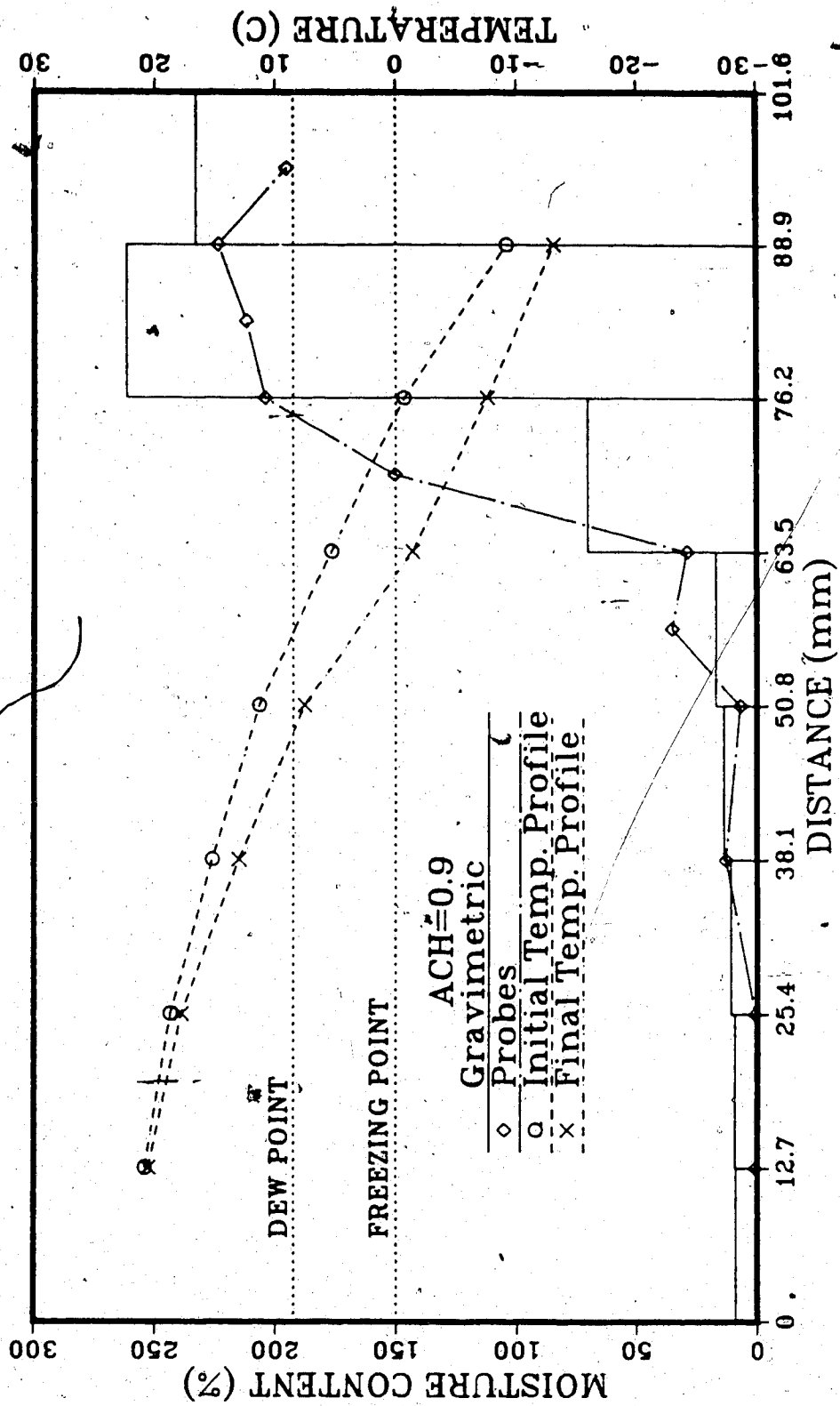


Figure 4.20 Temperature profiles and the final moisture distribution within the cellulose (ACH=0.9)

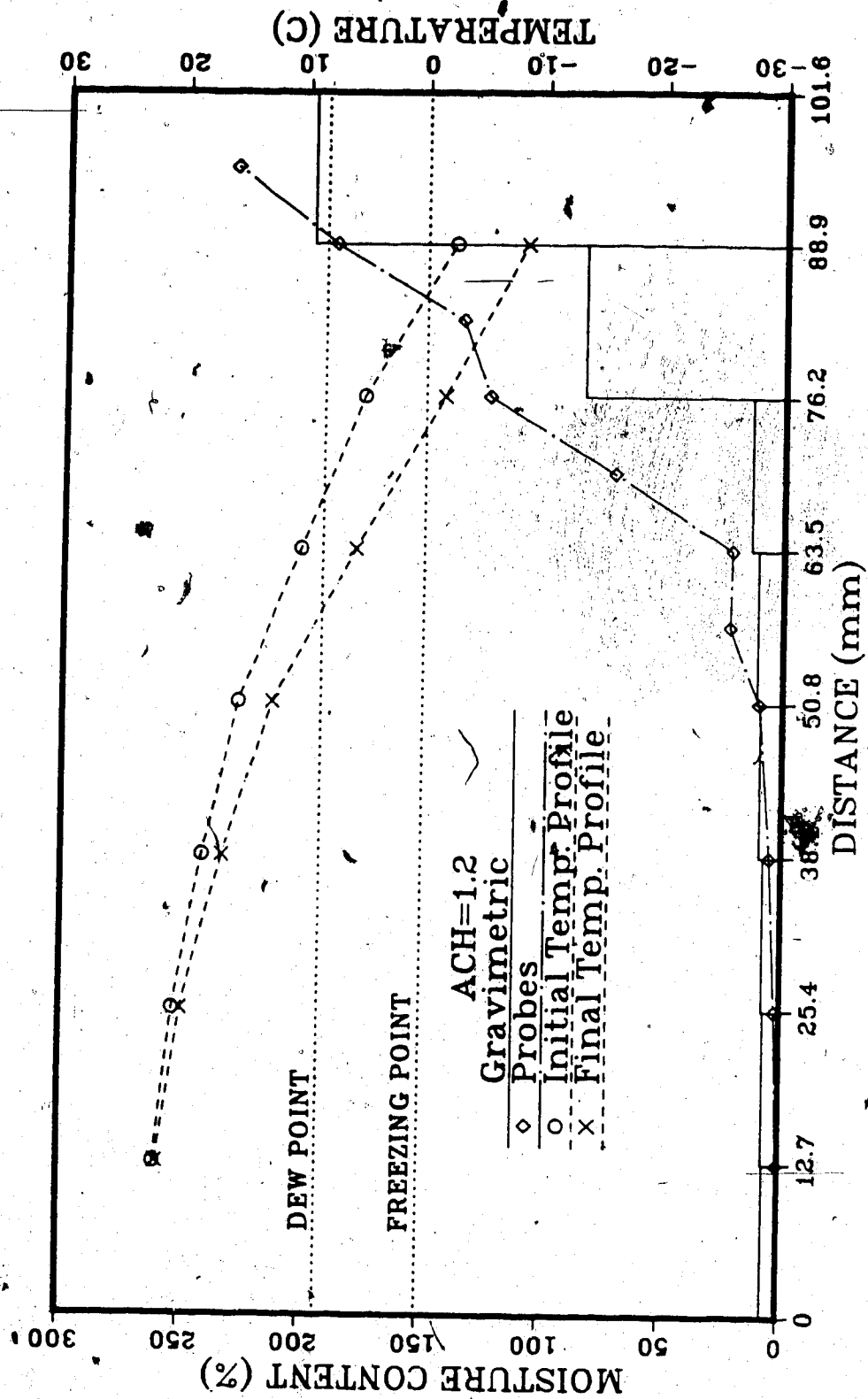


Figure 4.21 Temperature profiles and the final moisture distribution within the cellulose (ACH=1.2).

Figures 4.22 and 4.23 show the total moisture accumulation obtained from drying for each test plotted against the exfiltration rate (ACH) and number of air changes, respectively. Since the total number of air changes for all tests were the same, the total amount of moist air that flowed through the cellulose was the same for each test. However, results indicate that the total moisture accumulation decreased as exfiltration rate increased. The results reinforce the explanations mentioned earlier that as exfiltration rate increased, the thickness of the frozen layer decreased because the 0 °C isotherm was closer to the cold side.

Table 4.6 summarizes the exfiltration rate and amount of water consumed during each test as well as the overall moisture accumulation obtained from drying of the test sample. The results generally show that a smaller fraction of the water vapour passing through the cellulose condensed and froze as exfiltration rate increased. The temperature profiles in Figures 4.2 to 4.5 indicate that as the exfiltration rate increased, the temperature of the air leaving the cellulose on the cold boundary also increased. If the air leaving the cellulose is assumed to be saturated, then as the exfiltration rate increased, more moisture was carried by the air into the cold room. This resulted in less overall moisture accumulation within the insulation.

From the results presented so far, it seems that

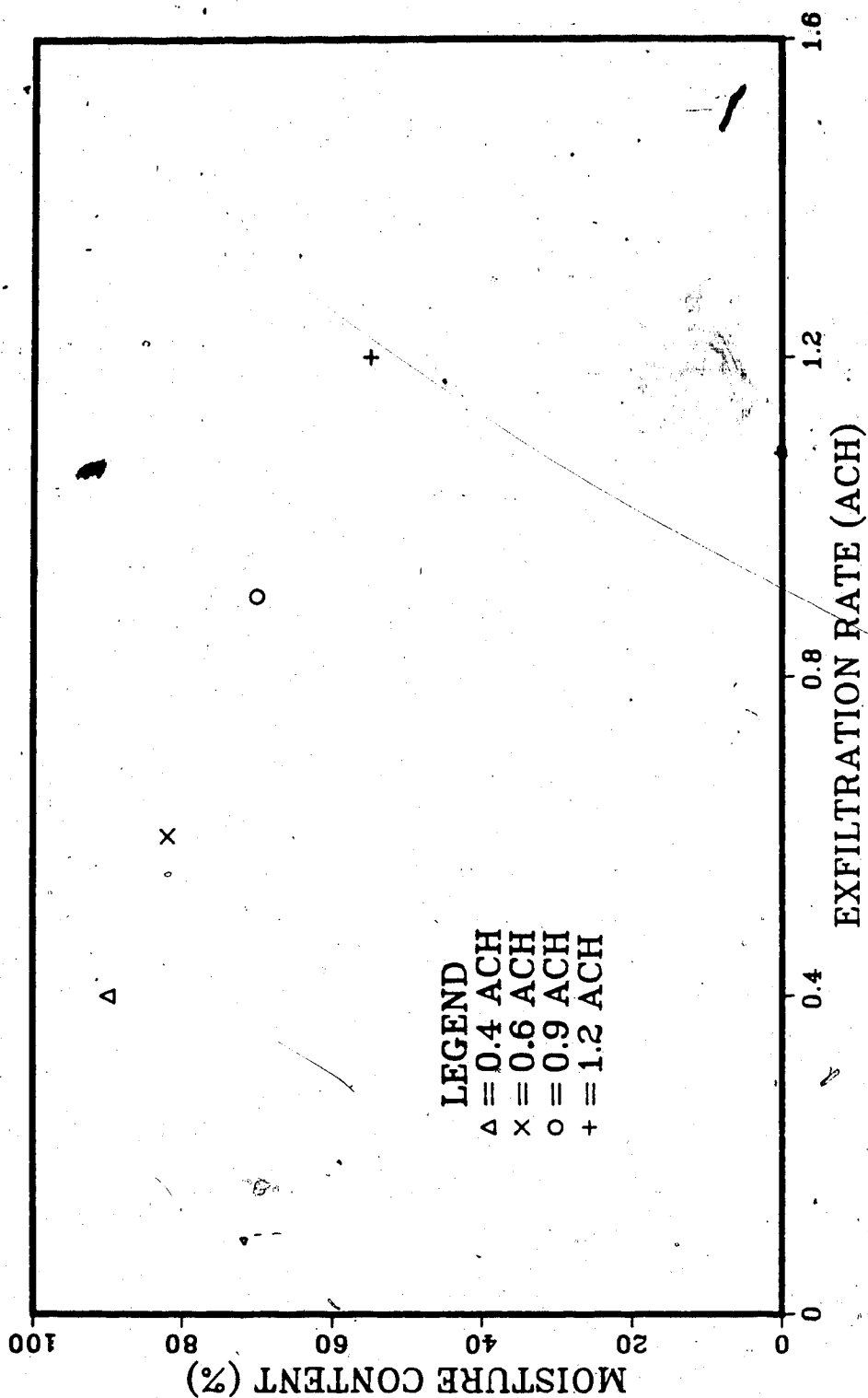


Figure 4.22 Overall moisture accumulation versus exfiltration rate for each test.

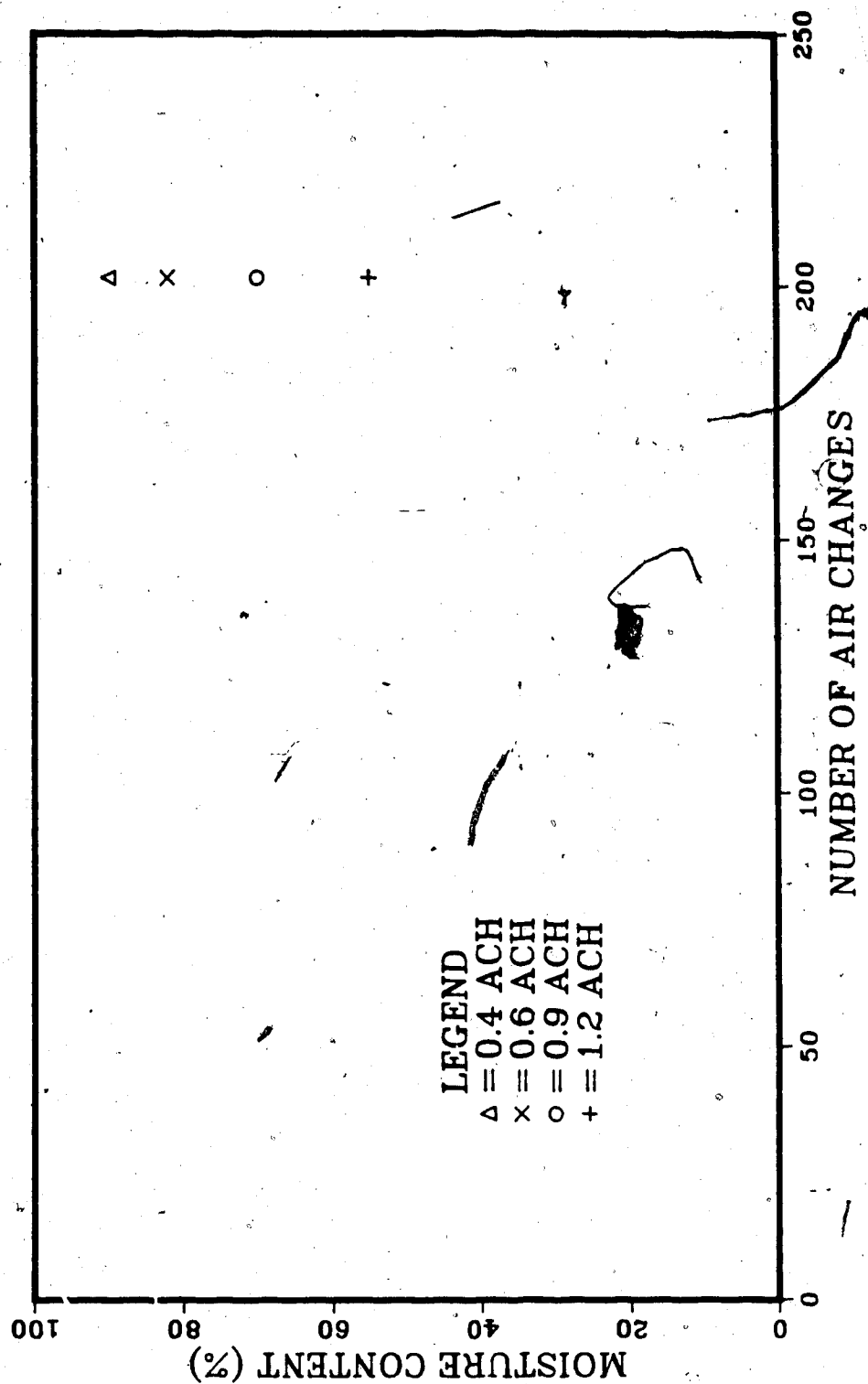


Figure 4.23 Overall moisture accumulation versus total number of air changes for each test.

Table 4.6 Summary of the overall moisture accumulation and water consumption for each test.

Exfiltration Rate (ACH)	0.4	0.6	0.9	1.2
Duration of the test (hours)	504	336	224	168
Total Water Consumption (mL)	1332	1352	1410	1437
Total Amount of Moisture Accumulation (g)	1041	948	809	636
Total Moisture Accumulation as % of Water Consumption (%)	78	70	57	44

Table 4.7 Thickness of the frozen portion of the cellulose by locating the 0 °C

Exfiltration Rate (ACH)	0.4	0.6	0.9	1.2
Thickness of the Frozen Portion from the Temperature Profile (mm)	54.6	47.3	40.0	28.3

the average moisture content in the unfrozen portion of the cellulose equilibrated quickly at about 20 % by weight. Using the measured temperature profile and locating the 0 °C isotherm, the thickness of the frozen portion can be estimated for each test (Table 4.7). The results given in Table 4.7 indicate a significant decrease in the thickness of the frozen portion with an increase in the exfiltration rate. Subtracting the 20 % moisture content in the unfrozen portion from the overall moisture accumulation and dividing by the dry weight of the frozen portion yields an average moisture content of 150 ± 5 % within the frozen portion for each test. Averaged over the entire test period, that is approximately 0.75 % moisture by weight accumulated in the frozen portion per air change.

The tests that were performed in this investigation represent a special situation where part of the insulation was below freezing. The situation is typical of Canadian winters where the outside temperature is normally below freezing. The process of moisture migration and accumulation for insulation experiencing above freezing and sub-freezing temperature is different. Gupta and Churchill [1977] have pointed out that if the temperature within porous insulation is above freezing, then moisture will migrate from the warm temperature side towards the cold temperature side and results in a build-up of moisture at the cold side where condensation

occurs. Because of the high concentration of moisture at the cold side, a migration of moisture in the opposite direction can occur due to gravity and capillary action. However, in the case where part of the insulation is below freezing temperature, the moisture still migrates from the warm temperature side towards the cold temperature side, but the moisture will be solidified after reaching the 0°C isotherm. Significant moisture migration in the reverse direction does not occur. Also at below 0°C , the vapour pressure over ice is lower than that over water at the same temperature. For example, at -5°C , the saturation vapour pressure over ice is approximately 402 Pa as compared to 422 Pa over water. Thus, the vapour pressure in the frozen portion of the insulation is lower than the vapour pressure in the above freezing portion. With this constant vapour pressure difference, moisture tends to diffuse from higher to the lower vapour pressure region. Therefore, the sub-freezing portion of the insulation where moisture is frozen continues to act as a "sink" for both heat and moisture transfer. If the sub-freezing temperature gradient is maintained long enough, almost all the moisture in the above freezing temperature portion of the insulation will migrate towards the sub-freezing portion. Therefore, the portion of the insulation where the temperature is above freezing will be relatively dry and the sub-freezing portion will have high moisture content in the form of frost or ice.

At the end of each test, the cellulose was carefully examined for the extent of moisture accumulation. No visible settling of the cellulose was noted nor any visible liquid water was found anywhere within the cellulose. The top portion of the cellulose was frozen together and easily peeled away from the bottom portion where the cellulose remained relatively dry and loose (Plate 4.1). Extensive frost formation within the frozen portion of the cellulose was found in each test (Plates 4.2 and 4.3). The results of the probe measurement, the gravimetric analysis and the temperature profile indicate that the thickness of the frozen layers correspond to the 0 °C isotherms and confirm the moisture transfer mechanism mentioned previously. These results suggest that if the boundary temperatures were constant, the frozen layer will increase or decrease in thickness when the filtration velocity is changed. The moisture front occurred at the 0 °C isotherm and significant moisture accumulation and formation of frost within the cellulose only began at the interface onward to the cold boundary. Results of this kind can form the basis for a model to predict moisture accumulation within porous insulation. By knowing the exfiltration rate and the temperature profile within the cellulose, the 0 °C isotherm can be located and the average moisture build-up within the frozen and unfrozen portions of the cellulose can be estimated. The present investigation only provided



Plate 4.1. Photo showing the top frozen portion of the cellulose separated easily from the bottom dry portion.

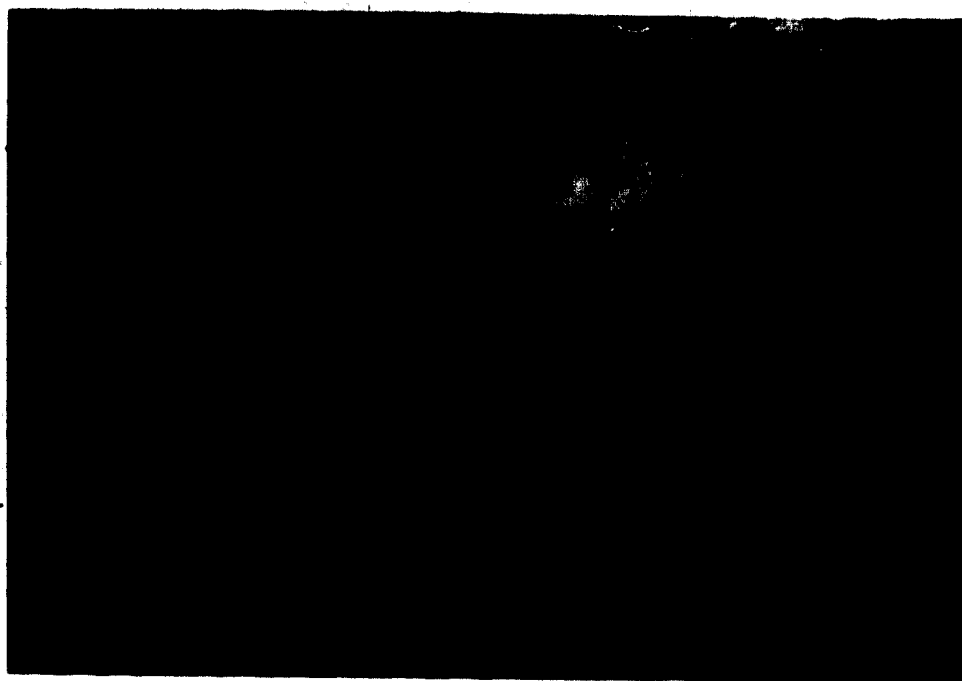


Plate 4.2 Photo of the frost formation within the cellulose under a microscope.



Plate 4.3 Photo of the frost formation within the cellulose under a microscope.

some more insights into the process of moisture migration and accumulation in porous insulation. Testing of different materials at various orientations and test conditions are needed to accurately model the moisture problems in buildings.

Looking at the tests from the energy point of view, the convective heat losses associated with exfiltration is given as

$$Q_e = q \rho C_p \Delta T \quad (4.3)$$

where Q_e is the heat loss in W, q is the flow rate of the air in m^3/s , ρ is the density of the air in kg/m^3 , C_p is the specific heat of the air in $\text{J}/\text{kg}\cdot\text{K}$, and ΔT is the temperature difference in K. The exfiltrative heat loss are 5.6, 8.3, 12.5 and 16.6 W for the 0.4, 0.6, 0.9 and 1.2 ACH test respectively. The conductive heat loss is estimated from Fourier's Law

$$Q_c = -k A \frac{\Delta T}{\Delta x} \quad (4.4)$$

where Q_c is the conductive heat loss in W, k is the effective thermal conductivity of the cellulose in $\text{W}/\text{m}\cdot^\circ\text{C}$, A is the cross-sectional area in m^2 and $\Delta T/\Delta x$ is the temperature gradient in $^\circ\text{C}/\text{m}$. The value for the effective thermal conductivity is approximated from Equation 3.1 at the mean temperature and moisture content existed within

the cellulose. The temperature gradient is estimated from the measured temperature profile. The respective conductive heat losses for the 0.4, 0.6, 0.9 and 1.2 ACH are 7.3, 6.8, 6.6 and 5.9 W. The latent heat loss due to the release of latent heat when moisture accumulated within the cellulose can be approximated by

$$Q_L = \dot{m}_m L \quad (4.5)$$

where Q_L is the latent heat loss in W, \dot{m}_m is the rate of moisture accumulation within the cellulose in kg/s and L is the latent heat in J/kg. The latent heat losses are 1.7, 2.3, 2.9 and 3.0 W for the 0.4, 0.6, 0.9 and 1.2 ACH ~~test~~ respectively. Table 4.8 summarizes the heat losses due to various components for each test. The total heat loss increases with the exfiltration rate. Clearly, as the exfiltration rate increased, more heat energy was supplied to the cellulose and the internal temperature was ~~raised~~. By warming up the cellulose, the overall moisture accumulation was reduced at the expense of higher heat losses.

4.7 Summary

By varying only the exfiltration rate, results of the temperature profiles, moisture distributions and overall moisture accumulations within the cellulose from each test can be compared and analysed. The temperature

Table 4.8 Summary of estimated heat losses due to convection, conduction and latent heat for each test.

Exfiltration Rate (ACH)	0.4	0.6	0.9	1.2
Convective Heat Loss (W)	5.6	8.3	12.5	16.6
Conductive Heat Loss (W)	7.3	6.8	6.6	5.9
Latent Heat Loss (W)	1.6	2.2	2.8	3.0
Total Heat Loss (W)	14.5	17.3	21.9	25.5

profiles show that the temperatures within the cellulose increased with the exfiltration rate. The final moisture distribution within the cellulose obtained from the gravimetric analysis agreed with the probe measurements taken at the end of each test. Results of the moisture distributions and the corresponding temperature profile indicate that significant moisture accumulation within the cellulose occurred only at the portion of the cellulose where the temperature was below freezing. The transient moisture distributions as measured by the probes also indicate that moisture accumulation equilibrated quickly at about 20 % within the portion of the cellulose that was above freezing, but increased with time at the sub-freezing portion of the cellulose. The results of the moisture build-up within the cellulose with respect to time appeared to follow a straight line, indicating that the rate of moisture accumulation was constant for the duration of the test. This result of constant rate of moisture accumulation was supported by a fairly uniform exfiltration rate as measured by the gas analyser during the test. With higher exfiltration rate, the temperature of the air leaving the cellulose was also increased. If the air leaving the cellulose is assumed to be saturated, then more moisture was carried by the air into the cold room. Therefore, the overall moisture accumulation decreased as the exfiltration rate increased.

Observations made at the end of each test show no

visible liquid water within the cellulose. The top portion of the cellulose was frozen together with extensive frost formation while the bottom portion remained dry and loose. The existence of a distinct dry and wet portion within the cellulose tends to confirm the theory that sub-freezing temperature within the porous insulation acts as a "sink" for moisture transfer and eventually dries up the moisture in the above freezing portion of the porous insulation. Results show a roughly 20 % moisture content within the dry portion and 150 % within the wet portion of the cellulose at the end of each test. The consistent pattern suggests the possibility of a model to predict the moisture migration and accumulation in porous insulation. However, more experimental data at different test conditions are needed to complete such a model.

CHAPTER 5

CONCLUSIONS AND RECOMMENDATIONS

The influence of the exfiltration rate on the amount and distribution of moisture within a slab of 102 mm thick cellulose fibre insulation was studied. With both the temperatures and humidities on either side of the cellulose and the total amount of moist air exfiltrated through the cellulose held the same in each test, the following conclusions can be drawn from the results.

1) Higher exfiltration rates result in more energy being supplied to the insulation and therefore less overall moisture accumulation.

2) Sub-freezing temperatures within the cellulose behave as a "sink" for moisture accumulation; therefore, the cellulose was separated into a wet (150 % moisture content by weight) and dry (20 % moisture content by weight) portion.

3) Visual inspection at the end of each test showed no visible liquid condensation anywhere within the cellulose. The absence of liquid condensation between the dew point and freezing point temperatures within the cellulose suggests a strong local diffusional effect that drives the moisture into the sub-freezing portion of the cellulose.

4) Convective heat loss associated with exfiltration

of warm air represents a major portion of the total heat loss.

Results from the present investigation suggest the possibility of a model in predicting the process of moisture migration and accumulation in porous materials. However, moisture migration in building under real life conditions are far more complex. With the interaction of wind, cyclic environmental conditions, multi-dimensional heat and mass transfers, non-uniform leakage characteristics of the building envelope, etc., prediction of moisture migration becomes a very difficult task. The need to simplify the problem without losing any generality is a must for any model. A systematic testing of porous materials in different orientations and environments is essential to gain more insight and better understanding of the process of moisture migration and accumulation in buildings. With more laboratory results and analytical studies on the subject, moisture problems in buildings can be resolved without affecting the living comfort.

REFERENCES

- ASHRAE Handbook of Fundamentals, American Society of Heating, Refrigerating, and Air-Conditioning Engineers, Inc., 1981.
- ASTM C177-76, "Standard Test Method for Steady-State Thermal Transmission Properties by Means of the Guarded Hot Plate," Annual Book of ASTM Standards, Vol. 04.06, American Society for Testing and Materials, 1985.
- ASTM E741-83, "Standard Test Method for Determining Air Leakage Rate by Tracer Dilution," Annual Book of ASTM Standards, Vol. 04.07, American Society for Testing and Materials, 1985.
- ASTM C666-73, "Standard Test Method for Resistance of Concrete to Rapid Freezing and Thawing," Annual Book of ASTM Standards, Vol. 04.02, American Society for Testing and Material, 1985.
- Berlad, A.L., Tutu, N., Yeh, Y-J., Jaung, R., Krajewski, R., Hoppe, R., and Salzano, F.J., "Air Intrusion Effects on the Performance of Permeable Insulation System," Thermal Insulation Performance, ASTM STP 718, D.L. McElroy and R.P. Tye, Eds. American Society for Testing and Materials, 1980, pp.181-194.
- Carslaw, H.S., and Jaeger, J.C., Conduction of Heat in Solids, Second Edition, Oxford University Press, New York, 1959, pp.256-262.
- Dechow, F.J. and Epstein, K.A., "Laboratory and Field Investigations of Moisture Absorption and Its Effect on Thermal Performance of Various Insulations," ASTM STP 660, R.P. Tye, Ed., American Society for Testing and Materials, 1978, pp.234-260.
- Dworjadkin, A. and Malinowski, R., "Volume Changes of Light Weight Cellular Concrete by Repeated Wetting and Drying," Moisture Problems in Buildings, RILEM/CIB Symposium, Helsinki, 1965, Report 2-35.
- Ford, J.K., "Humidity Measurement and Modeling In Residential Attic," ASTM STP 779, Moisture Migration in Buildings, M. Lieff and H.R. Trechsel, Eds. American Society for Testing and Materials, 1982, pp.160-190.

- Gupta, J.P. and Churchill, S.W., "Moisture Transfer in Porous Medium under a Temperature Gradient," Energy Conservation in Heating, Cooling, and Ventilating Buildings, Vol. 1, C.J. Hoogendoorn and N.H. Afgan, Eds. 1978, pp.71-81.
- Gurr, C.G., Marshall, T.J., and Hutton, J.R., "Movement of Water in Soil due to a Temperature Gradient," Soil Science, 74(5), Nov. 1952, pp.335-45.
- Handegord, G.O.P., "Prediction of Moisture Performance of Walls," ASHRAE Transactions, Vol. 91, 1985, pp.1501-1508.
- Huang, C.L.D., Siang, H.H., and Best, C.H., "Heat and Moisture Transfer in Concrete Slabs," Int. J. Heat Mass Transfer, Vol. 22, 1979, pp.257-266.
- Hutcheon, N.B., and Handegord, G.O.P., Building Science for a Cold Climate, John Wiley and Son, 1983, p.28.
- Joy, F.A., "Thermal Conductivity of Insulation Containing Moisture," Symposium on Thermal Conductivity, ASTM STP 217, American Society for Testing and Materials, 1957, pp.65-80.
- Klute, A., "A Numerical Method for Solving the Flow Equation for Water in Unsaturated Materials," Soil Science Vol. 73, 1952, pp.105-116.
- Langlais, G., Hyrien, M., and Klarsfeld, S., "Influence of Moisture on Heat Transfer Through Fibrous-Insulating Materials," Thermal Insulation, Materials, and Systems for Energy Conservation in the '80s, ASTM STP 789, F.A. Govan, D.M. Greason, J.D. McAllister, Eds., American Society for Testing and Materials, 1983, pp.563-581.
- Lowe, P.R., "An Approximating Polynomial for the Computation of Saturated Vapour Pressure," J. Appl. Meteor., Vol. 16, 1977, pp.100-103.
- Modi, D.K. and Benner, S.M., "Moisture Gain of Spray-Applied Insulations and Its Effect on Effective Thermal Conductivity --Part 1," Journal of Thermal Insulation, Vol. 8, 1985, pp.259-277.
- Niskanen, E., "On the Strength and Elasticity Characteristics of Finnish Structured Birch Plywood as a Function of Moisture Content," Moisture Problems in Buildings, RILEM/CIB Symposium, Helsinki, 1965, Report 1-5.

Ogniewicz, Y., and Tien, C.L., "Analysis of Condensation in Porous Insulation," Int. J. Heat Mass Transfer. Vol. 24, 1981, pp.421-430.

Shuman, E.C., "Some Effects of Moisture Migration and Persistence in Building Materials," Moisture Migration in Buildings, ASTM STP 779, M. Iieff and H.R. Trechsel, Eds., American Society for Testing and Materials, 1982, pp.65-79.

Sneck, T., "Corrosion of Metals in Buildings as a Moisture Problem," Moisture Problems in Buildings, RILEM/CIB Symposium, Helsinki, 1965, Report 5-1.

Tenwolde, A., "Steady-State One-Dimensional Water Vapor Movement by Diffusion and Convection in a Multilayered Wall," ASHRAE Transactions, Vol. 91, Part 1, 1985, pp.322-341

Van der Held, E.F.M. and Van Drunen, F.G., "A Method of Measuring the Thermal Conductivity of Liquids," Physika, Vol. 15, No. 10, 1949, pp.865-881.

Wilson, A.G. and Garden, G., "Moisture Accumulation in Walls due to Air Leakage," Moisture Problems in Buildings, RILEM/CIB Symposium, Helsinki, 1965, Report 2-9.

Wise, A.F.E., "Ventilation of Buildings: A Review with Emphasis on the Effects of Wind," Energy Conservation in Heating, Cooling and Ventilating Building, Vol. 1, C.J. Hoogendoorn and N.H. Afgan, Eds., 1978, pp.135-153.

Yarbrough, D.W. and Toor, I.A., "Effect of Air Movement on Thermal Resistance of Loose-Fill Thermal Insulation," Thermal Insulation, Materials and Systems for Energy Conservation in the '80s, ASTM STP 789, F.A. Govan, D.M. Greason, and J.D. McAllister, Eds., American Society for Testing and Materials, 1983, pp.529-541.

APPENDIX A

MIRAN 1A GAS ANALYSER CALIBRATION PROCEDURE

A closed-loop calibration system is used to calibrate the MIRAN 1a Gas Analyser (Figure A.1). The following procedure is taken to determine the relationship between the output voltage (approximately 0 to 1 volt) and the SF₆ concentration (from 0 to about 5 ppm) :

- 1) The MIRAN 1A Gas Analyser and the closed-loop calibration pump are purged with clean air to remove any contaminant within the system. The total volume of the cell in the gas analyser and the calibration system is 5.64 litres. A digital voltmeter is connected to the output of the gas analyser.
- 2) The zero is set so that zero output voltage corresponds to zero concentration of SF₆.
- 3) A 503 mL mixing tube is purged with clean air. 10 mL of clean air sample is drawn from the mixing tube using a syringe and replaced with 10 mL of pure SF₆. A ping pong ball inside the mixing tube is used to mix the SF₆ and the air to give a uniform concentration inside the mixing tube.
- 4) 100 µL of the uniform mixture is drawn from the mixing tube and injected into the closed-loop calibration system through the septum on the pump connection. The output voltage is recorded after each

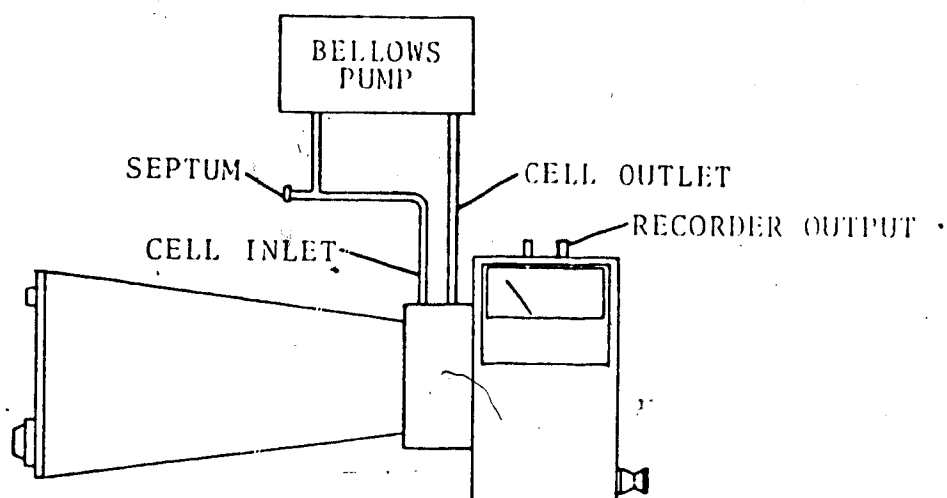


Figure A.1 Closed-loop schematic calibration system
for the MIRAN 1A Gas Analyser.

injection of the mixture. This procedure is repeated 15 times with each injection produces an increase in SF_6 concentration of 0.35 ppm in the closed-loop calibration system.

5) A fourth order least-square polynomial is used to fit the calibration points to obtain a calibration curve.

Typical calibration curve is shown in Figure A.2.

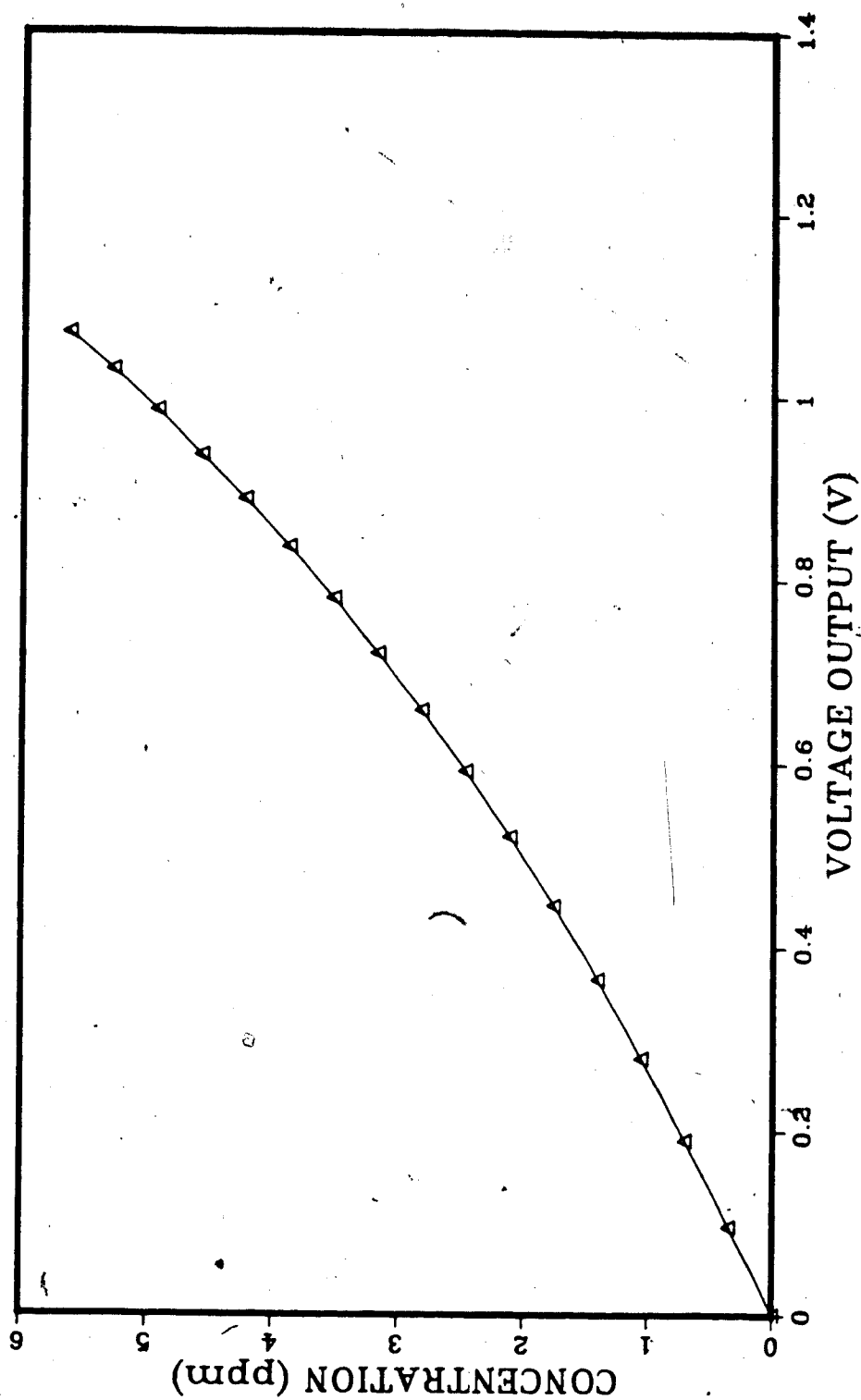


Figure A.2 Typical calibration curve for the MIRAN 1A Gas Analyser.

APPENDIX B

SOLUTION OF THE CONTINUITY EQUATION FOR THE TRACER GAS DECAY METHOD

The tracer gas decay test method is based on the continuity equation. The rate of change of the tracer gas in the test space, $V(dc/dt)$, is the difference between the tracer gas injected into the test space, F , and the tracer gas leaving the test space due to exfiltration, cE ,

$$V \left(\frac{dc}{dt} \right) = F - cE \quad (B.1)$$

where V is the volume of the test space in m^3 , c is the concentration of the tracer gas in part per million (ppm), t is the time in s, F is the tracer gas injection rate in L/s and E is the exfiltration rate in L/s. Initially, tracer gas is injected into the test space to give a safe but easily measured concentration. After injection stops, F is identically zero and Equation B.1 becomes

$$V \left(\frac{dc}{dt} \right) = -cE \quad (B.2)$$

Rearranging the terms in Equation B.2 yields

$$\frac{dc}{c} = - \frac{E}{V} dt \quad (B.3)$$

The solution to Equation B.3 is

$$\ln c(t) = - \frac{E}{V} t + D \quad (B.4)$$

where D is a constant and the term E/V is called the exfiltration rate, I . Taking the exponential of both side, Equation B.4 becomes

$$c(t) = \exp (-It + D) \quad (B.5)$$

Substituting the initial condition of $c=c_0$ at $t=0$ into Equation B.5,

$$c(t) = c_0 \exp (-It)$$

$$\text{or } \ln \frac{c(t)}{c_0} = -It \quad (B.6)$$

A plot of concentration versus time on a semi-log graph gives a straight line if the tracer gas concentration is uniform in the test space and the exfiltration rate is constant. The slope of the straight line is the exfiltration rate.

APPENDIX C

THEORY OF THE INFINITE LINE HEAT SOURCE

The differential equation of heat conduction is

$$\frac{1}{a} \frac{\partial \theta}{\partial t} = \frac{\partial^2 \theta}{\partial x^2} + \frac{\partial^2 \theta}{\partial y^2} + \frac{\partial^2 \theta}{\partial z^2} \quad (C.1)$$

where a is the thermal diffusivity of the material, θ is the temperature, t is the time and x , y and z are the Cartesian coordinates. The theoretical treatment of the line heat source theory is based on the assumptions of a line heat source of infinite length and negligible thickness buried along the z -axis in an infinite homogeneous and isotropic material. If heat is liberated at a rate of $\Phi(t)$ per unit time per unit length of the line heat source, then the differential equation of heat conduction in cylindrical coordinates is

$$\frac{1}{a} \frac{\partial \theta}{\partial t} = \frac{\partial^2 \theta}{\partial r^2} + \frac{1}{r} \frac{\partial \theta}{\partial r} \quad (C.2)$$

where $r^2 = x^2 + y^2$. The boundary conditions are

$$t = 0 : \theta = 0 \quad \partial \theta / \partial t = 0$$

$$t > 0, r = \infty : \theta = 0$$

$$t > 0, r = 0 : \Phi(t) = Q.$$

The solution to Equation C.2 is

$$\theta = \frac{Q}{4\pi k} \int_0^t \frac{\exp(r^2/4at)}{t} dt \quad (C.3)$$

By substituting $\beta^2 = r^2/(4at)$, Equation C.3 becomes

$$\begin{aligned} \theta &= \frac{Q}{2\pi k} \int_{\infty}^{\beta} \frac{\exp(\beta^2)}{\beta} d\beta \\ &= \frac{Q}{2\pi k} [I(\beta)] \end{aligned} \quad (C.4)$$

where the series $I(\beta)$ is

$$I(\beta) = D - \ln(\beta) + \frac{\beta^2}{2} - \frac{\beta^4}{8} + \dots \quad (C.5)$$

where D is a constant. If β is sufficiently small, then

$$\begin{aligned} I(\beta) &\doteq D - \ln(\beta) \\ &= D - \ln\left(\frac{r}{(4at)^{1/2}}\right) \end{aligned} \quad (C.6)$$

Therefore, Equation C.4 can be written as

$$\theta = \frac{Q}{2\pi k} \left\{ D - \ln\left[\frac{r}{(4at)^{1/2}}\right] \right\} \quad (C.7)$$

If θ_1 and θ_2 are the temperature rise corresponding to the time t_1 and t_2 at a radial distance r away from the

line heat source, then Equation C.7 can be written as

$$\begin{aligned}\theta_1 - \theta_2 &= \frac{Q}{2\pi k} \left\{ \ln \left[\frac{r}{(4at_2)^{1/2}} \right] - \ln \left[\frac{r}{(4at_1)^{1/2}} \right] \right\} \\ &= \frac{Q}{4\pi k} \ln \left(\frac{t_2}{t_1} \right) \quad . \quad (C.8)\end{aligned}$$

Rewriting Equation C.8 in terms of thermal conductivity,

$$k = \frac{Q}{4\pi} \left[\frac{\ln(t_2/t_1)}{\theta_2 - \theta_1} \right] \quad . \quad (C.9)$$

Therefore, by measuring the temperature rise with respect to time and knowing the power input to the line heat source (Q), k can be obtained.

APPENDIX D

SOLUTION FOR THE ENERGY EQUATION

The energy equation for flow through a porous medium is

$$\rho u C_p \frac{dT}{dx} = k \frac{d^2 T}{dx^2} \quad (D.1)$$

where ρ is the density of the fluid, u is the filtration velocity, C_p is the specific heat of the fluid, T is the temperature, x is the distance, k is the thermal conductivity of the porous medium. Substituting $P = dT/dx$ and $dP/dx = d^2 T/dx^2$, Equation D.1 becomes

$$\rho u C_p P = k \frac{dP}{dx} \quad (D.2)$$

Rearranging the terms in Equation D.2 yields

$$\frac{dP}{P} = \frac{\rho u C_p}{k} dx \quad (D.3)$$

The solution for Equation D.3 is

$$\ln (P) = \frac{\rho u C_p x}{k} + D_1 \quad (D.4)$$

where D_1 is the integration constant. Taking the exponential of both side, Equation D.4 becomes

$$P = D_2 \exp\left(\frac{\rho u C_p x}{k}\right) \quad (D.5)$$

where $D_2 = \exp(D_1)$ is a constant. Substituting back $P = dT/dx$ into Equation D.5 yields

$$\frac{dT}{dx} = D_2 \exp\left(\frac{\rho u C_p x}{k}\right) \quad (D.6)$$

The solution to Equation D.6 is

$$T = D_2 \exp\left(\frac{\rho u C_p x}{k}\right) \frac{k}{\rho u C_p} + D_3 \quad (D.7)$$

where D_3 is an integration constant. Substituting the boundary conditions of $x=0$, $T=T_i$ and $x=l$, $T=T_o$ into Equation D.7 gives

$$T_i = D_2 \frac{k}{\rho u C_p} + D_3 \quad (D.8)$$

$$\text{and } T_o = D_2 \exp\left(\frac{\rho u C_p l}{k}\right) \frac{k}{\rho u C_p} + D_3 \quad (D.9)$$

Subtracting Equation D.9 from D.8 yields

$$T_i - T_o = D_2 \frac{k}{\rho u C_p} \left[1 - \exp\left(\frac{\rho u C_p l}{k}\right) \right] \quad (D.10)$$

$$\text{or } D_2 = \frac{\rho u C_p}{k} \frac{T_i - T_o}{[1 - \exp(\rho u C_p \ell / k)]} \quad (D.11)$$

Substituting Equation D.11 into Equation D.8 yields

$$T_i = \frac{\rho u C_p}{k} \frac{(T_i - T_o)}{[1 - \exp(\rho u C_p \ell / k)]} \frac{k}{\rho u C_p} + D_3$$

$$\text{or } D_3 = T_i - \frac{(T_i - T_o)}{[1 - \exp(\rho u C_p \ell / k)]} \quad (D.12)$$

Substituting Equations D.11 and D.12 into Equation D.7 and rearrange the terms yields

$$T = T_i - (T_i - T_o) \left[\frac{\exp(\rho u C_p x / k) - 1}{\exp(\rho u C_p \ell / k) - 1} \right] \quad (D.13)$$

APPENDIX E

PSYCHROMETRY OF MOIST AIR

The following relations are used to calculate the humidity ratio, density and specific heat capacity of moist air at a given environmental condition :

- 1) Atmospheric Pressure at a given Elevation [Hutcheon and Handegord, 1983]

$$P = P_{sl} \left[1 - \frac{Bh}{T_a} \right]^{\frac{g}{R_a B}} \quad (E.1)$$

where P is the atmospheric pressure at a given elevation, P_{sl} is the atmospheric pressure at sea level (101 325 Pa), B is constant (0.0065), h is the elevation in m, T_a is the air temperature (288 K), g is the gravitational constant (9.8 m²/s) and R_a is a gas constant for air (287.1 J/kg·K)

- 2) Saturation Vapor Pressure of Water at a given Temperature [Lowe, 1977]

$$es = 100(A0 + T(A1 + T(A2 + T(A3 + T(A4 + T(A5 + T(A6))))))) \quad (E.2)$$

where $A0=6984.505294$

$A1=-188.903910$

$A2=2.133357675$

$A3=-1.288580973 \times 10^{-2}$

$A4=4.393587233 \times 10^{-5}$

$A5=-8.023923082 \times 10^{-8}$

$A6=6.136820929 \times 10^{-11}$

and T is the temperature in K.

3) Humidity Ratio [ASHRAE Handbook, 1981]

$$W = 0.62198 \left[\frac{(RH)es}{P - (RH)es} \right] \quad (E.3)$$

where W is the humidity ratio in $(\text{kg H}_2\text{O})/(\text{kg dry air})$, RH is the relative humidity in decimal, es is the saturation water vapor pressure in Pa and P is the local atmospheric pressure in Pa.

4) Density of the Moist Air [ASHRAE Handbook, 1981]

$$\rho_a = \frac{P (1 + W)}{R_a T (1 + 1.6078W)} \quad (E.4)$$

where ρ_a is the density of the moist air in kg/m^3 .

5) Specific Heat Capacity of the Moist Air [ASHRAE Handbook, 1981]

$$C_{pa} = C_{pd} \left[1 + \left(\frac{C_{pv}}{C_{pd}} - 1 \right) \frac{W}{1 + W} \right] \quad (E.5)$$

where C_{pa} is the specific heat capacity of the moist air at constant pressure in $\text{J/kg}\cdot\text{K}$, C_{pd} and C_{pv} are the specific heat capacities of the dry air and water vapour (1005 and 1850 $\text{J/kg}\cdot\text{K}$) respectively.